NASA CR-137534

(NASA-CR-137534) INVESTIGATION OF ROTOR BLADE ELEMENT AIRLOADS FOR A TEETERING ROTOR IN THE BLADE STALL REGIME (SECOND WIND TUNNEL TEST) (Boeing Vertol Co., Philadelphia, Pa.) 104 p HC $5.50 CSCL 01A G3/02

N76-18069

Unclas 19075

INVESTIGATION OF ROTOR BLADE ELEMENT AIRLOADS FOR A TEETERING ROTOR IN THE BLADE STALL REGIME

by

L. U. Dadone
T. Fukushima

OCTOBER 1975

Prepared under Contract NAS2-7229 by

THE BOEING VERTOL COMPANY
Boeing Center, P.O. Box 16858
Philadelphia, Pennsylvania 19142

for

U.S. ARMY AIR MOBILITY RESEARCH AND DEVELOPMENT LABORATORY
Ames Research Center
Moffett Field, California

and

NATIONAL AERONAUTICS AND SPACE ADMINISTRATION

D210-10792-3

October 1975

INVESTIGATION OF ROTOR BLADE ELEMENT AIRLOADS FOR A TEETERING ROTOR IN THE BLADE STALL REGIME (SECOND WIND TUNNEL TEST)

by

L. U. Dadone
T. Fukushima

Prepared under Contract NAS2-7229 by
The Boeing Vertol Company
Boeing Center, P.O. Box 16858
Philadelphia, Pennsylvania 19142

for

NATIONAL AERONAUTICS AND SPACE ADMINISTRATION

SUMMARY

Following the test discussed in Volume I of this report, a second test was conducted in the NASA-Ames 7 x 10 ft low speed wind tunnel on a seven-foot diameter model of a teetering rotor. The objectives of the additional test were:

1. Acquire pressure data for correlation with laser and flow visualization measurements (Reference 1).

2. Explore rotor propulsive force limits by varying the advance ratio at constant lift and propulsive force coefficients.

3. Obtain additional data to define the differences between teetering and articulated rotors.

4. Verify the acceleration sensitivity of new experimental transducers.

TABLE OF CONTENTS

LIST OF ILLUSTRATIONS

LIST OF TABLES

LIST OF SYMBOLS

a	Lift curve slope	Radian $^{-1}$
A	Rotor disc area	ft
b	Number of blades	
c	Blade chord	
C_l	Blade element lift coefficient, $\frac{\text{Lift}}{qc}$	
C_m	Blade element pitching moment coefficient about the quarter chord, $\frac{\text{Moment}}{qc^2}$	
C_n	Blade element normal force coefficient, $\frac{\text{Normal Force}}{qc}$	
C_p	Pressure coefficient, p/q	
C_T/σ	Rotor thrust coefficient, $T/\sigma\rho AV_T^2$	
C_T'/σ	Rotor lift coefficient, $L/\sigma\rho AV_T^2$	
D	Rotor diameter	feet
k	Reduced frequency parameter $\frac{c\Omega}{2V}$	
M	Mach Number	
P	Rotor power	HP
p	Measured pressure	lb/in^2
q	Dynamic pressure, $\frac{1}{2}\rho V^2$	lb/ft^2
r	Blade radial station	feet
R	Blade radius	feet
Re	Reynolds Number based on chord $\frac{cV}{\nu}$	

U_p	Total of velocity components perpendicular to rotor disc plane at a blade station	feet/sec
V	Free stream velocity	feet/sec
V_T	Rotor tip speed	feet/sec
x	Blade element chordwise location measured from leading edge	in
X	Rotor propulsive force	pounds
$\bar{X}$	Rotor propulsive force coefficient, $X/qd^2\sigma$	
y	Blade element surface location measured perpendicular to chord line	feet
μ	Advance ratio, V_T	
α	Blade element angle of attack	degrees
α_{ME}	Angle of attack calculated from $(C_N-C_{N_O})/dC_N/d\alpha)$	degrees
α_s	Rotor shaft angle	degrees
α_{TPP}	Rotor tip path plane angle $\alpha_s - \beta_{ic}$	degrees
β	Blade flapping angle	degrees
β_{ic}	Cosine component of blade flapping angle	degrees
β_{is}	Sine component of blade flapping angle	degrees
θ_0	Blade collective pitch at center-line of rotation	degrees
$\theta_{.75R}$	Blade collective pitch at 75 percent radius	degrees
λ	Rotor inflow ratio	
ρ	Density of air	slugs/ft^3

σ	Rotor solidity, $\frac{bc}{\pi R}$	
ν	Kinematic viscosity	ft^2/sec
Ψ	Blade azimuth angle	degrees
Ω	Rotor speed	rad/sec

INTRODUCTION

Upon completion of the analysis of the data from the Wind Tunnel test of Reference 1, a second test was conducted to explore additional conditions of interest. However, in this second test the model rotor was limited in loads and the investigation was restricted to low tip speeds.

This test was conducted under the direction of G. Morehouse, Research Scientist at the Ames Directorate, U.S. Army Air Mobility Research and Development Laboratory. Dr. J. McCroskey, of the Ames Directorate, provided guidance during the test. R. George, also of the Ames Directorate, was responsible for instrumentation and data acquisition. R. Mann, of the Boeing Vertol Company, carried out the off-line data reduction.

1.0 TEST EQUIPMENT

The test equipment is described in Reference 1, of which the present report is an addendum. For completeness, some of the key information is repeated.

1.1 Wind Tunnel

The test was conducted in the 7 x 10 ft. (2.13 x 3.05 m) low speed wind tunnel at NASA-Ames, Moffett Field, California. This tunnel is of the closed circuit single return type, with a rectangular test section equipped with solid walls. Maximum wind tunnel speed is approximately 400 fps (122 m/sec).

1.2 Rotor Test Setup

The rotor test stand used in this test consists of a hub and a pylon mounted on a turntable. The turntable rests on a six component balance system. Rotor drive and slip ring assembly are located below the turntable floor. The pylon can be inclined from 0° forward to 25° by remote control.

The hub has been simplified by eliminating cyclic pitch controls, but there are provisions for remotely controlling the collective pitch.

The blades are set with a pre-cone angle of 1.5°. Blade flapping is measured at the center of rotation by means of a gear and potentiometer arrangement. The instrumented blade was equipped with a torsion gage at the 0.50 R station.

1.3 Rotor

The rotor is a reduced scale version of the modified UH-1D rotor tested in the Ames 40 x 80 ft. wind tunnel as described in Reference 3. The basic data for the blades in this test are

Airfoil designation	NACA 0012
Chord	4.25 in. (10.8 cm)
Number of blades	2
Diameter	7.0 ft. (2.13 m)
Twist	0°
Pre-cone angle	1.5°
Root cutout, r/R	0.119
Solidity	0.0644
Taper Ratio	1:1
Blade Lock No. (for one blade)	3.3
Location of pressure instrumentation, r/R	0.75

1.4 Surface Static Pressures

One of the rotor blades was equipped with 16 absolute static pressure transducers distributed along the 0.75 R span station. Table I shows the transducer assignment and describes how the transducers functioned during the test.

The transducers used in this test were KULITE Model LQL4-125-25. Their operating range was 0-20 psi, and their sensitivity was repeatedly checked out in the 0-4 psi range before and during the test. No change in sensitivity was detected. Figure 1 illustrates transducer installation.

Because of rotor speed limitations, the transducer output was generally very low and it had to be boosted by an additional amplification factor before being recorded.

Figure 2 and Table II illustrate the installation of the acceleration compensated transducers on the second blade.

1.5 Data Acquisition System

Since the data acquisition system was limited to 14 channels of information, two completely separate wind tunnel runs were necessary for each test condition. Table III shows the channel assignment and recording sequence. Data acquisition procedures are the same as discussed in Reference (1).

During the portion of the test dealing with acceleration compensated transducers, only one recording sequence was necessary. Transducer assignment, condition, and channel assignment are summarized in Table II.

1.6 Data Reduction System

The pressure data and other information recorded on the 14-channel analog tapes were transferred to the Boeing Vertol Company for processing through the Boeing Vertol flight test data reduction system.

Details of the data reduction procedure are discussed in Reference (1).

SPAN STATION: .75R
PROFILE: NACA 0012
TRANSDUCERS: KULITE LQL4-125-25

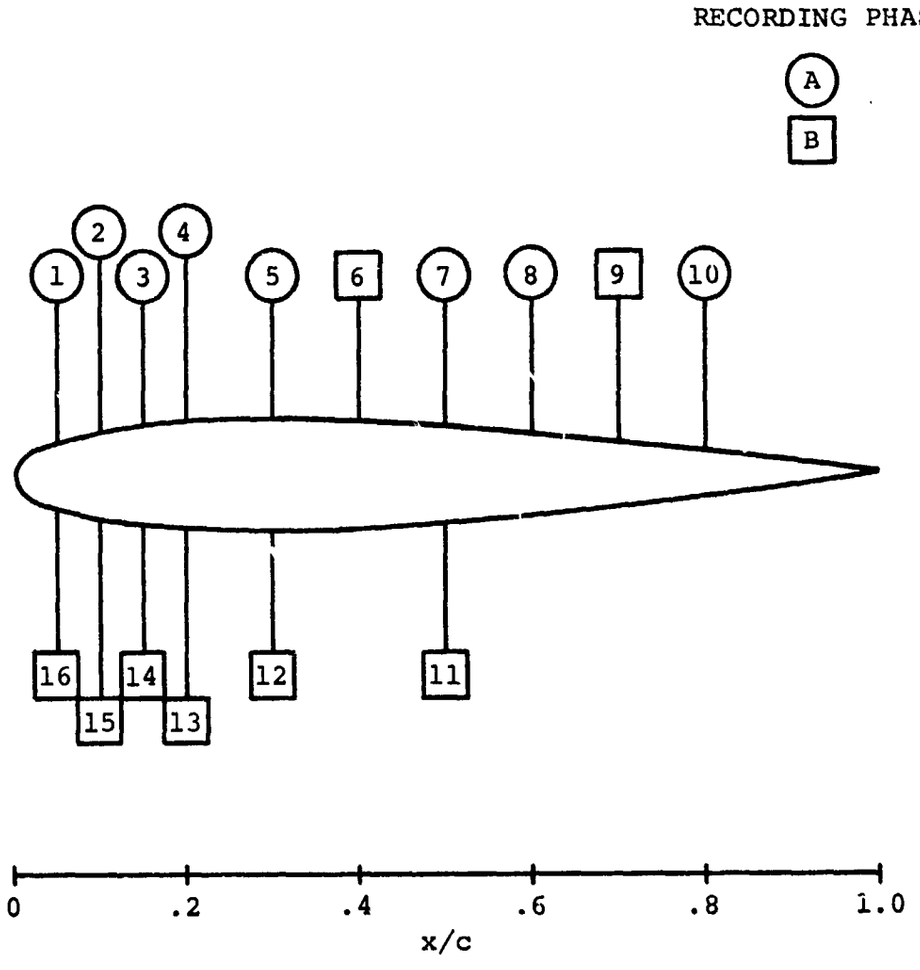

NOTE: TRANSDUCERS 15 AND 16 INOPERATIVE AT START OF TEST

FIGURE 1 PRESSURE TRANSDUCER DISTRIBUTION

TABLE I TRANSDUCER ASSIGNMENT AND CONDITION DURING TEST

TRANSDUCER NUMBER	CHORD STATION (X/C)	SURFACE	RECORDING PHASE	CONDITION
1	.05	UPPER	A	
2	.10		A	INOPERATIVE IN MANY CASES
3	.15		A	INOPERATIVE IN MANY CASES
4	.20		A	OCCASIONAL MALFUNCTION
5	.30		A	
6	.40		B	
7	.50		A	
8	.60		A	OCCASIONAL MALFUNCTION
9	.70		B	
10	.80		A	INOPERATIVE IN SOME CASES, AND CAUSING BAD C_N AND C_M INTEG
11	.50	LOWER	B	
12	.30		B	OCCASIONAL MALFUNCTION
13	.20		B	
14	.15		B	MOSTLY INOPERATIVE
15	.10		B	INOPERATIVE
16	.05		B	INOPERATIVE REPLACED WITH $C_P = 1.0$

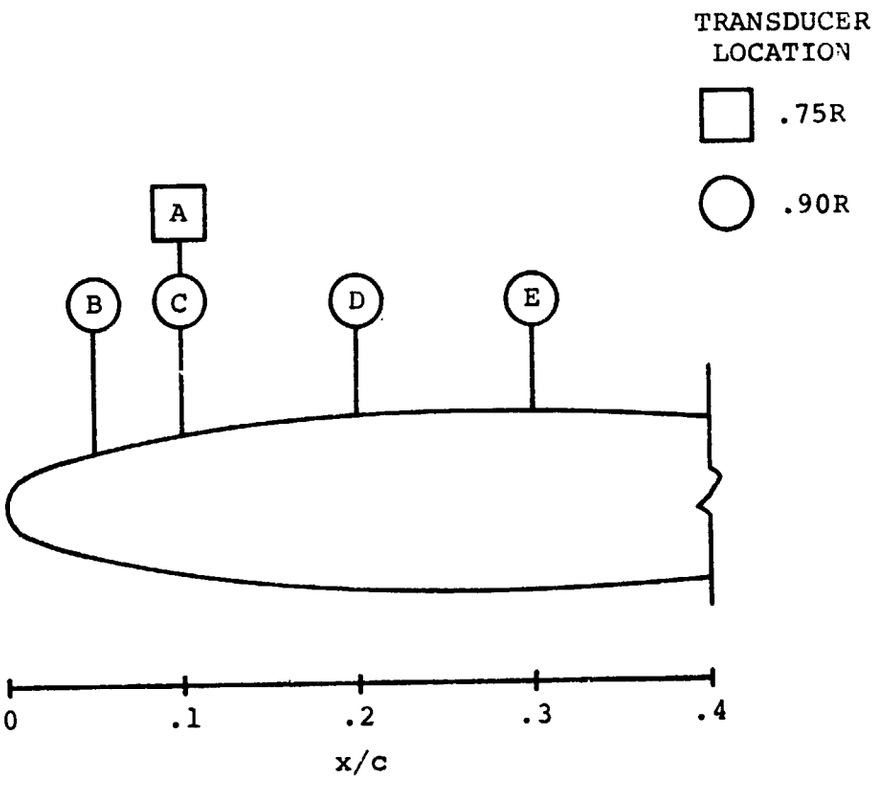

TRANSDUCER	DESCRIPTION
A	PERPENDICULAR TO CHORDLINE
B (INOPERATIVE)	PARALLEL TO CHORDLINE FACING OUTBOARD
C	PERPENDICULAR TO CHORDLINE
D	PARALLEL TO CHORDLINE FACING L.E.
E	PARALLEL TO CHORDLINE FACING 45° TOWARDS L.E.

FIGURE 2 LOCATION OF ACCELERATION COMPENSATED TRANSDUCERS

TABLE II - CHANNEL ASSIGNMENT AND CONDITION OF ACCELERATION COMPENSATED TRANSDUCERS

CHANNEL	TRANSDUCER(*)	OTHER CHANNEL INFORMATION	TRANSDUCER CONDITION
1	1		
2	2		
3	A		
4	4		
5	5		
6	C		
7	D		
8		TIME CODE	
9	B		INOPERATIVE
10	E		
11		FLAPPING	
12		1/REV SIGNAL	
13		FM TIME CODE	
14		VOICE IDENT.	

(*) TRANSDUCERS A, B, C, D, E ARE ACCELERATION COMPENSATED. OTHER TRANSDUCERS ARE THE SAME AS USED IN THE FIRST PART OF THIS TEST.

TABLE III TAPE RECORDER CHANNEL ASSIGNMENT AND RECORDING SEQUENCE

CHANNEL NUMBER	RECORDING PHASE A	RECORDING PHASE B
1	TR 1	TR 9
2	TR 2	TR 11
3	TR 3	TR 6
4	TR 4	TR 12
5	TR 5	TR 13
6	TR 7	TR 14
7	TR 8	TR 15
8	TIME CODE	
9	TR 10	TR 16
10	BLADE TORSION	
11	ROOT FLAPPING ANGLE	
12	RPM	
13	TIME CODE-FM	
14	VOICE ID	+1 VOLT D.C.

2.0 TEST PROGRAM

2.1 Summary of Test Conditions

Objectives of this wind tunnel test were:

(a) Acquire pressure data for correlation with laser and flow visualization measurements.

(b) Explore rotor propulsive force limits by varying the advance ratio of the rotor at constant lift and propulsive force coefficients.

(c) Obtain additional data to define the difference between teetering and articulated rotors.

(d) Verify the acceleration sensitivity of new experimental transducers.

The conditions at which final data were reduced and analyzed are shown in Table IV.

A more detailed list of test conditions is shown in Table V in the Appendix. The data on the acceleration compensated transducers is summarized in Table VI.

2.2 Test Procedure

The test procedure was almost the same as outlined in Reference (1). The only significant difference was that Phase A and Phase B recording sequences were separated into two distinct test runs, each with its own wind-off-zero.

2.3 Instrumentation Problems

Several of the pressure transducers did not function at all from the beginning of the test, and others malfunctioned periodically during the test. Specific instances will be pointed out when the data are reviewed in detail. For remarks on transducer condition, see also Tables I and II. Because of periodic transducer malfunctions, the integrated values of normal force and pitching moment are often inaccurate.

2.4 Data Reduction

The data reduction procedure was the same as followed during the first test, described in Reference (1). An additional difficulty, however, was introduced by changes in sensitivity made to compensate for the reduced transducer output at low

2.4 (continued)

tip speeds. Each sensitivity factor required a separate digitizing sequence because the existing data reduction system does not have provisions for sensitivity changes within a sequence of test runs.

2.5 Data Analysis

The data analysis procedure was the same as described in detail in Reference (1). Since the leading edge transducer on the lower surface was not functioning, a fixed value of $C_p = 1.0$ was assigned to the lower surface pressure at $x/c = 0.05$.

TABLE IV SUMMARY OF WIND TUNNEL TEST CONDITIONS

TEST POINT	C_T'/σ	μ	V_{TIP} (FPS)	DESCRIPTION OF RUN	OBJECTIVE
1.01	.131	.278	109.9	MATCH CONDITIONS FROM REF. 2 AND FLOW VISUALIZATION TESTS	EXPLORE TIP VORTEX PROXIMITY EFFECTS
02	.074	.188	110.0		
03	.123	.249	238.2		
04*	.100	.289	110.7		
05	.100	.289	110.7		
06	.084	.189	238.2		
07	.099	.191	238.7		
2.01	.074	.304	270.1	ADVANCE RATIO VARIATION AT MODERATE ROTOR LIFT LEVELS	STUDY PHENOMENA ASSOCIATED WITH DEGRADATION IN ROTOR PROPULSIVE FORCE
02	.074	.405	270.6		
03	.079	.455	269.8		
04	.079	.353	269.7		
05	.108	.348	270.3	ADVANCE RATIO VARIATION IN PRESENCE OF STALL	
06	.104	.302	270.5		
07*	.108	.408	270.6		
3.01	.070	.350	270.2	SHAFT ANGLE SWEEP AT CONSTANT COLLECTIVE $\theta_{.75} = 12.77°$	REPEAT TEST POINTS 17.03 TO 17.07 FROM FIRST TEST AT REDUCED TIP SPEED
02	.088	.350	270.2		
03	.107	.352	269.8		
04	.120	.351	269.9		
05	.137	.349	269.7		
06	.083	.344	270.9	SHAFT ANGLE SWEEP AT REDUCED COLLECTIVE $\theta_{.75} = 8.83°$	VERIFY EFFECT OF REDUCED FLAPPING EXCURSIONS
07	.102	.343	270.7		
08*	.070	.348	270.5		
09	.147	.349	271.0	SAME AS T.P. 3.05	REPEATABILITY CHECK
10	.079	.402	270.3	SAME AS T.P. 2.02	

(*) UNSATISFACTORY DATA NOT SHOWN IN REPORT

3.0 TEST RESULTS AND DISCUSSION

3.1 Tip Vortex Proximity Effects

Test conditions 1.01 through 1.07 were run to obtain a record of the 0.75R pressures in a flow environment already explored by other means, such as flow visualization with tufts (unpublished NASA data) or laser measurements (Reference 2). In each case, data were acquired first at the very low tip speeds of the original tests, and then at higher speeds to improve transducer performance. Changes in flow conditions to alter tip vortex location were also tried.

For a thorough interpretation of the results, it would have been necessary to evaluate the blade loading with a rotor performance analysis method including tip vortex effects. Since such an effort was beyond the scope of this study, the data are presented with limited comments.

3.1.1 Test Points 1.01 and 1.05, $\mu = 0.28$, $V_T = 110$ fps

Test point 1.01 was taken to correlate with previous flow visualization data (unpublished). Test point 1.05 was taken at a substantially reduced shaft angle for comparison. Both runs were at very low tip speeds but, since several transducers did not operate properly, the integrated loads have not been computed. The time history plots in Figure 3, Test Point 1.01, show evidence of a double stall event, where the first stall event appears at $\Psi = 200°$ and the second one at $\Psi = 310°$. The leading edge pressures display a third peak in the first quadrant, but such pressure peak does not seem to be associated with stall.

It can be also observed that, while the first stall event ($\Psi = 200°$) is gradual, as the pressure peak moves progressively from the leading edge to the trailing edge, the second stall event takes place almost simultaneously along the entire chord.

Figure 4 shows selected pressure time histories for Test Point 1.05, run at a reduced shaft angle. No significant separation is evident.

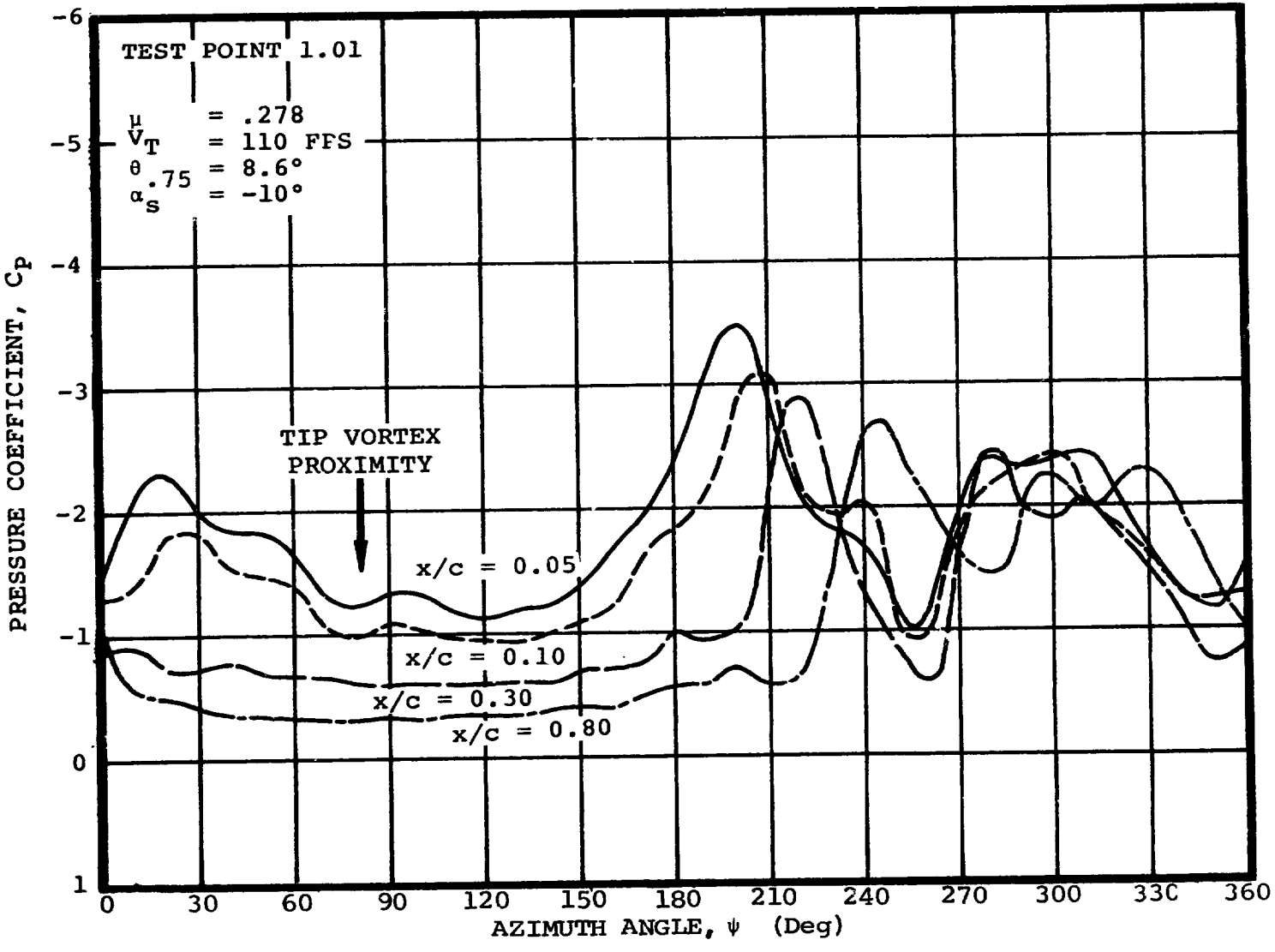

Figure 3 TIME HISTORIES OF UPPER SURFACE PRESSURES MEASURED AT r/R = 0.75

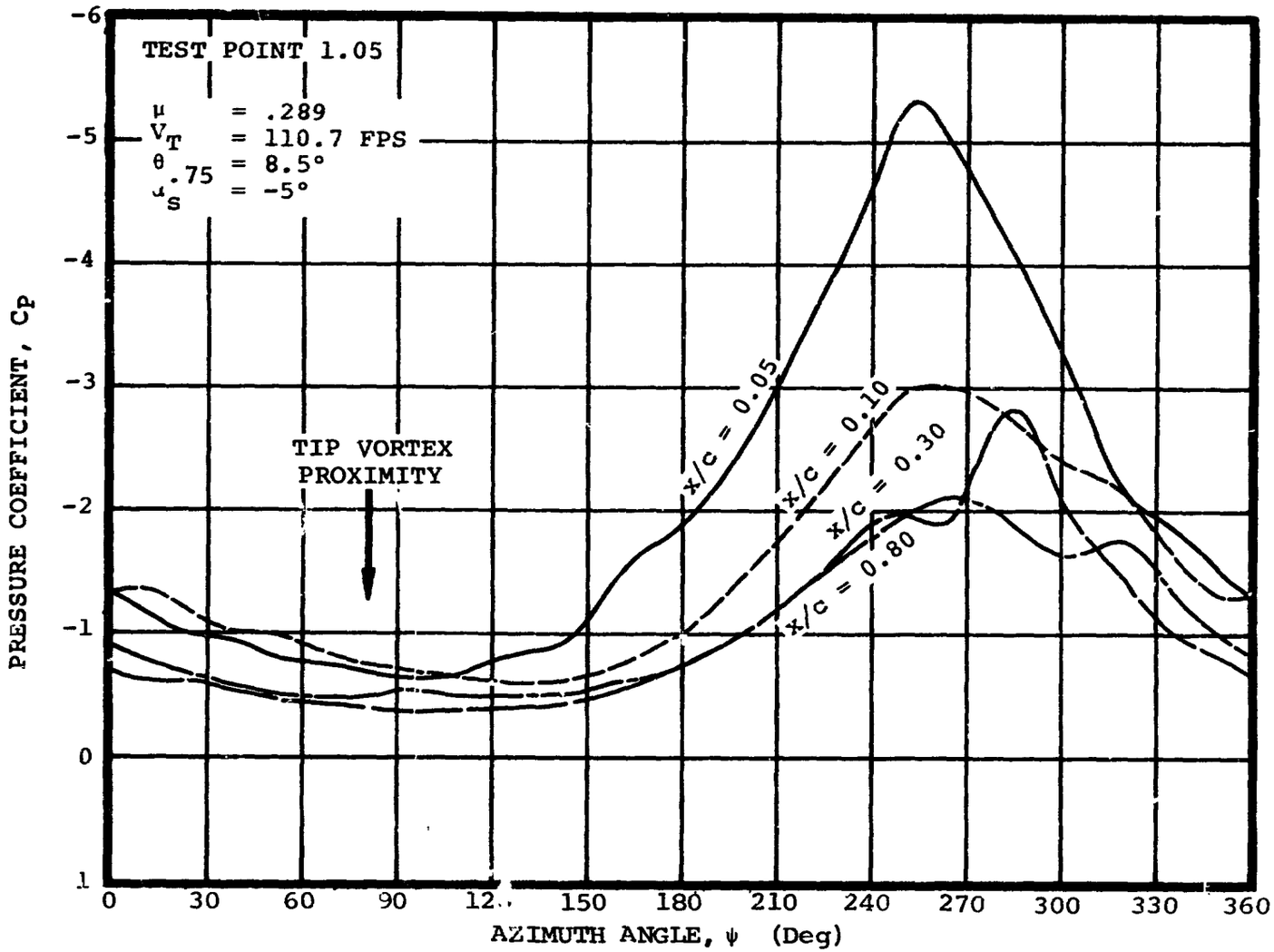

Figure 4 TIME HISTORIES OF UPPER SURFACE PRESSURES MEASURED AT r/R = 0.75

3.1.2 Test Points 1.02, 1.06 and 1.07, at $\mu = 0.19$

Test point 1.02 was run at a tip speed of 110 fps for correlation with laser measurements reported in Reference (2). Test points 1.06 and 1.07 were run at 238 fps.

Correlation with the lift estimated from the bound vorticity measurements of Reference (2) is very good, as shown in Figure 5, where the measured value of $(\Gamma/c\Omega R) = 0.145$ corresponds to a lift coefficient $C_l = 0.298$*.

As indicated in Figure 5 and the following figures, vortex intersection or vortex proximity effects are possible at $\Psi = 105°$ and $\Psi = 295°$.

The normal force and pitching moment time histories of Test Point 1.02 show a series of stall/reattachment events on the retreating side. In the main stall event the pitching moment breaks before the lift, but the largest nose down pitching moment is reached after the maximum normal force has been attained, which is consistent with the observations of Reference (1). Figure 6 shows selected pressure time histories for Test Point 1.02, and Figure 7 shows the variation in pressure distributions at selected azimuth locations.

Test Point 1.06 was run at the same conditions as Test Point 1.02, except for the tip speed which was increased from 110 to 238 fps. The increased tip speed all but eliminated the stall events of Test Point 1.02. In fact, the fluctuations observed in the fourth quadrant could be at least in part attributed to vortex proximity effects. Normal force and pitching moments for Test Points 1.06 and 1.07 are shown in Figure 8. Pressure time histories are shown in Figures 9 and 10.

* By the relation $C_l = \left(\frac{2}{c}\right)\left(\frac{\Gamma}{\Omega R}\right)\left(\frac{1}{\mu + r/R}\right)$.

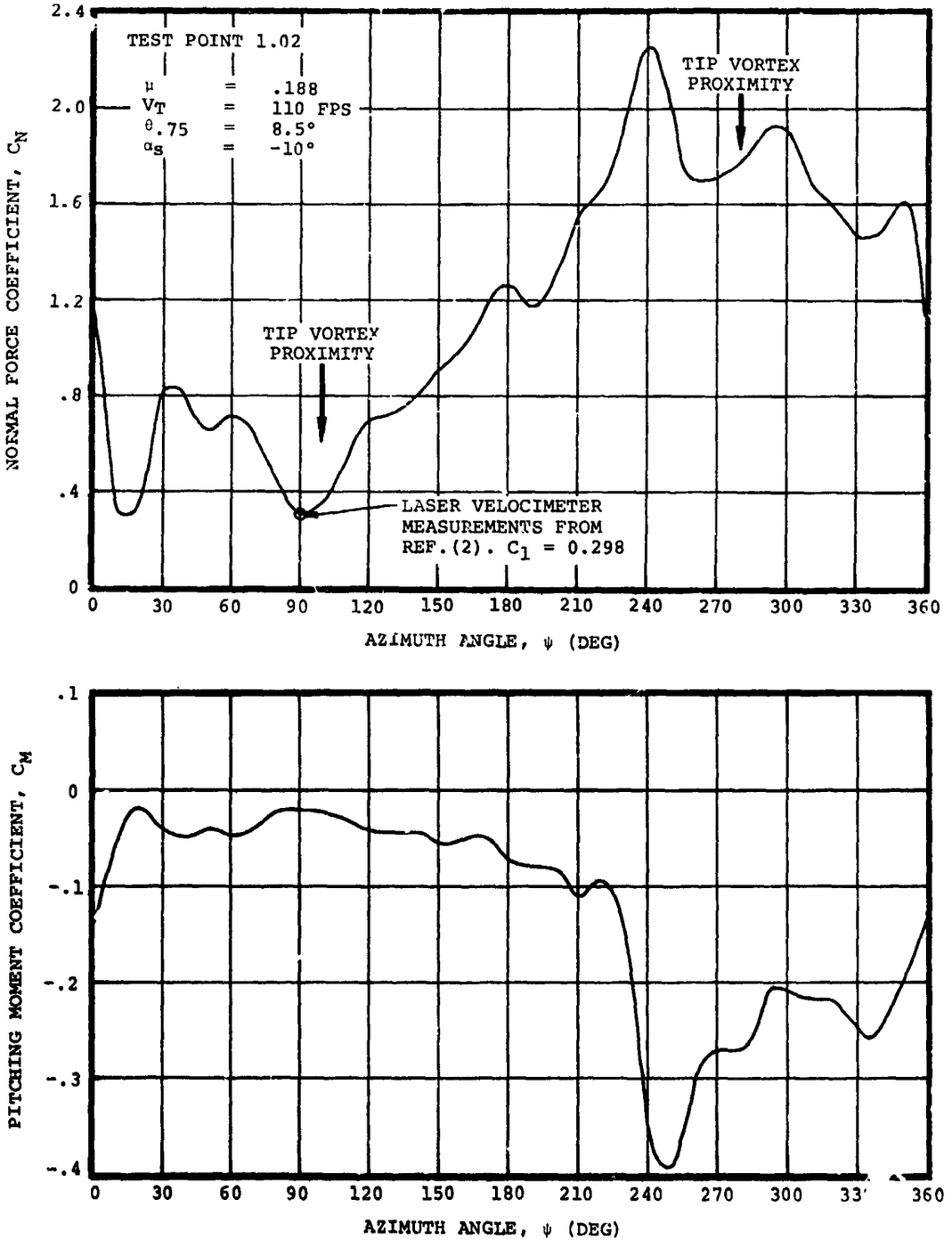

Figure 5 NORMAL FORCE AND PITCHING MOMENT COEFFICIENTS OBTAINED FROM INTEGRATED PRESSURES AT r/R = 0.75

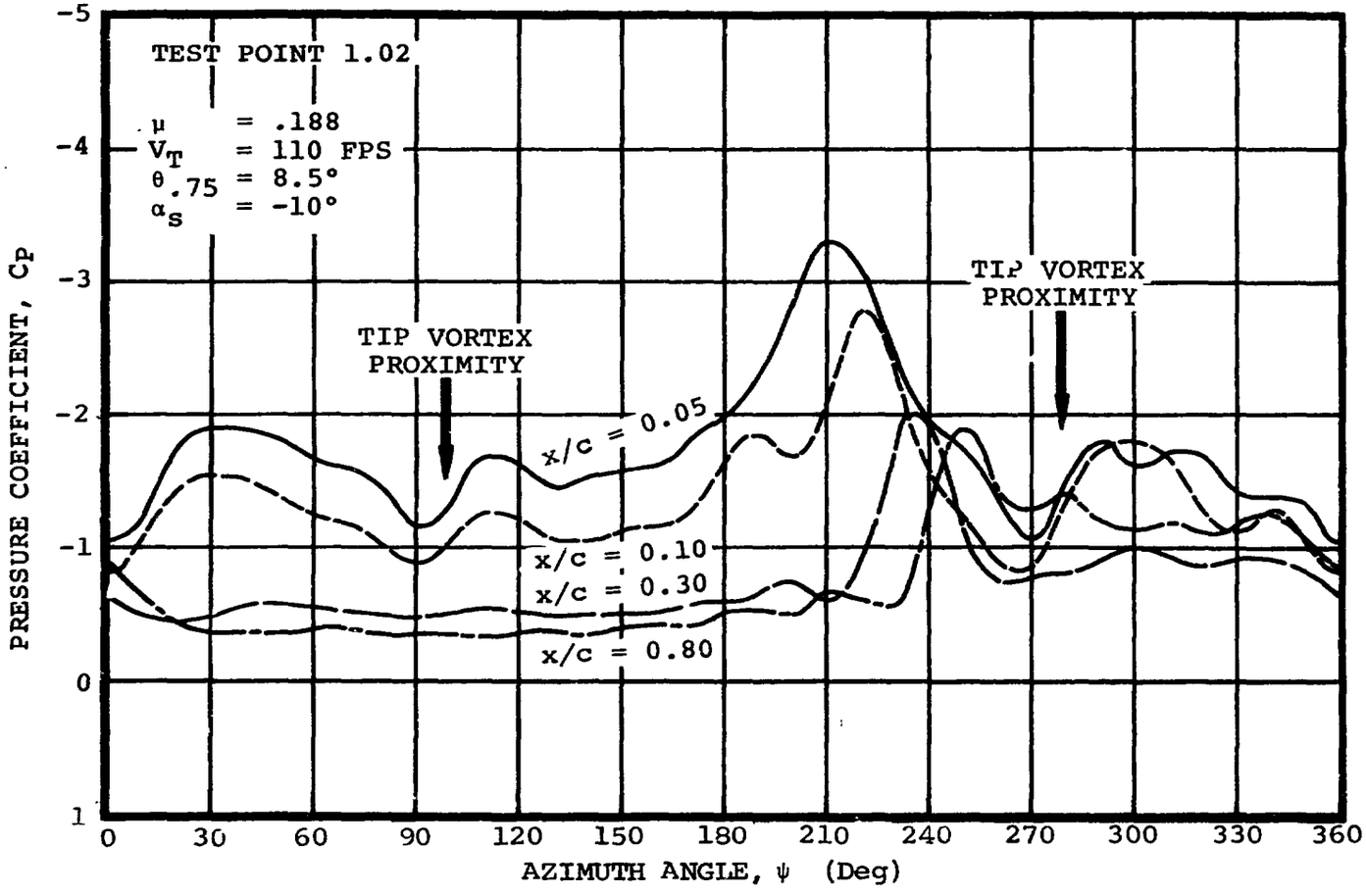

Figure 6 TIME HISTORIES OF UPPER SURFACE PRESSURES MEASURED AT r/R = 0.75

TEST POINT	μ	V_T (FPS)	α_{SHAFT} (DEG)	α_{TPP} (DEG)	$\theta_{.75}$ (DEG)	$C_{T'}/\sigma$	X/qD^2_o
1.02	.188	110.0	-10.0°	-2.6°	8.5°	.074	.4

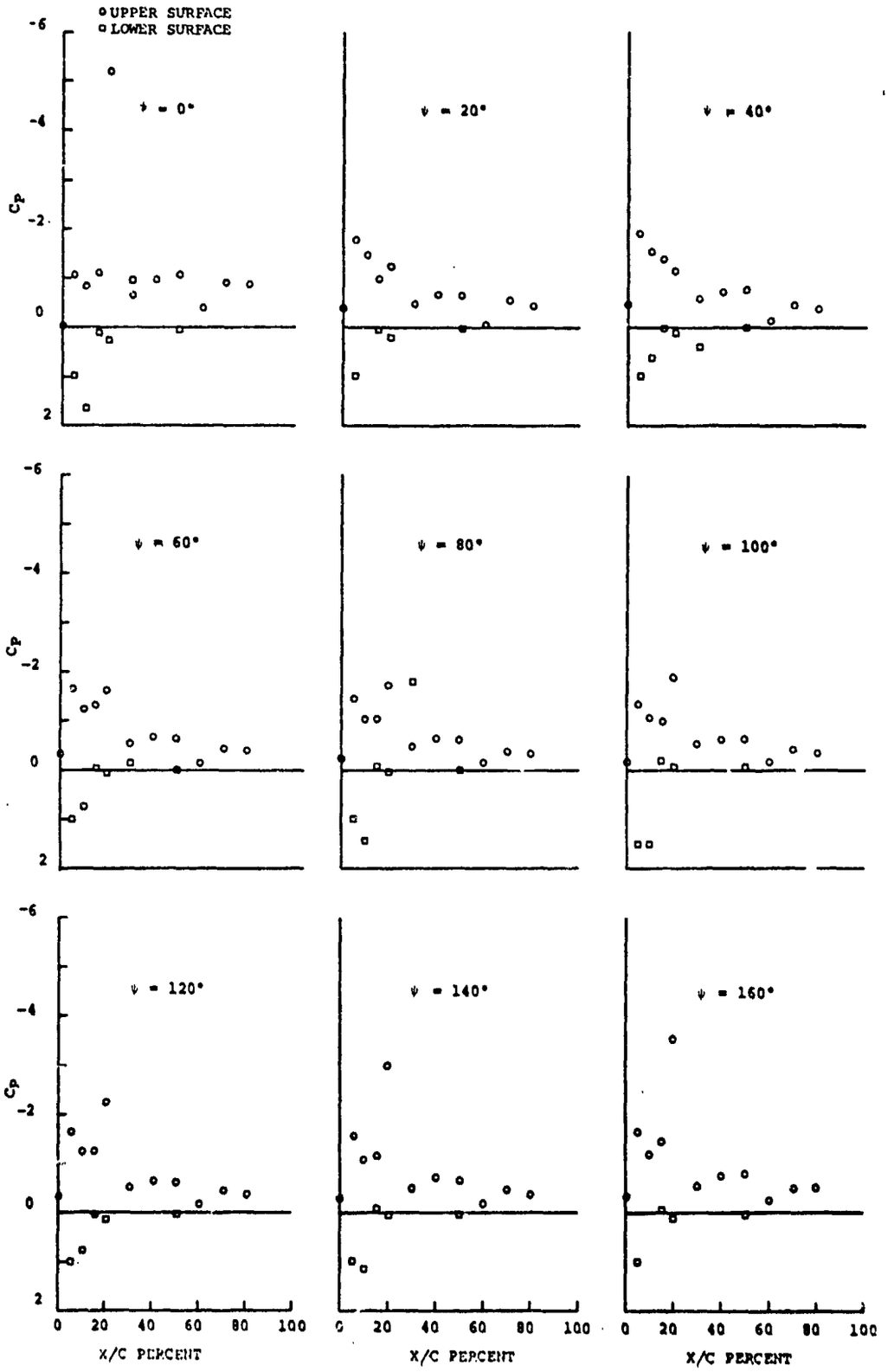

Figure 7 PRESSURE DISTRIBUTIONS MEASURED AT r/R = 0.75

TEST POINT	μ	V_T (FPS)	α_{SHAFT} (DEG)	α_{TPP} (DEG)	$\theta_{.75}$ (DEG)	$C_{T'}/\sigma$	$X/qD^2\sigma$
1.02	.188	110.0	-10.0°	-2.6°	8.5°	.074	.4

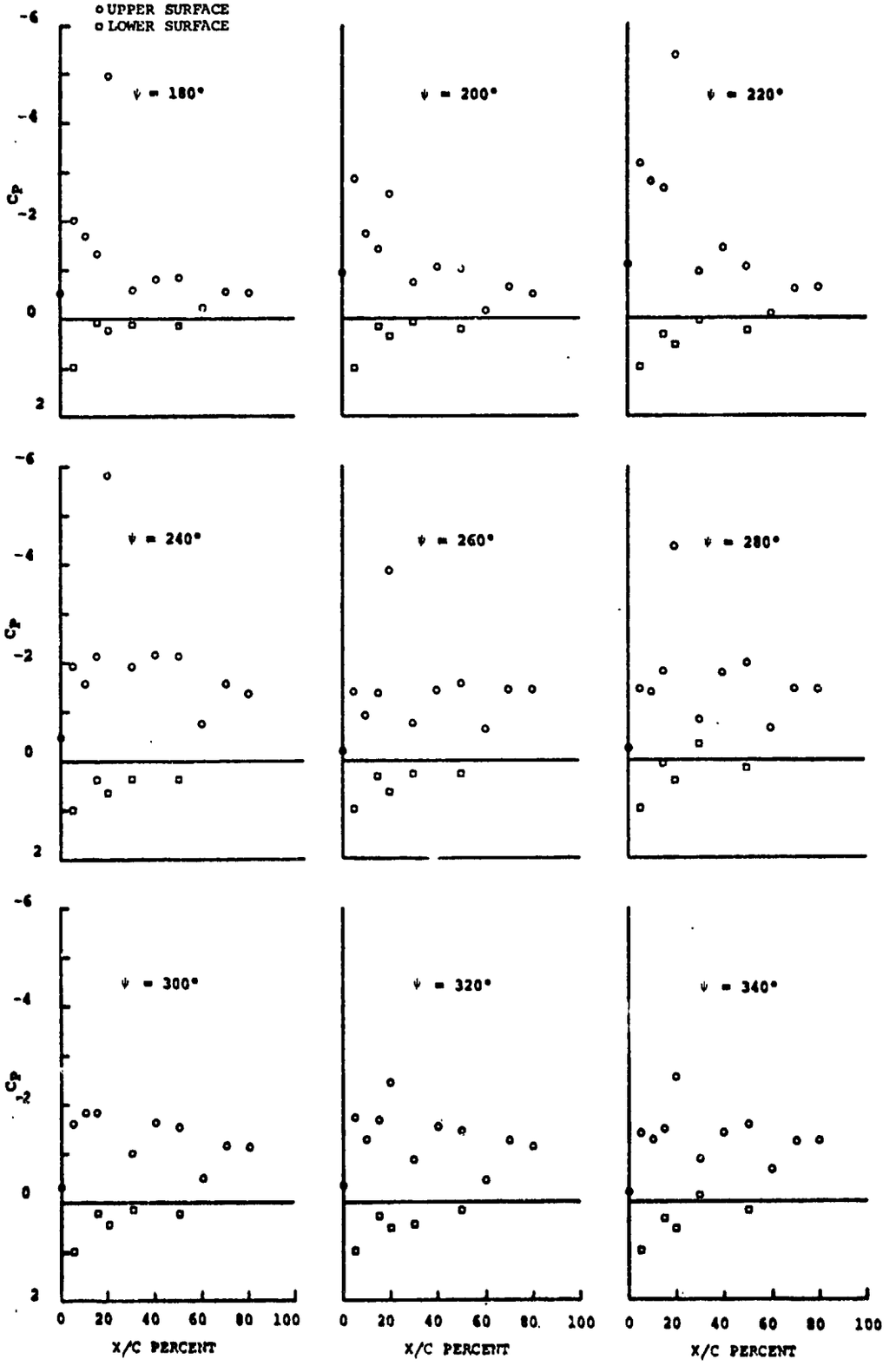

Figure 7 (Continued) PRESSURE DISTRIBUTIONS MEASURED AT r/R = 0.75

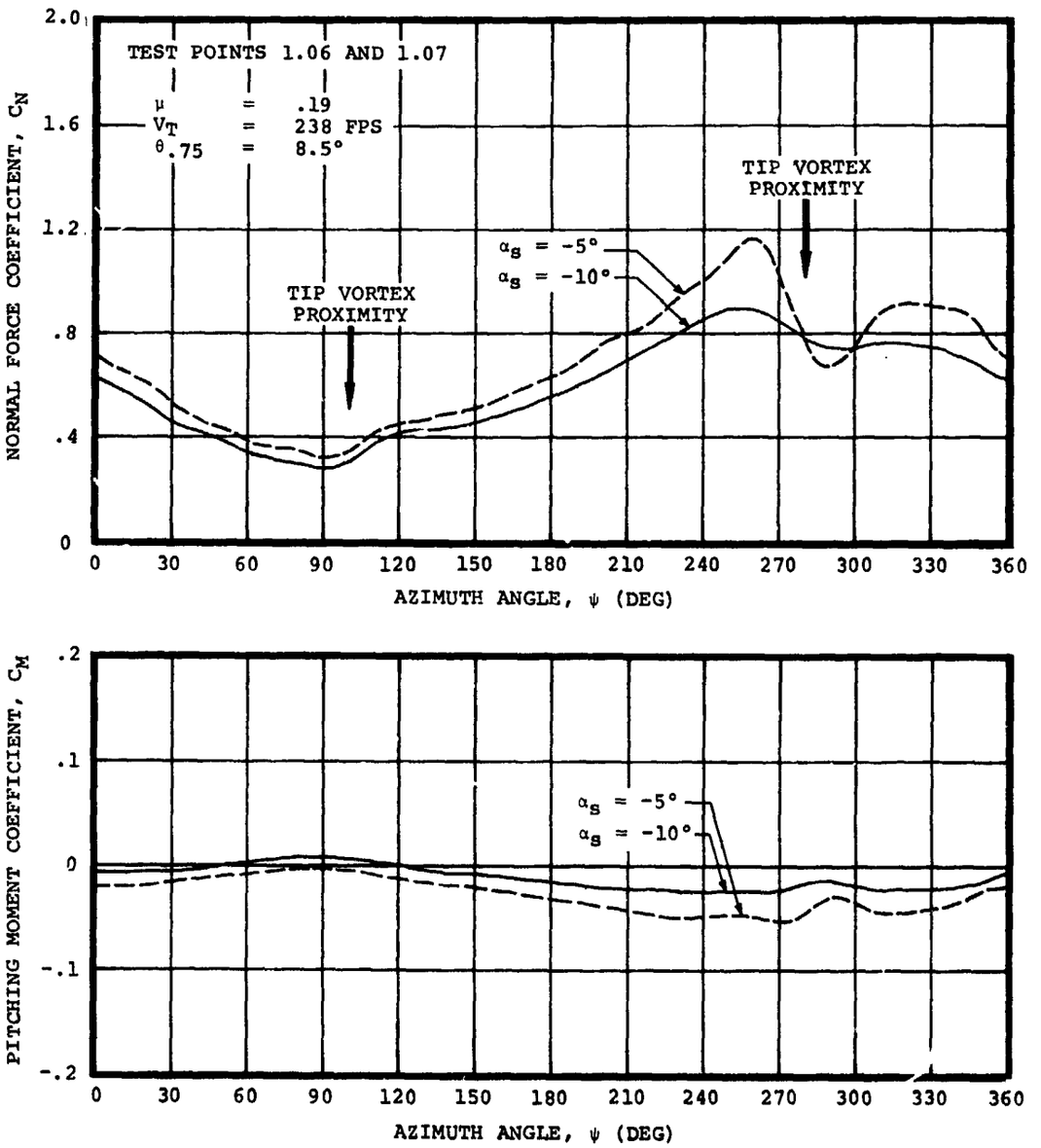

Figure 8 NORMAL FORCE AND PITCHING MOMENT COEFFICIENTS OBTAINED FROM INTEGRATED PRESSURES AT r/R = 0.75

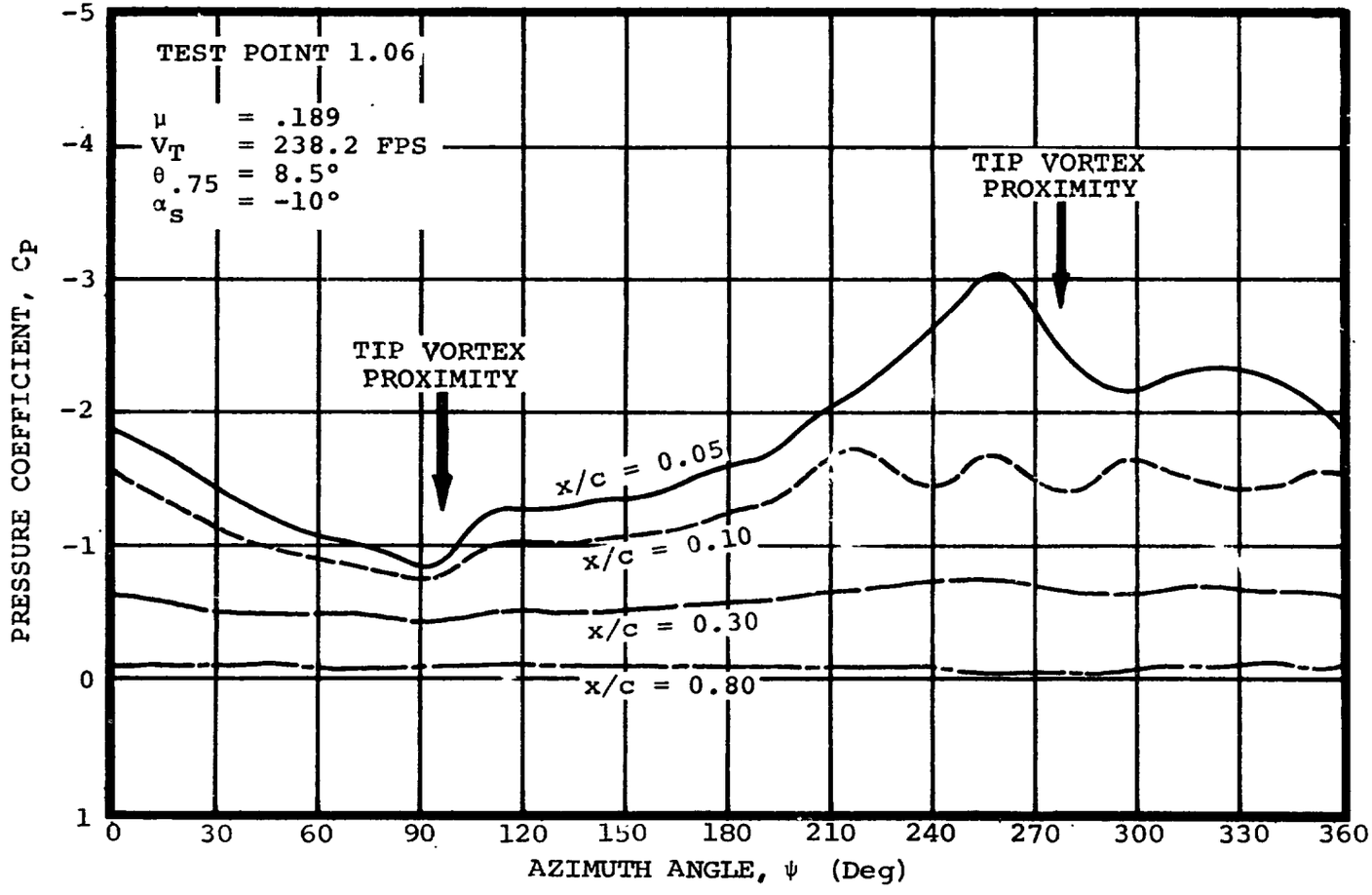

Figure 9 TIME HISTORIES OF UPPER SURFACE PRESSURES MEASURED AT r/R = 0.75

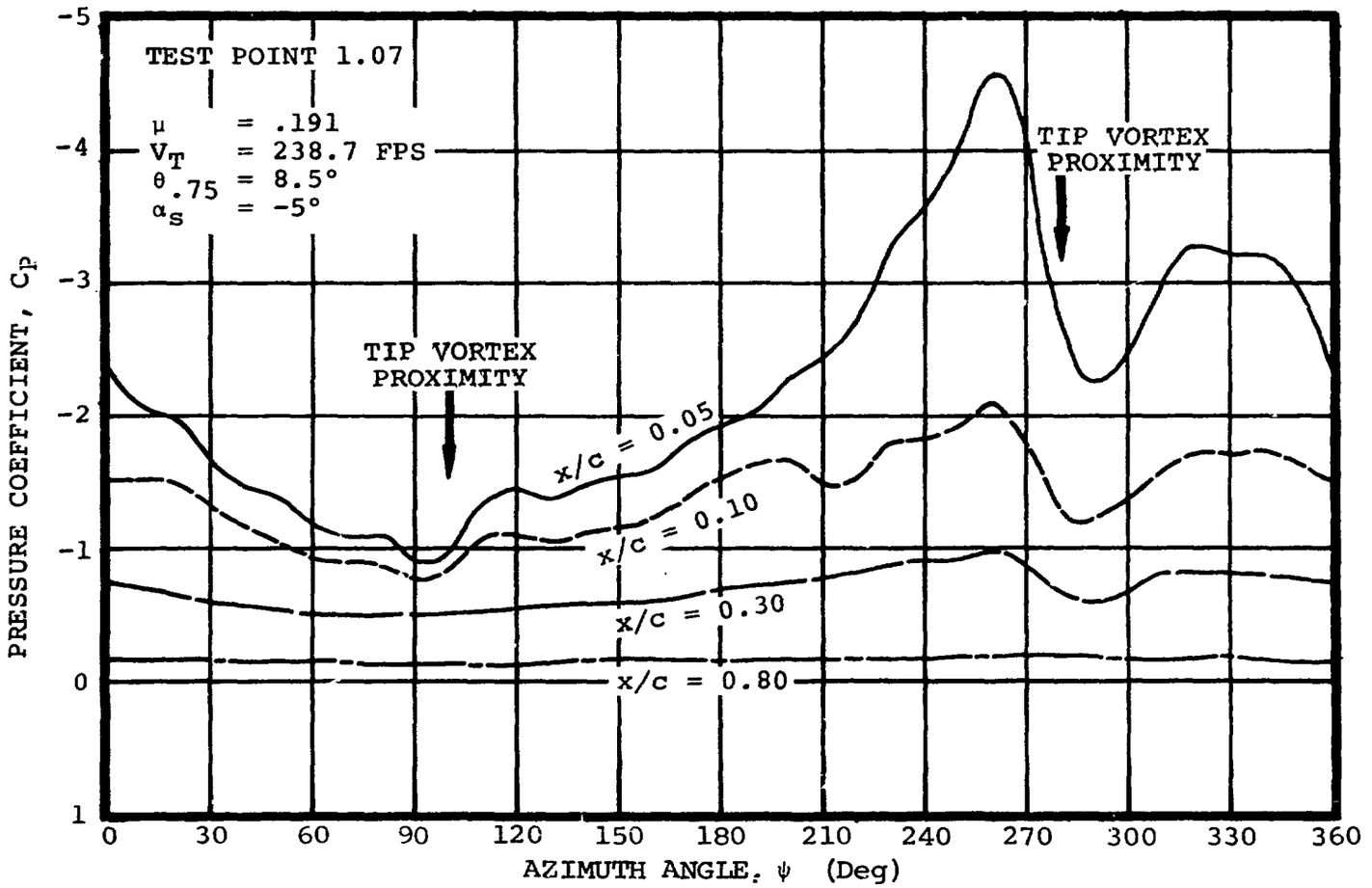

Figure 10 TIME HISTORIES OF UPPER SURFACE PRESSURES MEASURED AT r/R = 0.75

3.1.3 Test Point 1.03, μ = 0.25

Figure 11 shows four time histories of upper surface pressures. Pressure distributions at selected azimuth locations are shown in Figure 12. Because of transducer malfunctions, the integrated loads were in error and are not presented.

At this test condition, vortex proximity effects at r/R = 0.75 are possible at $\Psi \cong 95°$ from a half spiral, and at $\Psi \cong 50°$ from one full spiral.

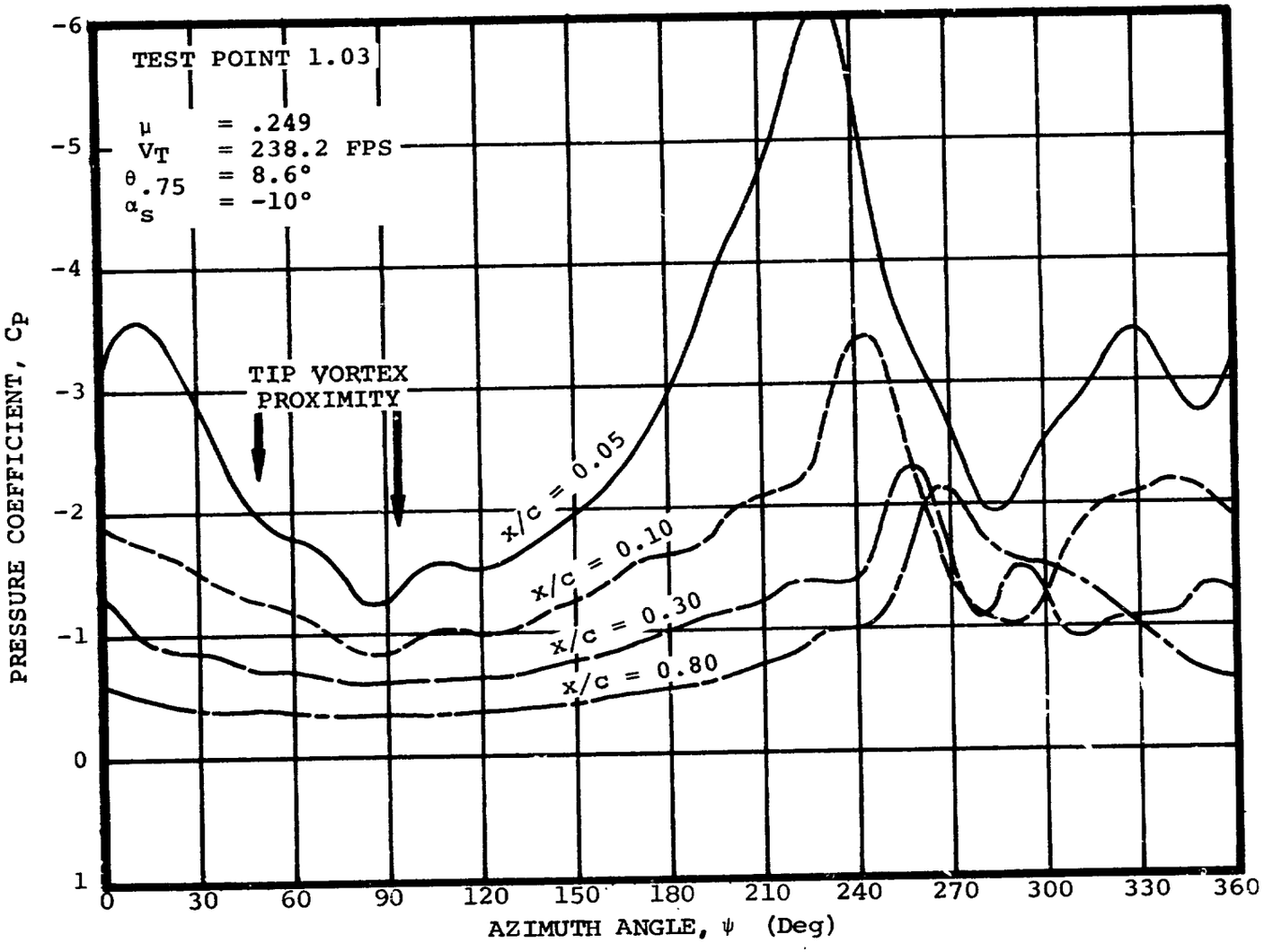

Figure 11 TIME HISTORIES OF UPPER SURFACE PRESSURES MEASURED AT r/R = 0.75

TEST INT	μ	V_T (FPS)	α_{SHAFT} (DEG)	α_{TPP} (DEG)	$\theta_{.75}$ (DEG)	C_T/σ	$X/qD^2\sigma$
1.03	.249	238.2	-10.0°	-0.9°	8.579°	.123	.25954

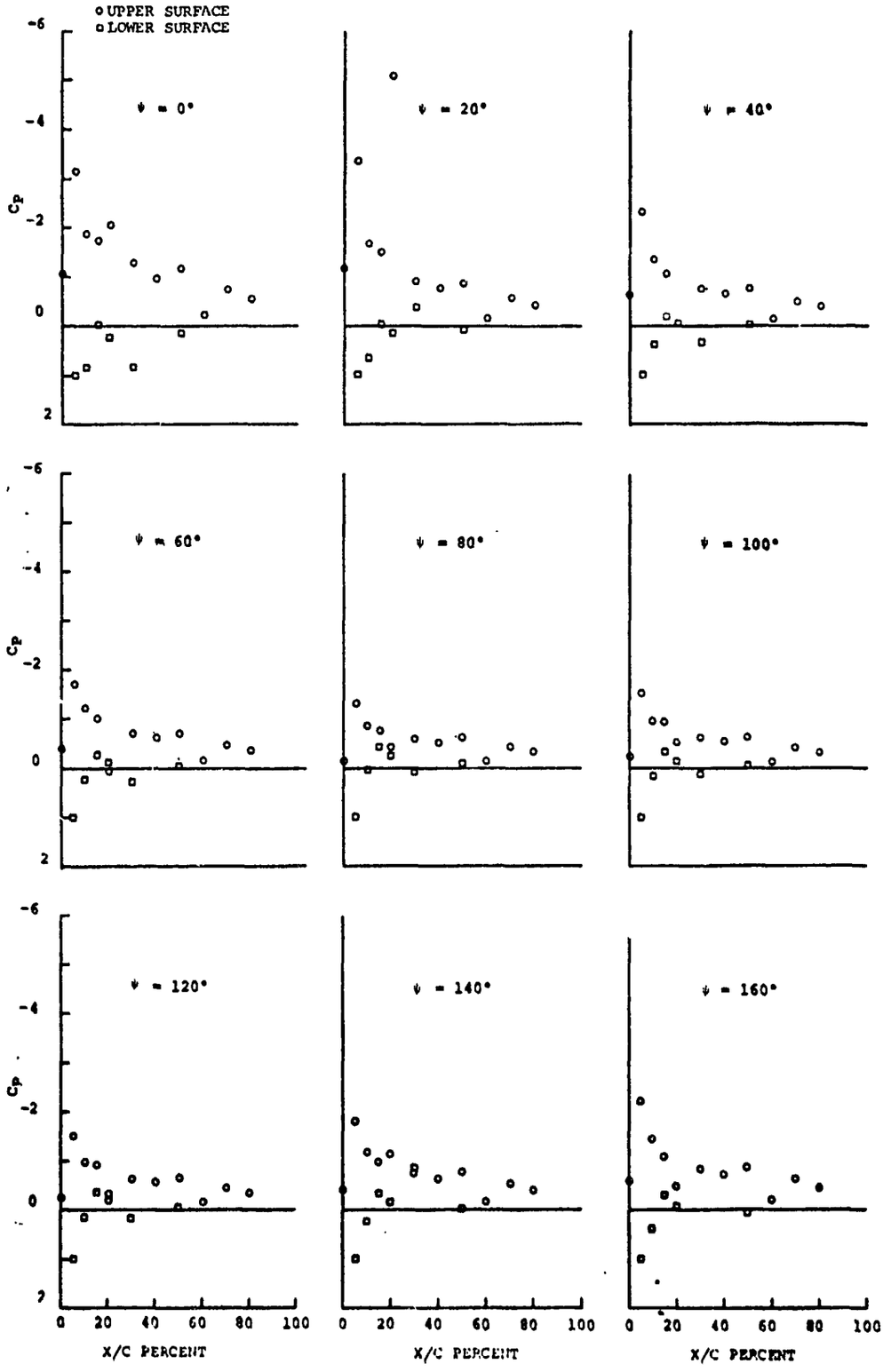

Figure 12 PRESSURE DISTRIBUTIONS MEASURED AT r/R = 0.75

TEST POINT	μ	V_T (FPS)	α_{SHAFT} (DEG)	α_{TPP} (DEG)	$\theta_{.75}$ (DEG)	C_T/σ	$X/qD^2\sigma$
1.03	.249	238.2	-10.0°	-0.9°	8.579°	.123	.25954

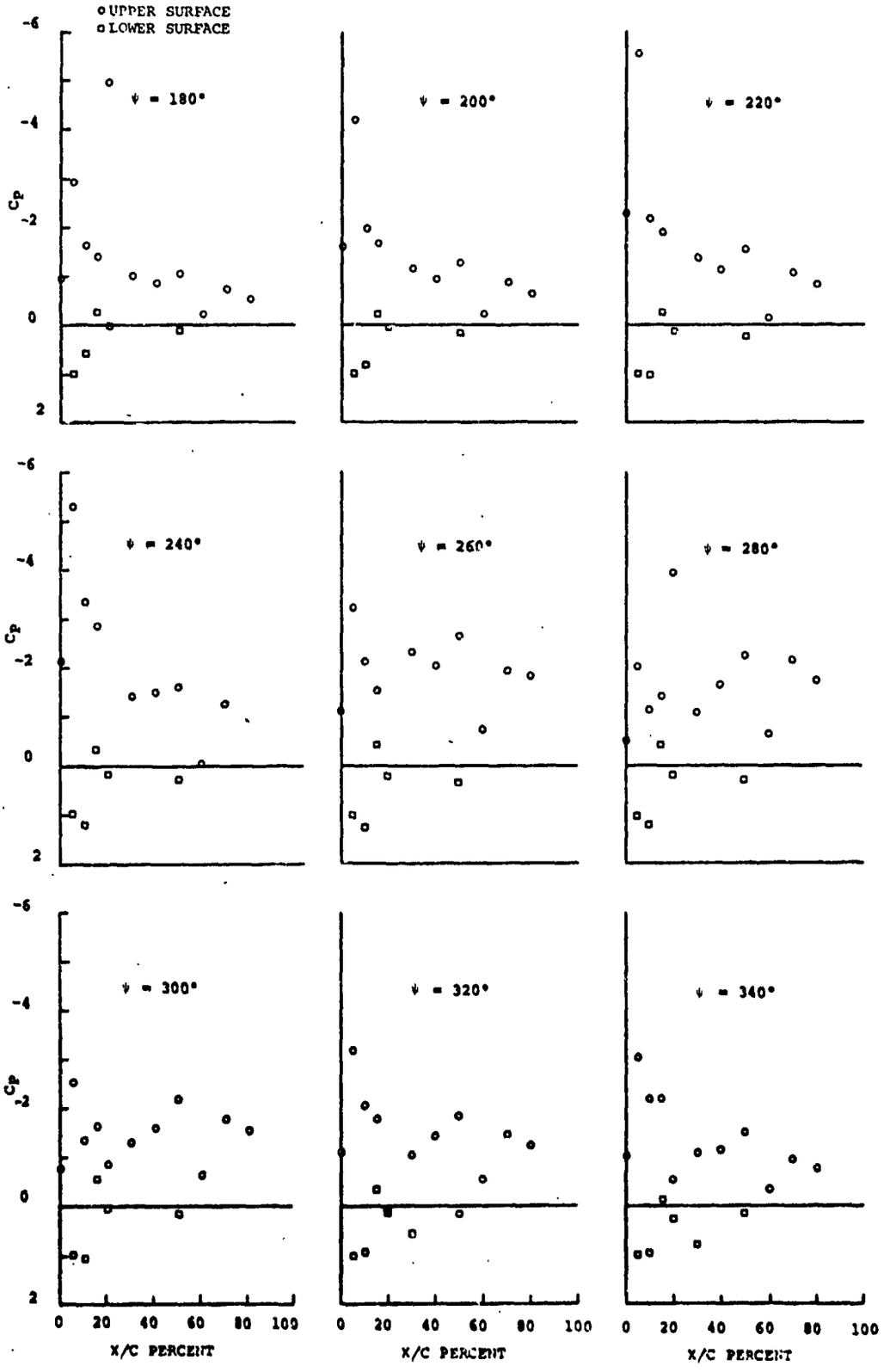

Figure 12 (Continued) PRESSURE DISTRIBUTIONS MEASURED AT r/R = 0.75

3.2 Investigation of Propulsive Force Limits

To gain insight into the flow phenomena responsible for the degradation in propulsive force with increasing advance ratio, the model rotor was run at constant lift coefficient, constant propulsive force coefficient and constant tip speed over a range of tunnel velocities. Two rotor lift coefficient levels were selected to vary the conditions for stall inception.

This investigation was not as useful as expected for two possible reasons:

a. Instrumentation problems.

b. The degradation in propulsive force on helicopter rotors is associated with compressibility effects which could not be simulated because of model loads limitations.

3.2.1 Advance Ratio Variation at Moderate Rotor Lift Levels (Test Points 2.01 to 2.04)

Test Points 2.01 to 2.04 were run at approximately constant rotor lift, C_T'/σ, and constant propulsive force, $\bar{X}$, for advance ratios from $\mu = 0.3$ to $\mu = 0.45$. In order to maintain lift and propulsive force, the tip path plane was tilted progressively forward as the collective pitch angle was increased with increasing advance ratio.

Figure 13 compares the integrated normal force and pitching moment coefficients. Some of the data were deleted because of transducer problems. Except for some variation in pitching moments, there is no evidence of significant stall in the integrated loads, but, at the higher advance ratios, the pressure time histories indicate a moderate amount of leading edge separation immediately followed by reattachment.

Figures 14 through 17 show selected upper surface pressure time histories for advance ratios from $\mu = 0.3$ to 0.45. The only significant effect is the appearance of two distinct pressure peaks on the retreating side at advance ratios above 0.35. The first pressure peak collapses at the leading edge (at $d\alpha/dt>0$) and spreads downstream in a gradual stall pattern. The second pressure peak is established while $d\alpha/dt<0$ following a flow reattachment process starting at about 0.30c and moving rapidly to the leading edge. The single pressure peak at 0.30c is in sequence with the stall pattern following the collapse of the first leading edge peak. The time interval between the two pressure peaks appears to become larger with increasing advance ratio.

Figures 18 and 19, respectively, show pressure distributions for the $\mu = 0.3$ and $\mu = 0.45$ test conditions. In Figure 19, the "first" pressure peak can be observed at $\psi = 240°$, with collapse at $\psi = 260°$ and 280°, and the "second" pressure peak indicating flow reattachment at $\psi = 320°$.

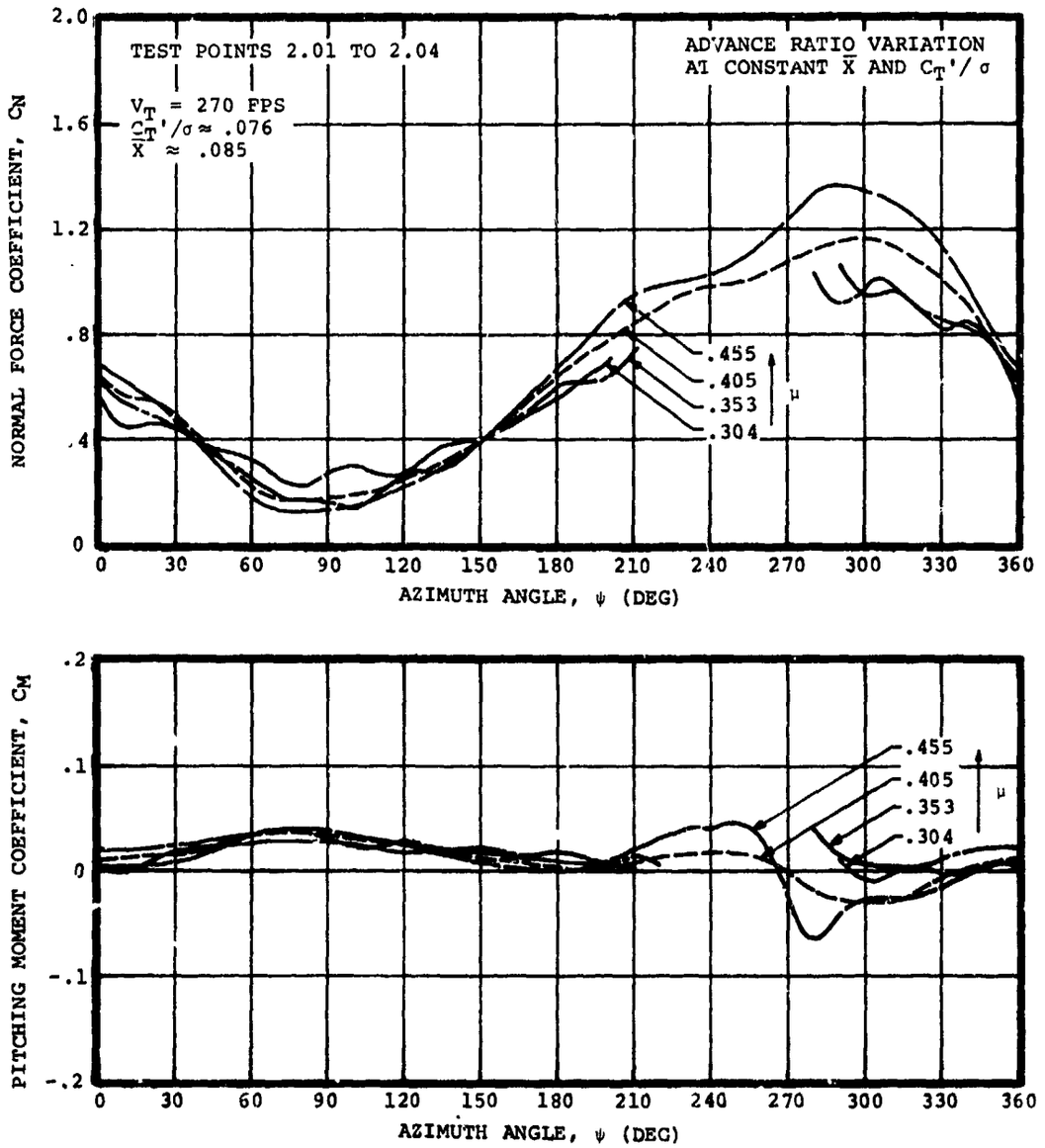

Figure 13 NORMAL FORCE AND PITCHING MOMENT COEFFICIENTS OBTAINED FROM INTEGRATED PRESSURES AT r/R = 0.75

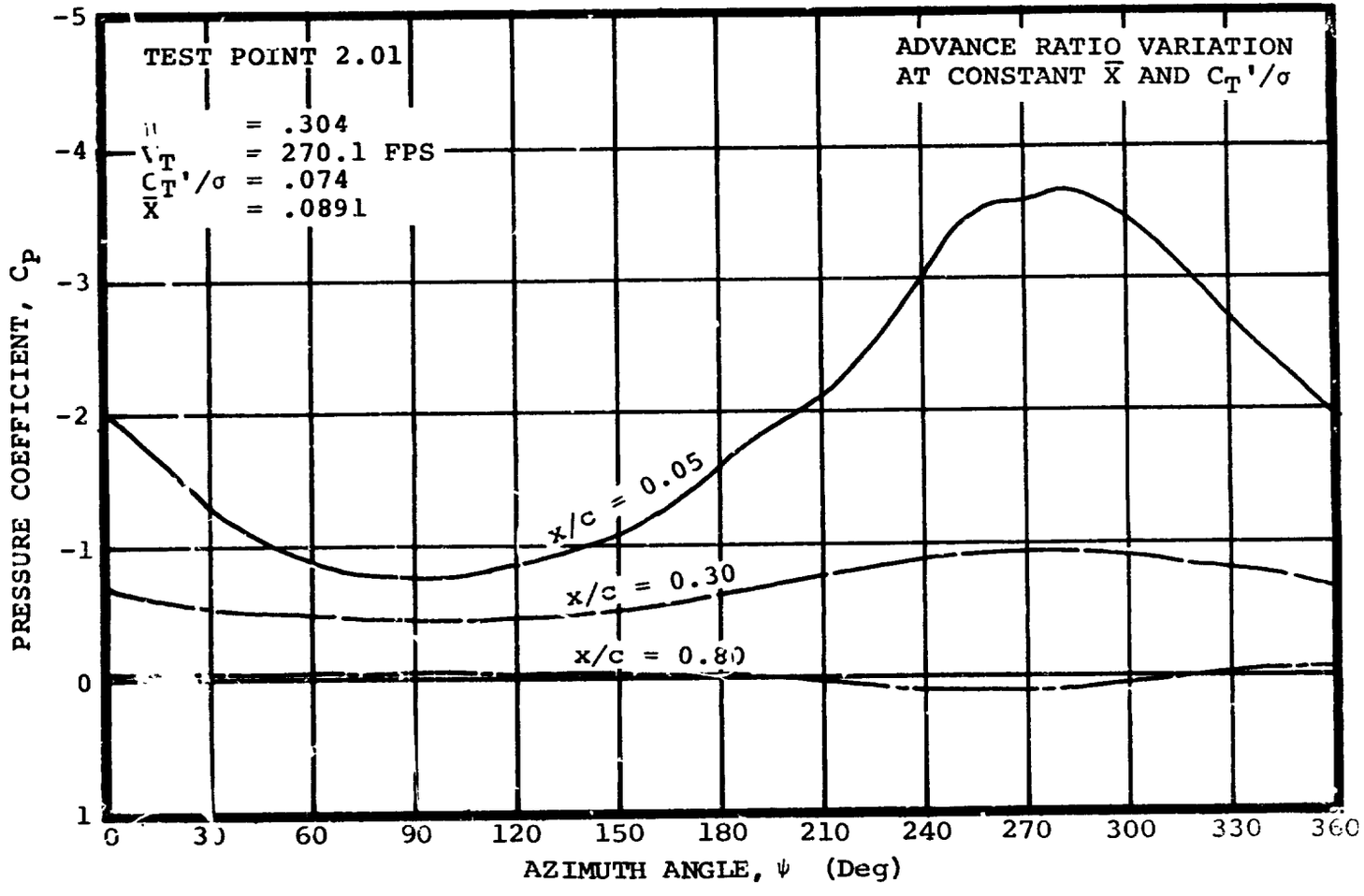

Figure 11 TIME HISTORIES OF UPPER SURFACE PRESSURES MEASURED AT r/R = 0.75

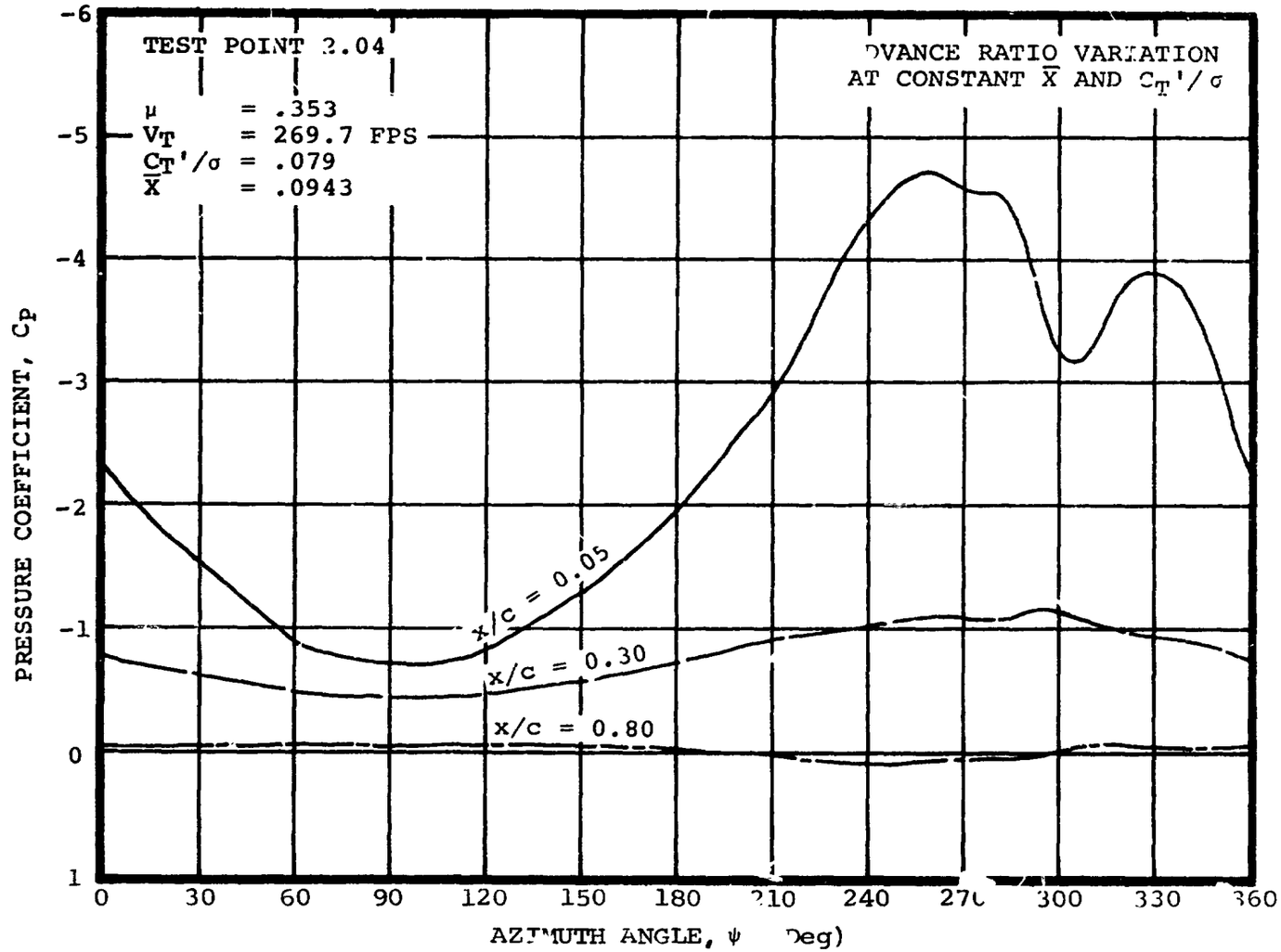

Figure 15 TIME HISTORIES OF UPPER SURFACE PRESSURES MEASURED AT r/R = 0.75

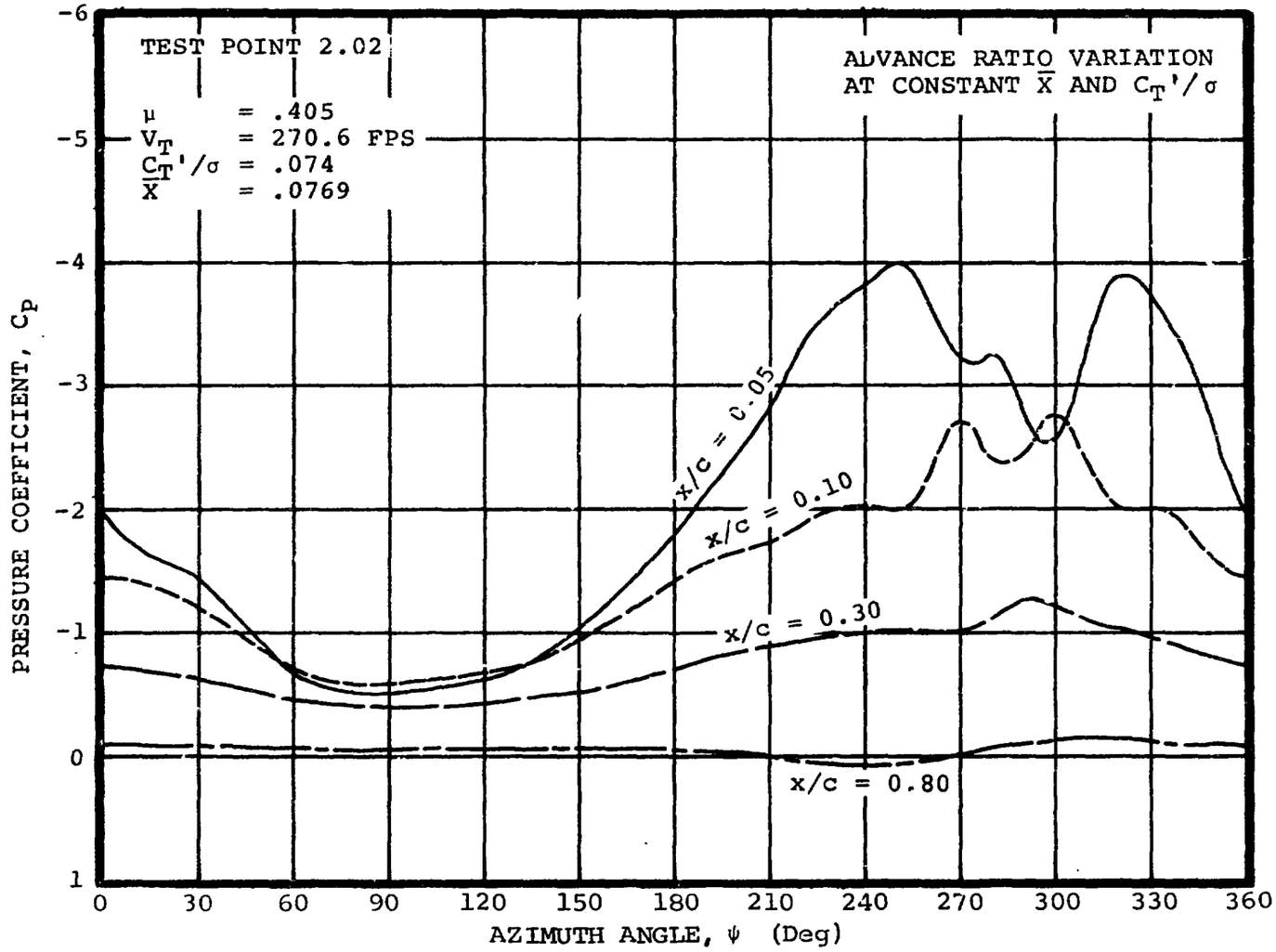

Figure 16 TIME HISTORIES OF UPPER SURFACE PRESSURES MEASURED AT r/R = 0.75

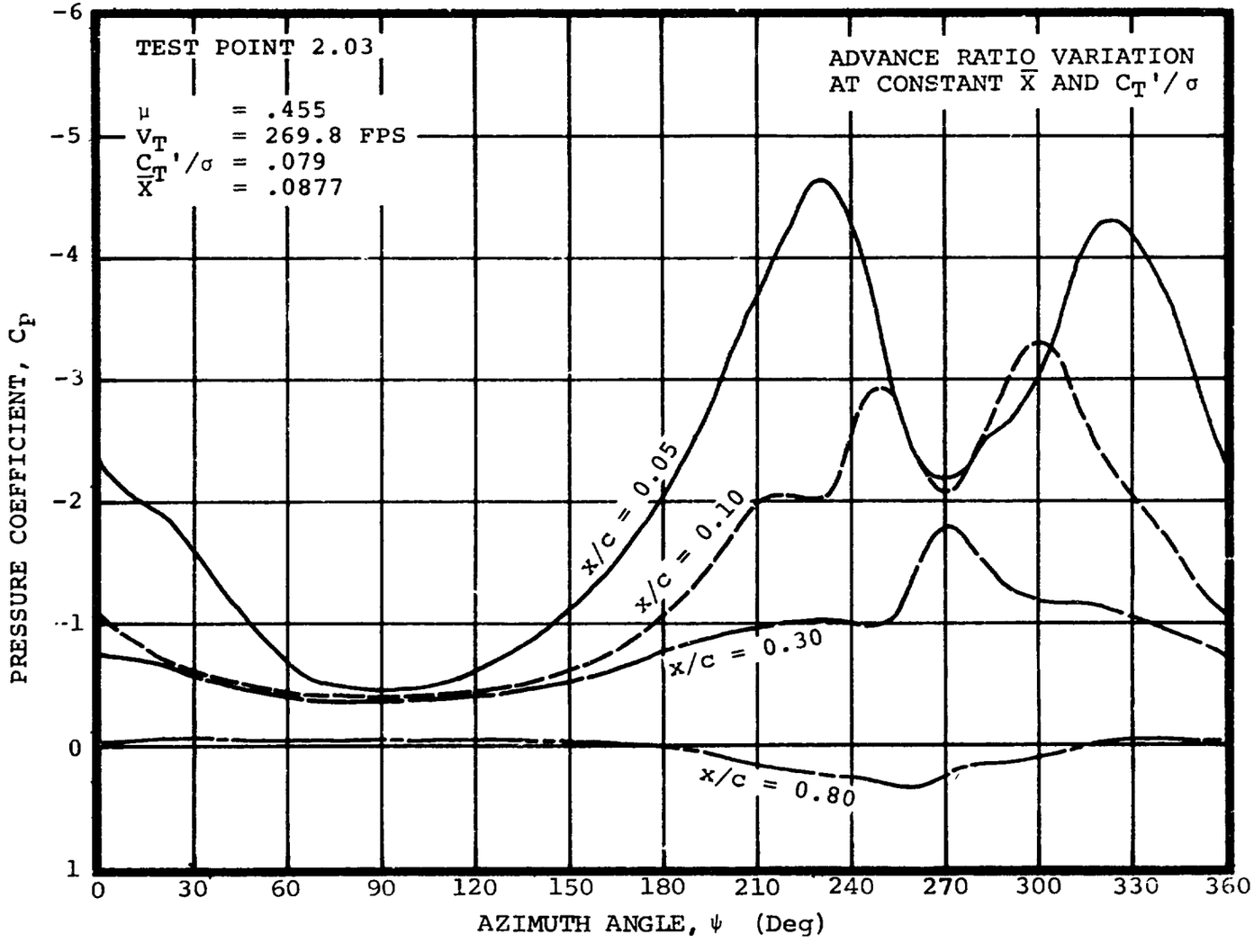

Figure 17 TIME HISTORIES OF UPPER SURFACE PRESSURES MEASURED AT r/R = 0.75

TEST POINT	μ	V_T (FPS)	α_{SHAFT} (DEG)	α_{TPP} (DEG)	$\theta_{.75}$ (DEG)	C_T/σ	$X/qD^2\sigma$
2.01	.304	270.1	-10.0°	-3.7°	8.5°	.074	.08906

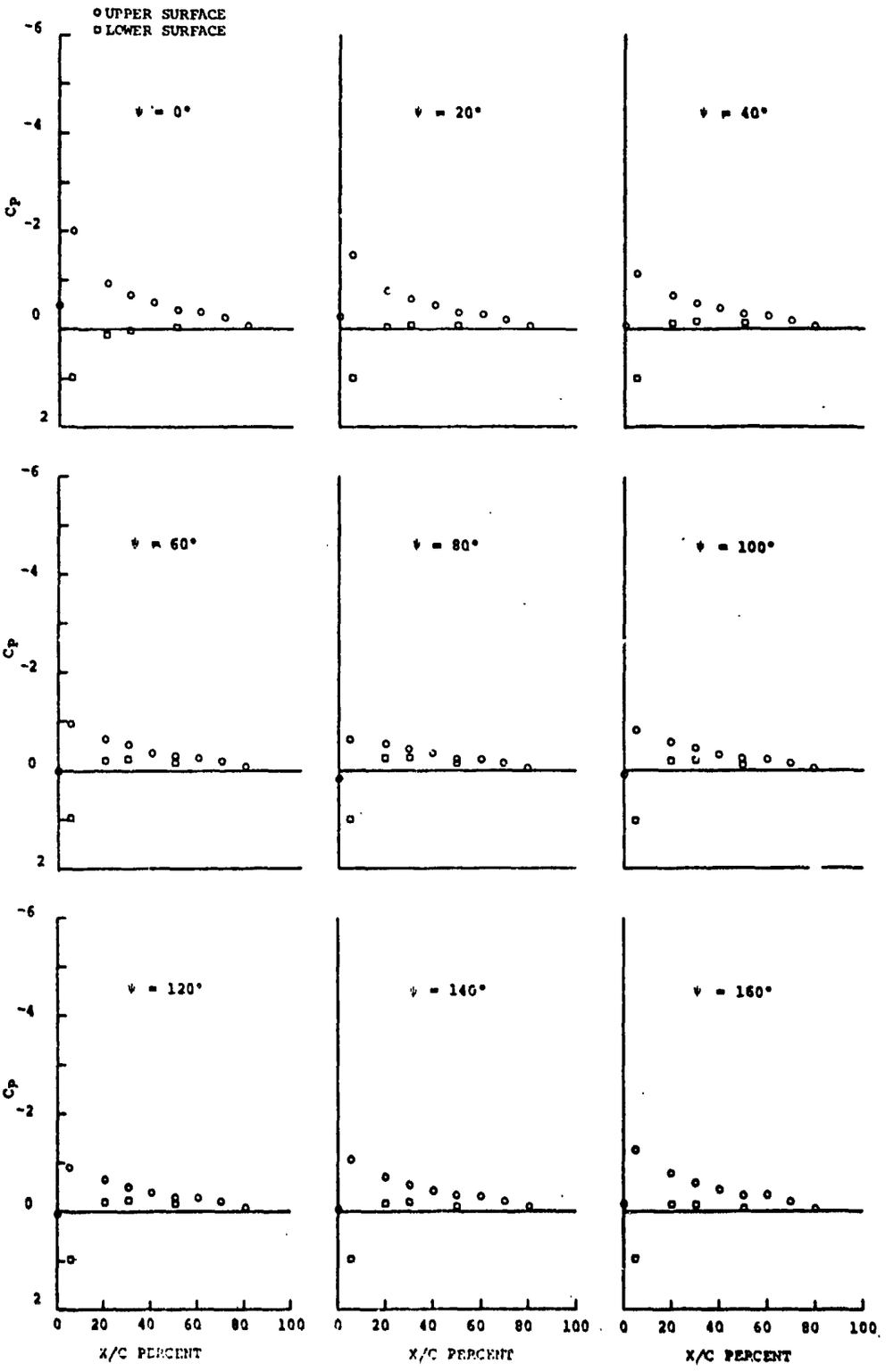

Figure 18 PRESSURE DISTRIBUTIONS MEASURED AT r/R = 0.75

TEST POINT	μ	V_T (FPS)	α_{SHAFT} (DEG)	θ_{TPP} (DEG)	$\theta_{.75}$ (DEG)	C_T/σ	$X/qD^2\sigma$
2.01	.304	270.1	-10.0°	-3.7°	8.5°	.074	.08906

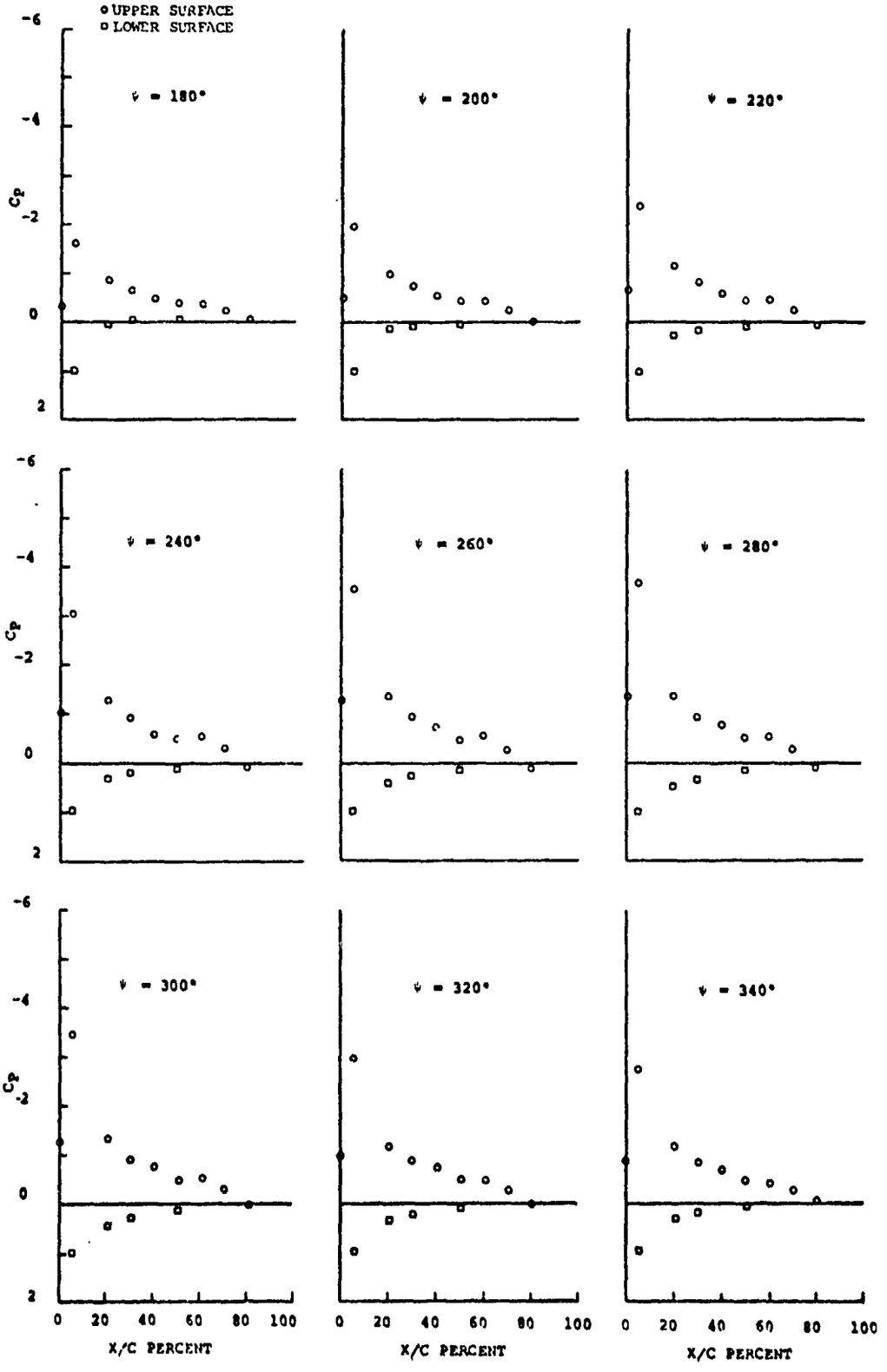

Figure 18 (Continued) PRESSURE DISTRIBUTIONS MEASURED AT r/R = 0.75

TEST POINT	μ	V_T (FPS)	α_{SHAFT} (DEG)	α_{TPP} (DEG)	$\theta_{.75}$ (DEG)	C_T'/σ	$X/qD^2\sigma$
2.03	.455	269.8	-20.5°	-8.4°	13.103°	.079	.08773

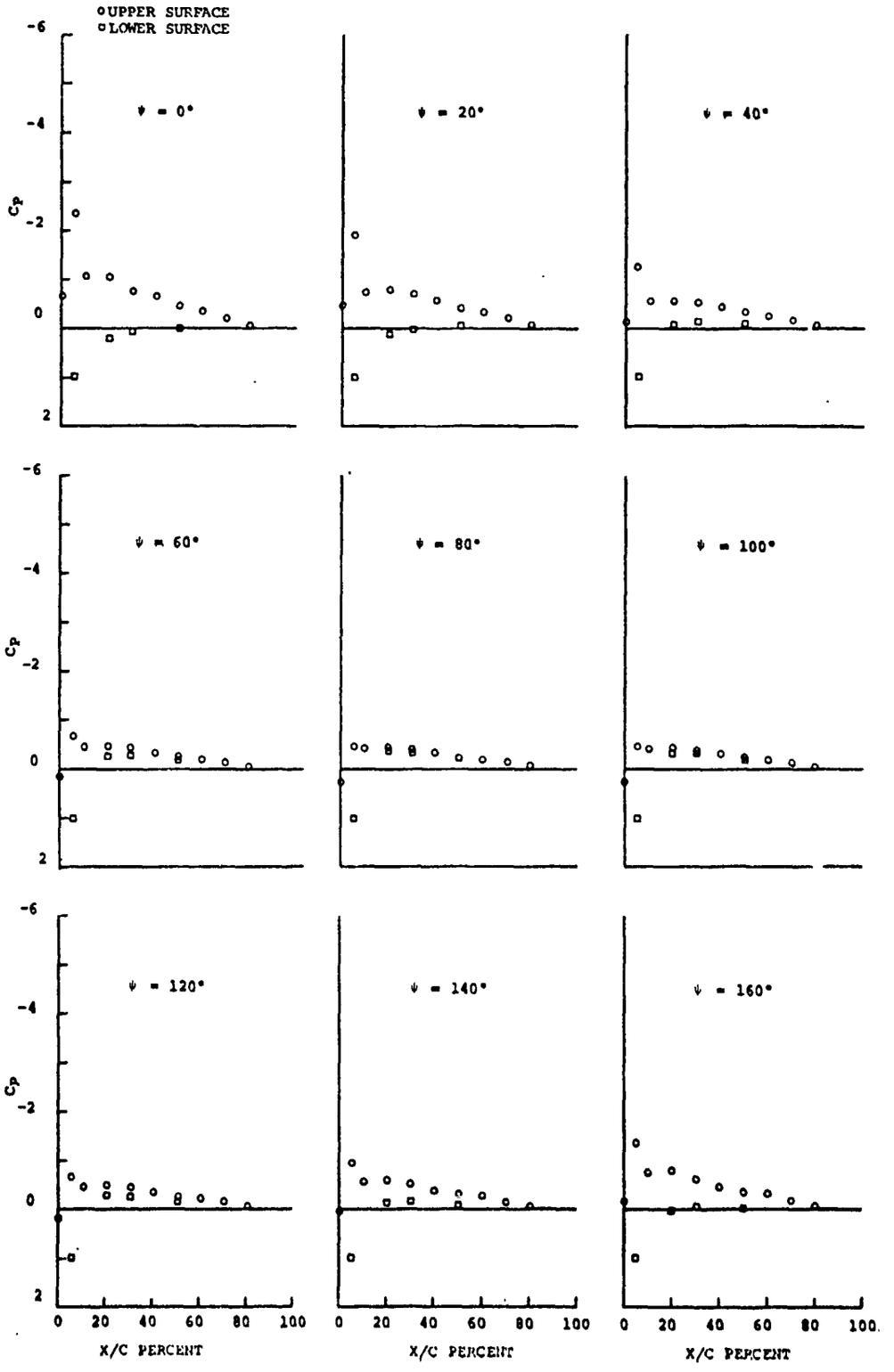

Figure 19 PRESSURE DISTRIBUTIONS MEASURED AT r/R = 0.75

TEST POINT	μ	V_T (FPS)	α_{SHAFT} (DEG)	α_{TPP} (DEG)	$\theta_{.75}$ (DEG)	C_T'/σ	$X/qD^2\sigma$
2.03	.455	269.8	-20.5°	-8.4°	13.103°	.079	.08773

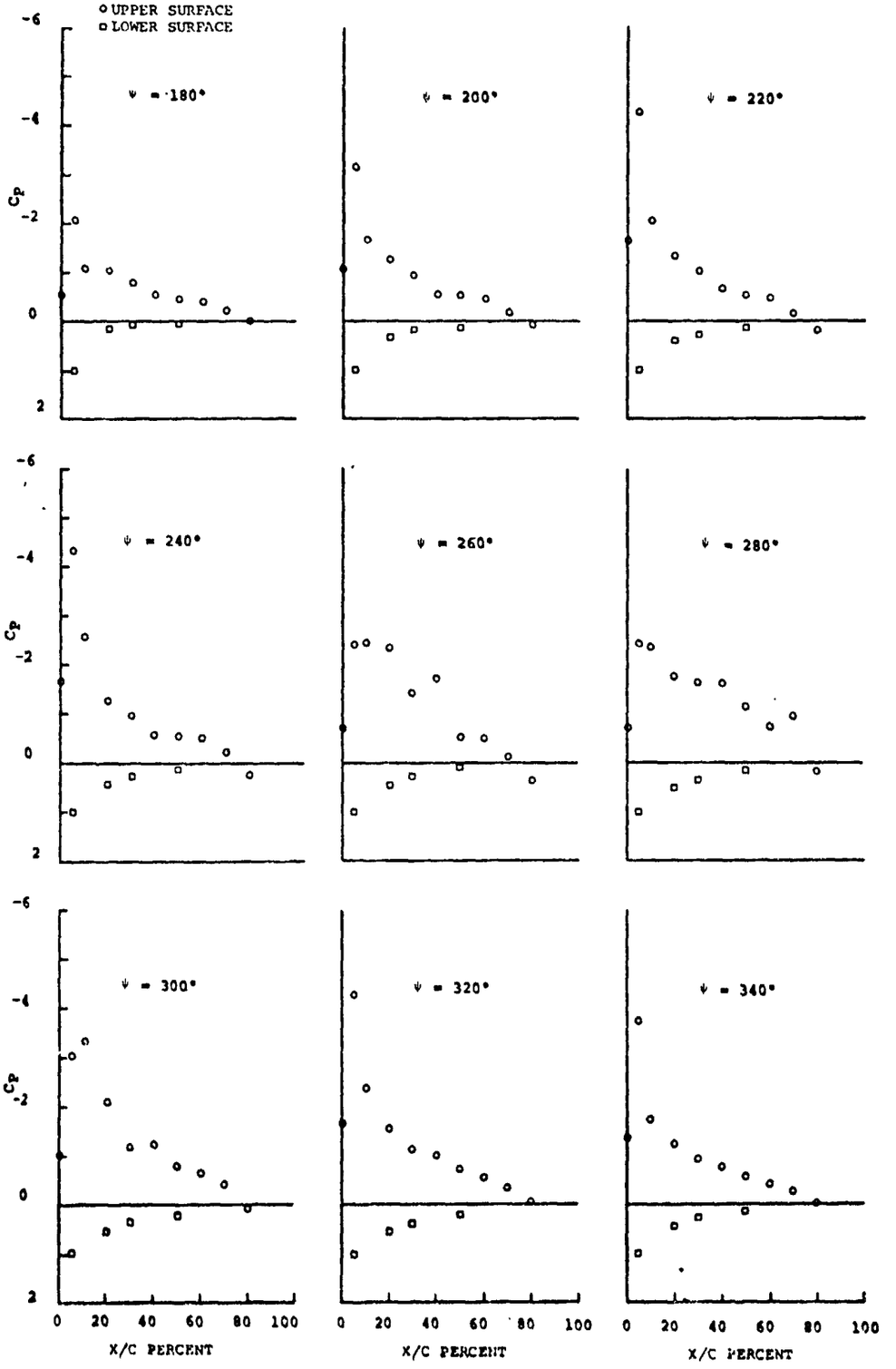

Figure 19 (Continued) PRESSURE DISTRIBUTIONS MEASURED AT r/R = 0.75

3.2.2 Advance Ratio Variation in Presence of Stall (Test Points 2.05 and 2.06)

The pressure data for Test Points 2.05 and 2.06 do not show evidence of the significant secondary pressure peaks observed at the lower thrust levels, but at the higher thrust levels of these test points rotor operation was limited to $\mu = 0.40$, with acceptable data at $\mu = 0.3$ and $\mu = 0.35$ only. At these lower advance ratios, the retreating blade stall has already been described in Reference (1) in conjunction with tests for shaft angle variation at constant collective angle.

Figure 20 shows time histories of normal force and pitching moment coefficients. In both test conditions, pitching moment stall occurs ahead of lift stall, but the maximum lift and maximum nose-down pitching moment levels are reached almost simultaneously.

In the fourth quadrant there is a second peak in the normal force coefficient, but this peak is reached without any flow reattachment and, therefore, without any significant recovery from pitching moment stall. Pitching moments remain very large for the duration of the second C_n peak.

Figures 22 and 23 show pressure time histories at $\mu = 0.3$ and $\mu = 0.35$ respectively. In both cases, there is one major collapse in leading edge pressures followed by some pressure fluctuations, but reattachment does not occur until the blade is back into the first quadrant. The peak in leading edge pressure coefficients takes place approximately 30° in azimuth ahead of the C_n peak, and it coincides with the largest nose-up values of the pitching moment coefficient just ahead of pitching moment stall.

Figures 23 and 24 show pressure distributions at selected azimuth locations. The pressure distributions confirm qualitatively that separation takes place at $\Psi > 240°$ and that full reattachment does not take place until the blade has returned to the first quadrant, $\Psi > 0°$.

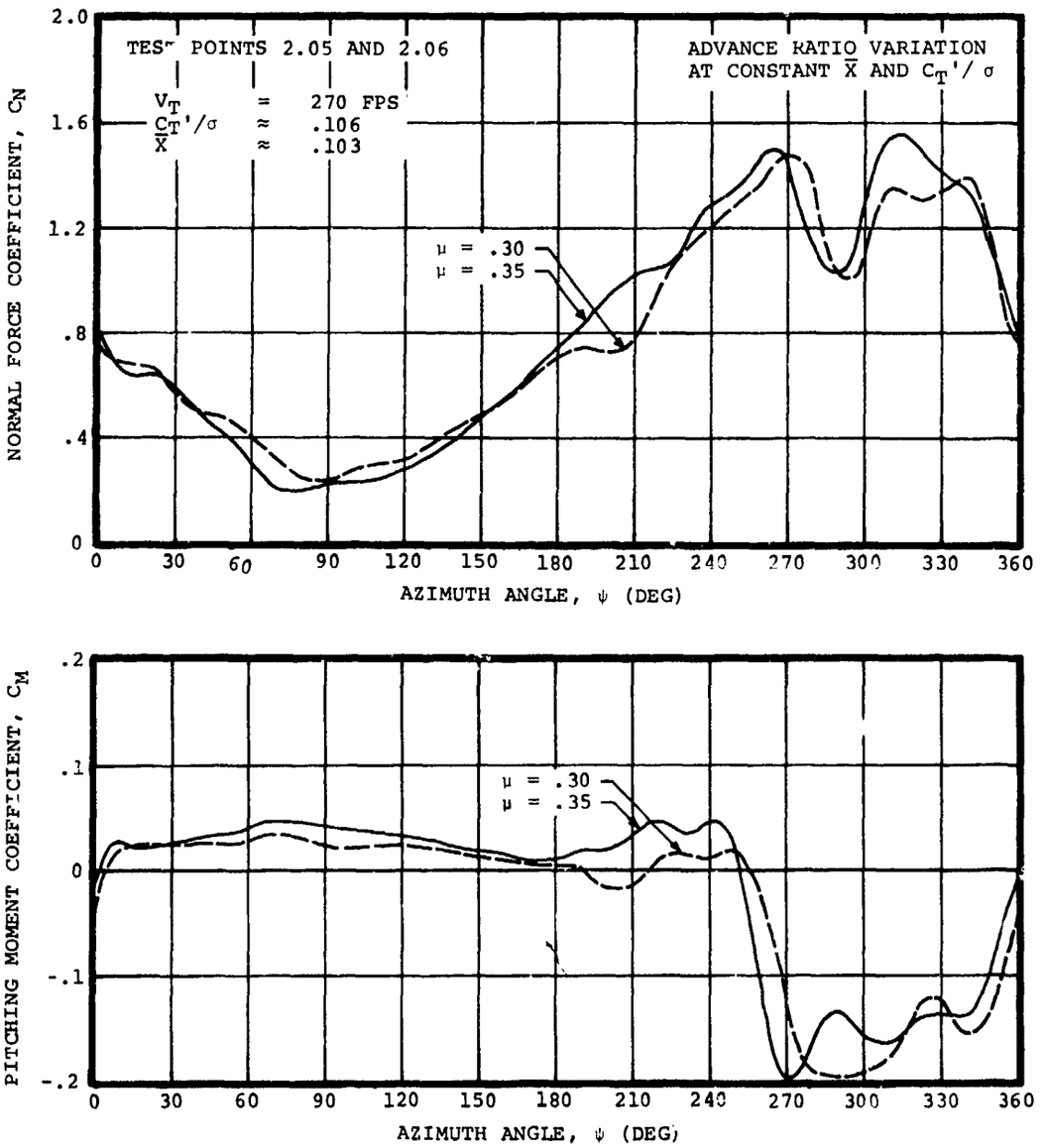

Figure 20 NORMAL FORCE AND PITCHING MOMENT COEFFICIENTS OBTAINED FROM INTEGRATED PRESSURES AT r/R = 0.75

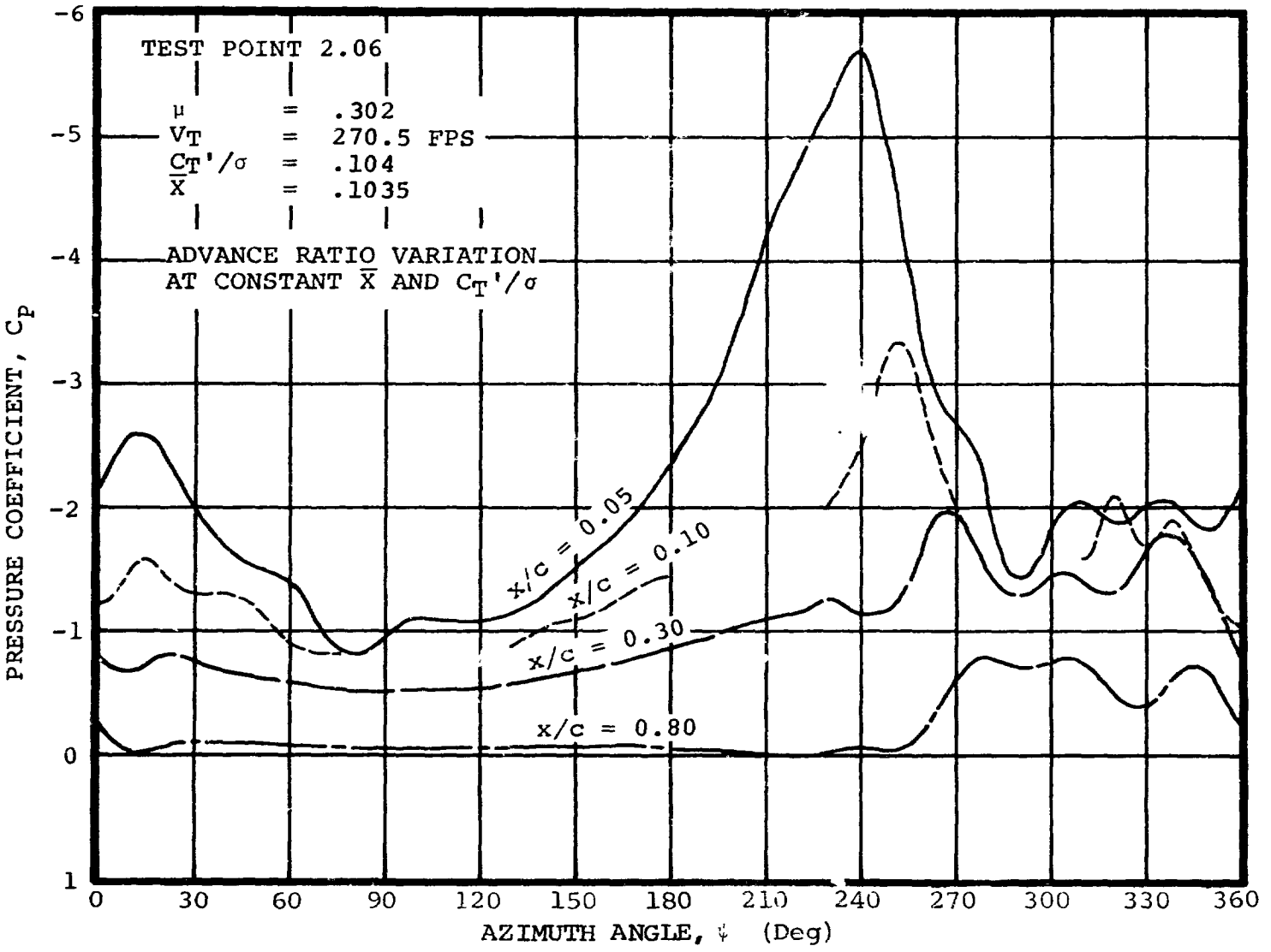

Figure 21 TIME HISTORIES OF UPPER SURFACE PRESSURES MEASURED AT r/R = 0.75

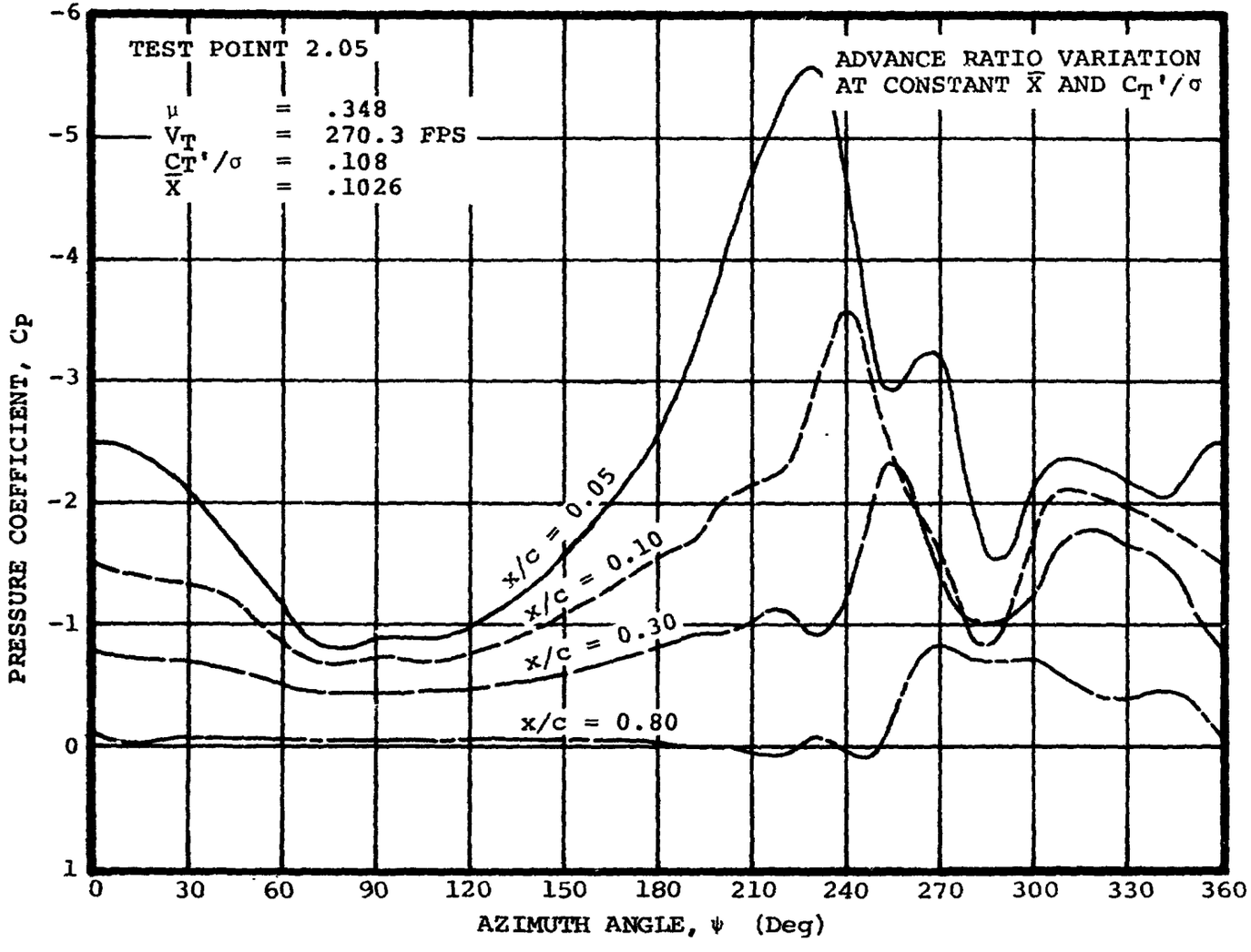

Figure 22 TIME HISTORIES OF UPPER SURFACE PRESSURES MEASURED AT r/R = 0.75

TEST POINT	μ	V_T (FPS)	α_{SHAFT} (DEG)	α_{TPP} (DEG)	$\theta_{.75}$ (DEG)	C_T'/σ	$X/qD^2\sigma$
2.06	.302	270.5	-9.5°	-0.7°	9.722°	.104	.10347

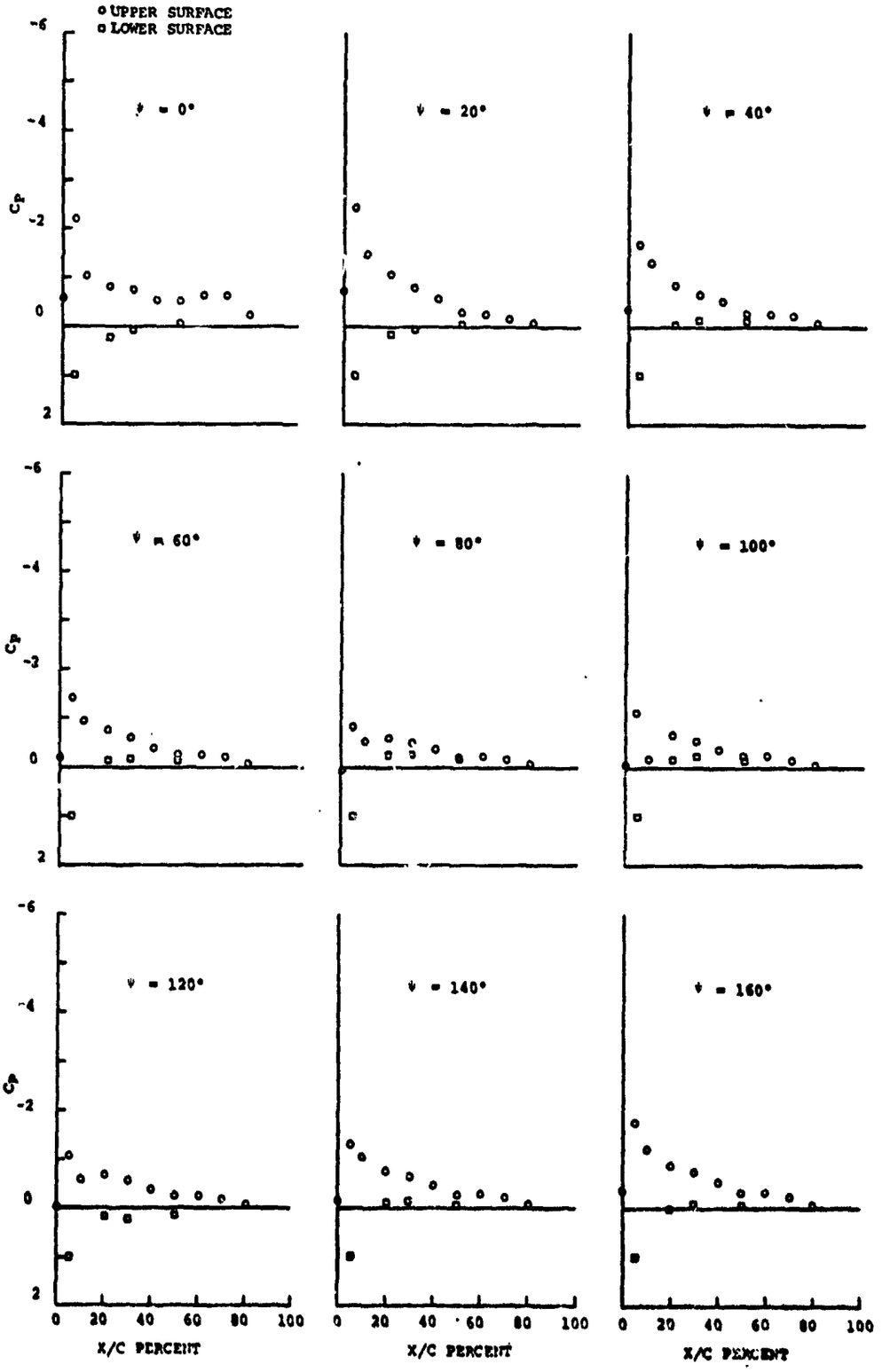

Figure 23 PRESSURE DISTRIBUTIONS MEASURED AT r/R = 0.75

TEST POINT	μ	V_T (FPS)	α_{SHAFT} (DEG)	α_{TPP} (DEG)	$\theta_{.75}$ (DEG)	C_T'/σ	$X/qD^2\sigma$
2.06	.302	270.5	-9.5°	-0.7°	9.722°	.104	.10347

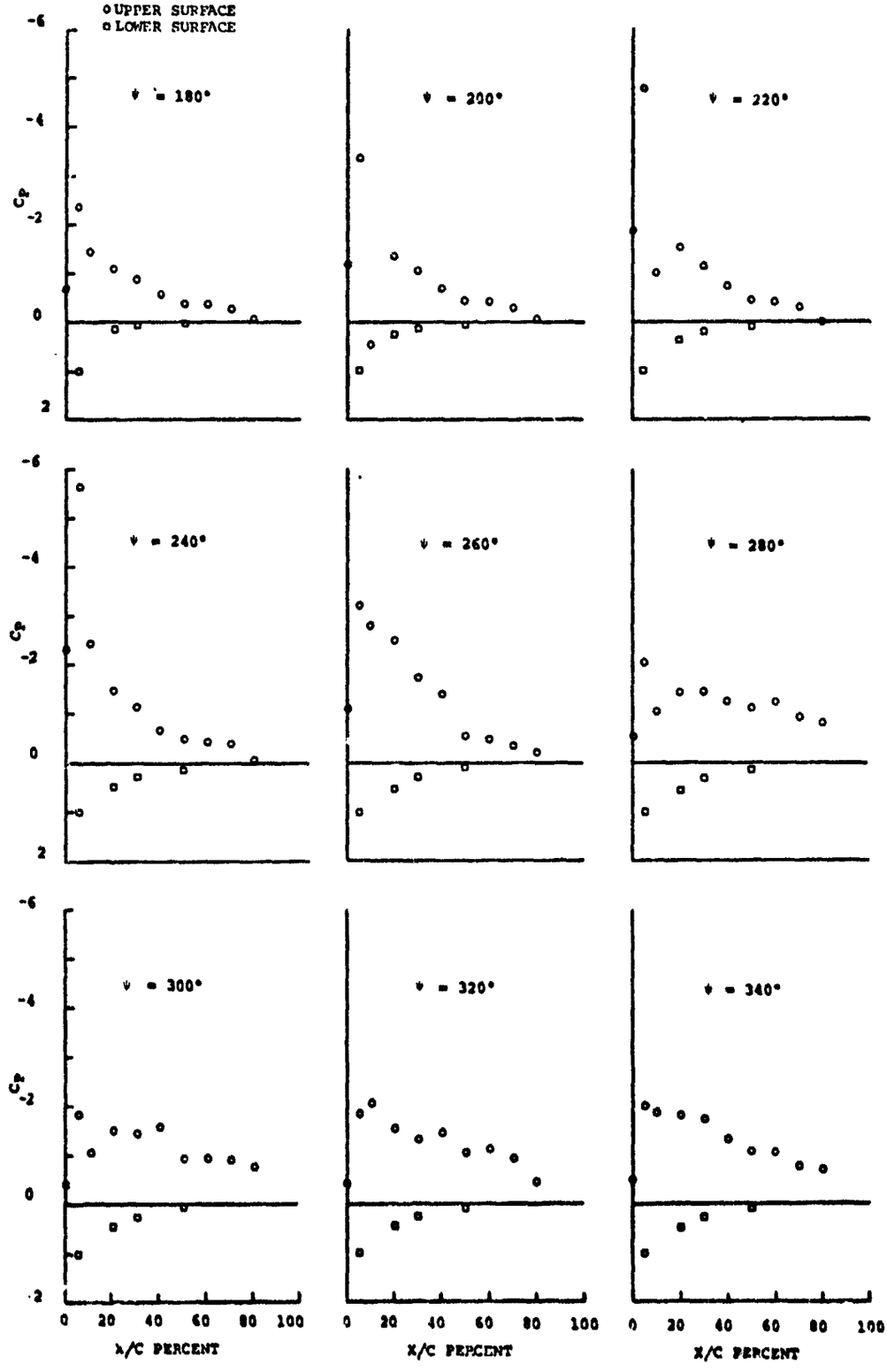

Figure 23 (Continued) PRESSURE DISTRIBUTIONS MEASURED AT r/R = 0.75

TEST POINT	μ	V_T (FPS)	α_{SHAFT} (DEG)	α_{TPP} (DEG)	$\theta_{.75}$ (DEG)	C_T/σ	$A/qD^2\sigma$
2.05	.348	270.3	-12.[illegible]°	-1.3°	12.33°	.108	.10259

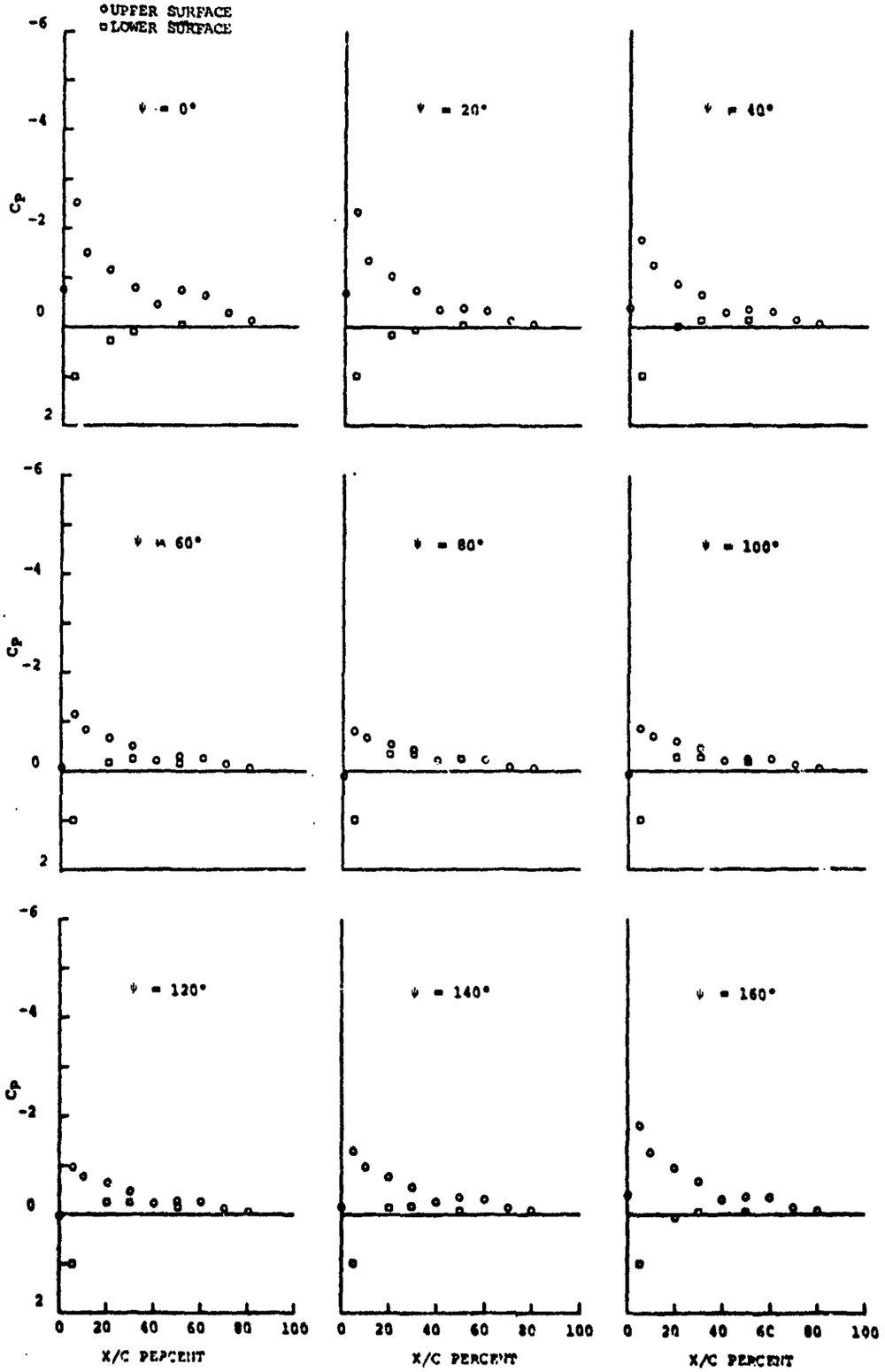

Figure 24 PRESSURE DISTRIBUTIONS MEASURED AT r/R = 0.75

TEST POINT	μ	V_T (FPS)	α_{SHAFT} (DEG)	α_{TPP} (DEG)	$\theta_{.75}$ (DEG)	C_T/σ	$X/qD^2\sigma$
2.05	.348	270.3	-12.0	-1.3°	12.33°	.108	.10259

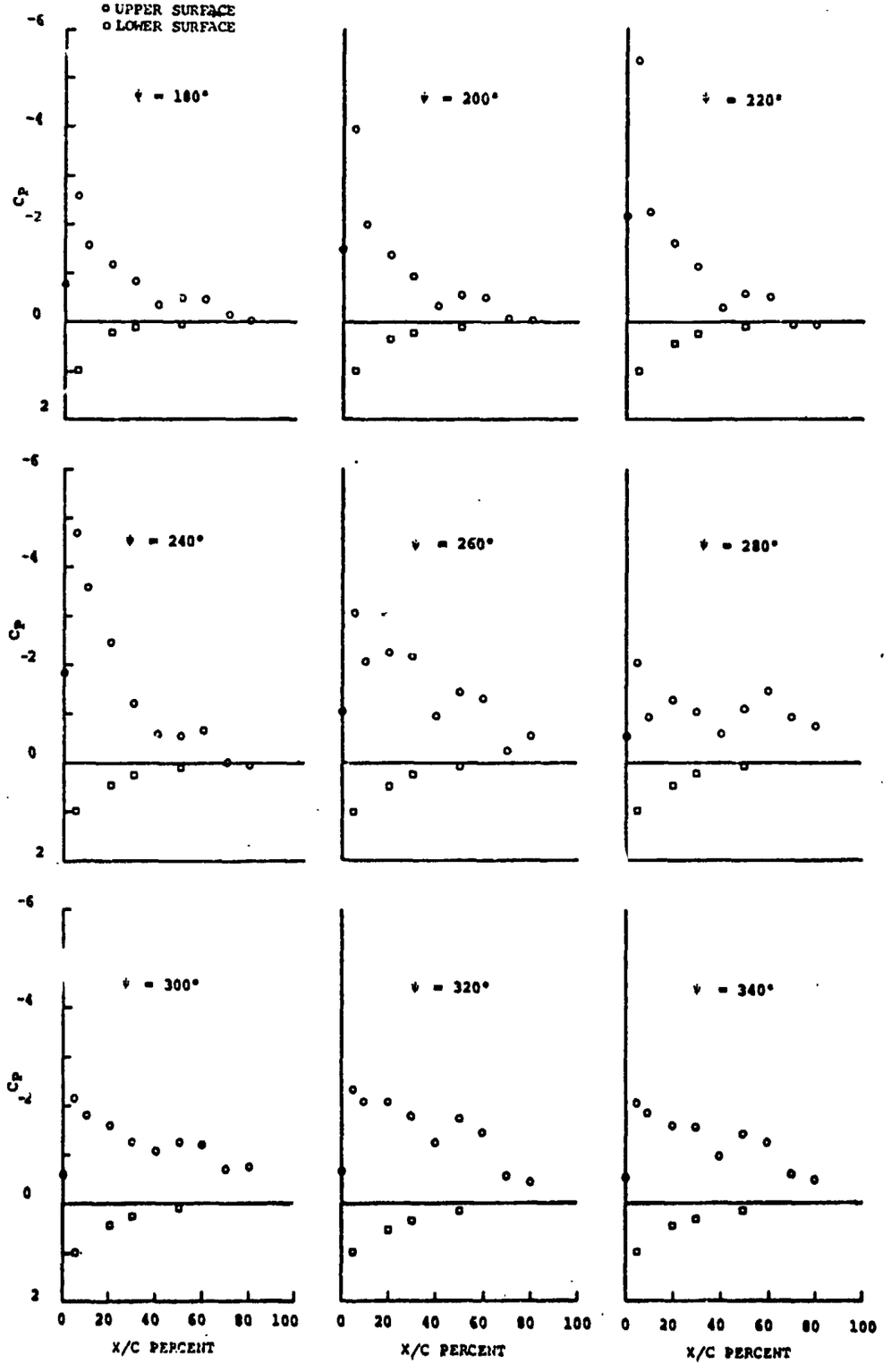

Figure 24 (Continued) PRESSURE DISTRIBUTIONS MEASURED AT r/R = 0.75

3.3 Additional Data for Comparison Between Teetering and Articulated Rotors

3.3.1 Shaft Angle Sweep at Constant Collective, $\theta_{.75} = 12.8°$ (Test Points 3.01 to 3.05)

Test Points 3.01 to 3.05 were acquired to provide an additional comparison with the articulated rotor data from Reference 4. Teetering and articulated rotors have been previously compared in Reference 1. The new data were obtained at a tip speed of 270 fps because of rotor limitations.

The data from the present test are in excellent agreement with the articulated rotor data, while the data in Reference 1 showed substantial differences. This is illustrated in Figure 25.

As shown in Figure 25, the boundary for the collapse in leading edge pressures for the teetering rotor, operating at V_T = 270 fps, is very close to the boundary for the articulated rotor operating at V_T = 500 fps. Except for an additional time delay, the same is true for the Cn_{max} and Cm_{max} boundaries associated with the first peak. This time delay could be due to the difference in airfoils (V23010-1.58 on the articulated rotor and NACA 0012 on the teetering rotor) or to dynamic stall changes associated with the reduction in tip speed.

Figure 26 summarizes the integrated normal force and pitching moment coefficients. Figures 27 through 31 show time histories of selected upper surface pressures.

As shown in Figure 26, second peaks in both normal force and pitching moment occur between ψ = 310° and ψ = 330° with complete reattachment taking place at $\psi \cong 10°$. Although the time of occurrence of the second set of peaks is correct, the magnitude of such peaks is subject to question because of transducer malfunction.

Figure 51 in the Appendix shows the summary of results from a flow visualization study conducted with tufts mounted on the rotor blade at conditions comparable to those of Test Points 3.05 and 3.09. The results of the flow visualization test are in qualitative agreement with the pressure data shown in Figure 31 as regards the collapse in leading edge pressures at $\psi > 210°$.

Figure 52, also in the Appendix, shows a flow visualization photograph at $\psi \approx 270°$ for conditions close to Test Point 3.05. The only difference is a tip speed reduction from 270 fps to 110 fps.

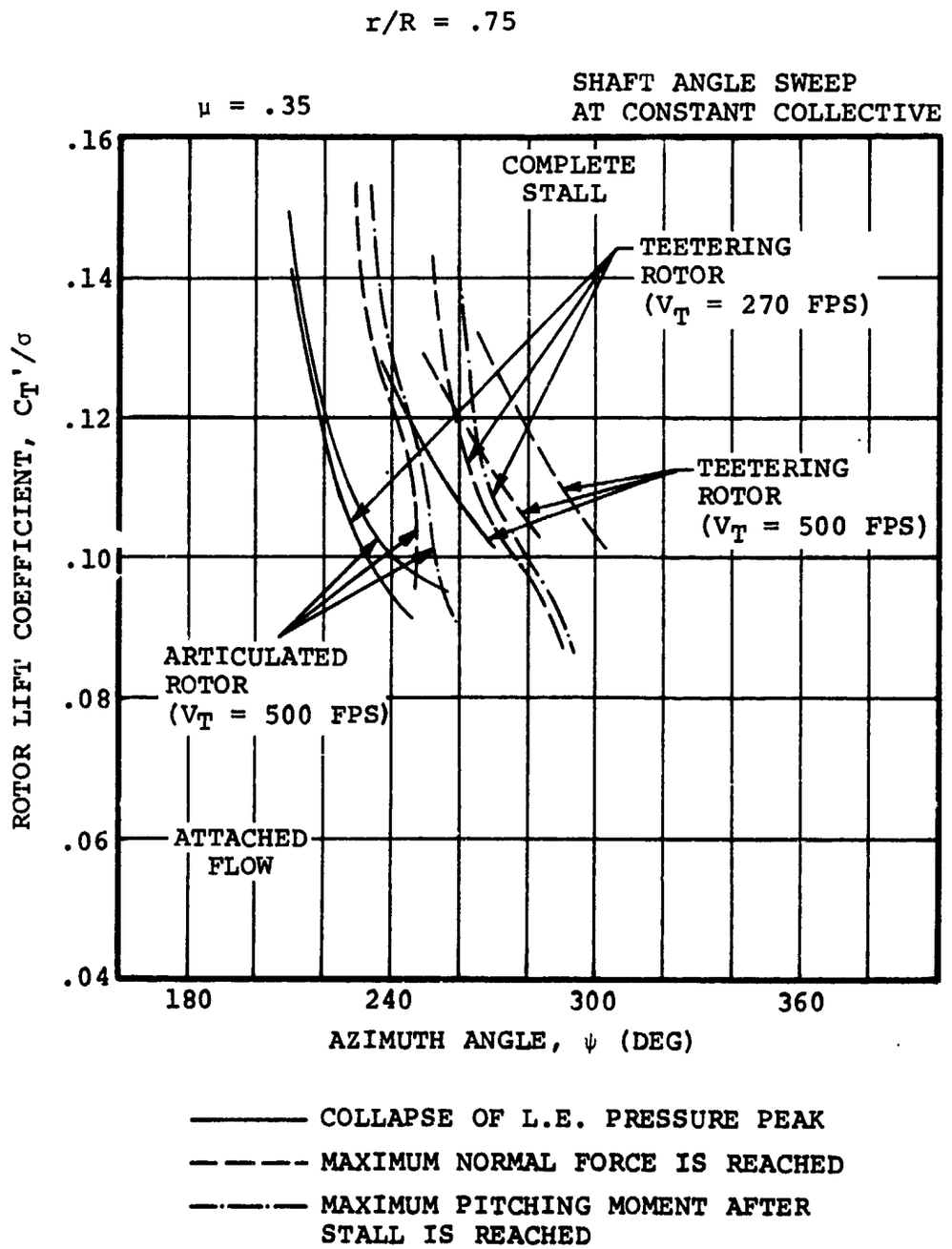

FIGURE 25. COMPARISON OF STALL BOUNDARIES OF TEETERING AND ARTICULATED ROTORS

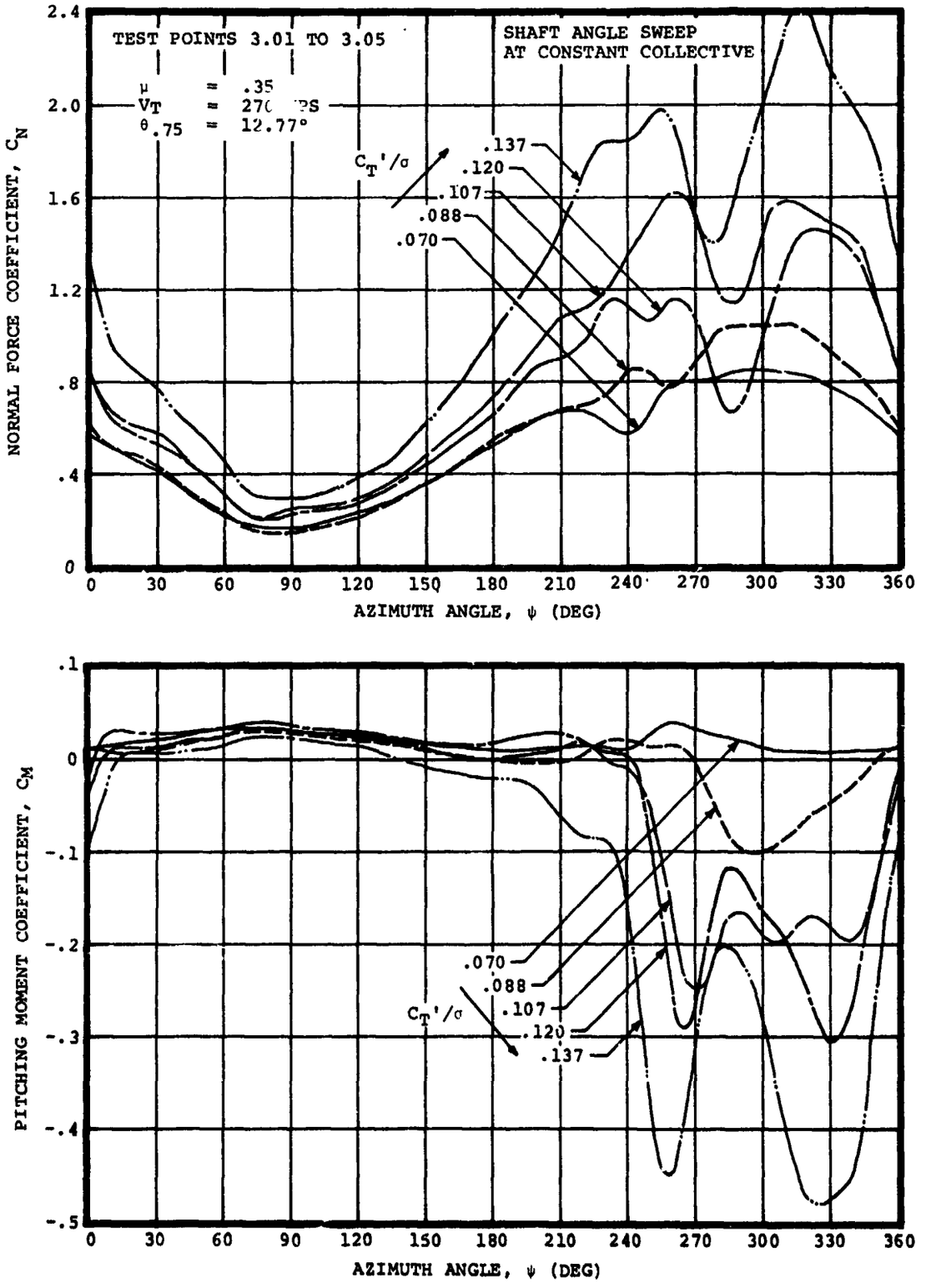

Figure 26 NORMAL FORCE AND PITCHING MOMENT COEFFICIENTS OBTAINED FROM INTEGRATED PRESSURES AT r/R = 0.75

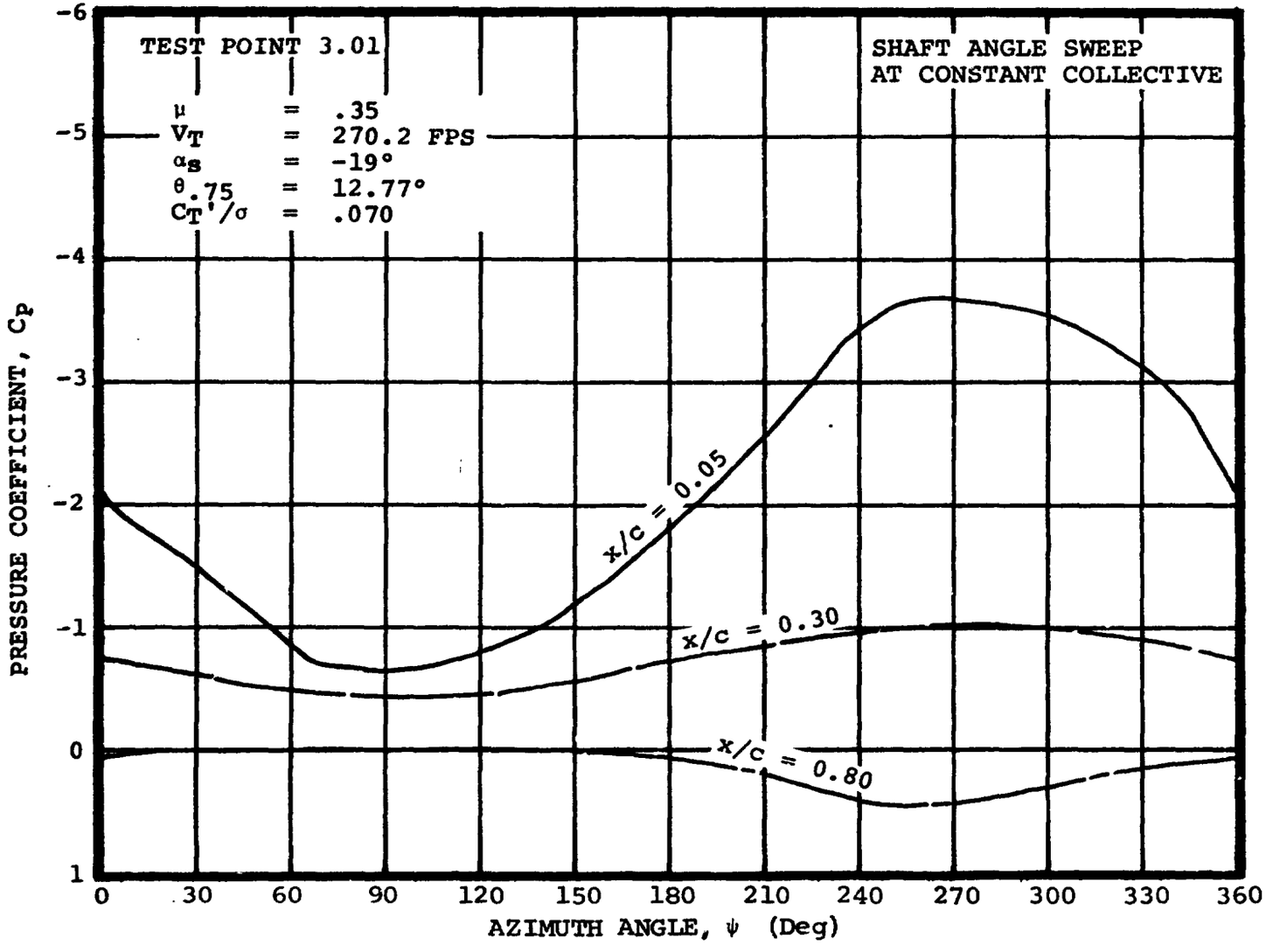

Figure 27 TIME HISTORIES OF UPPER SURFACE PRESSURES MEASURED AT r/R = 0.75

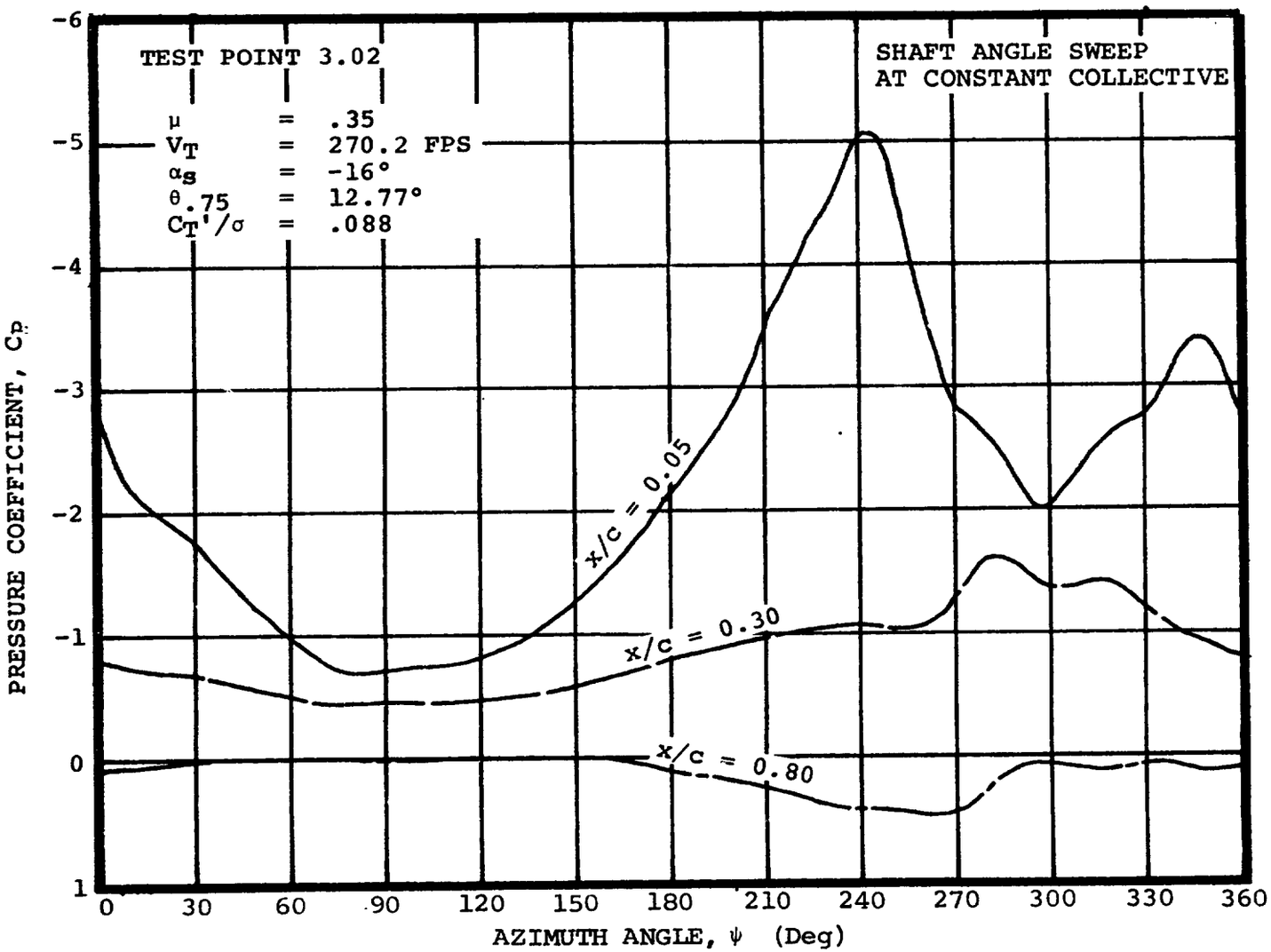

Figure 28 TIME HISTORIES OF UPPER SURFACE PRESSURES MEASURED AT r/R = 0.75

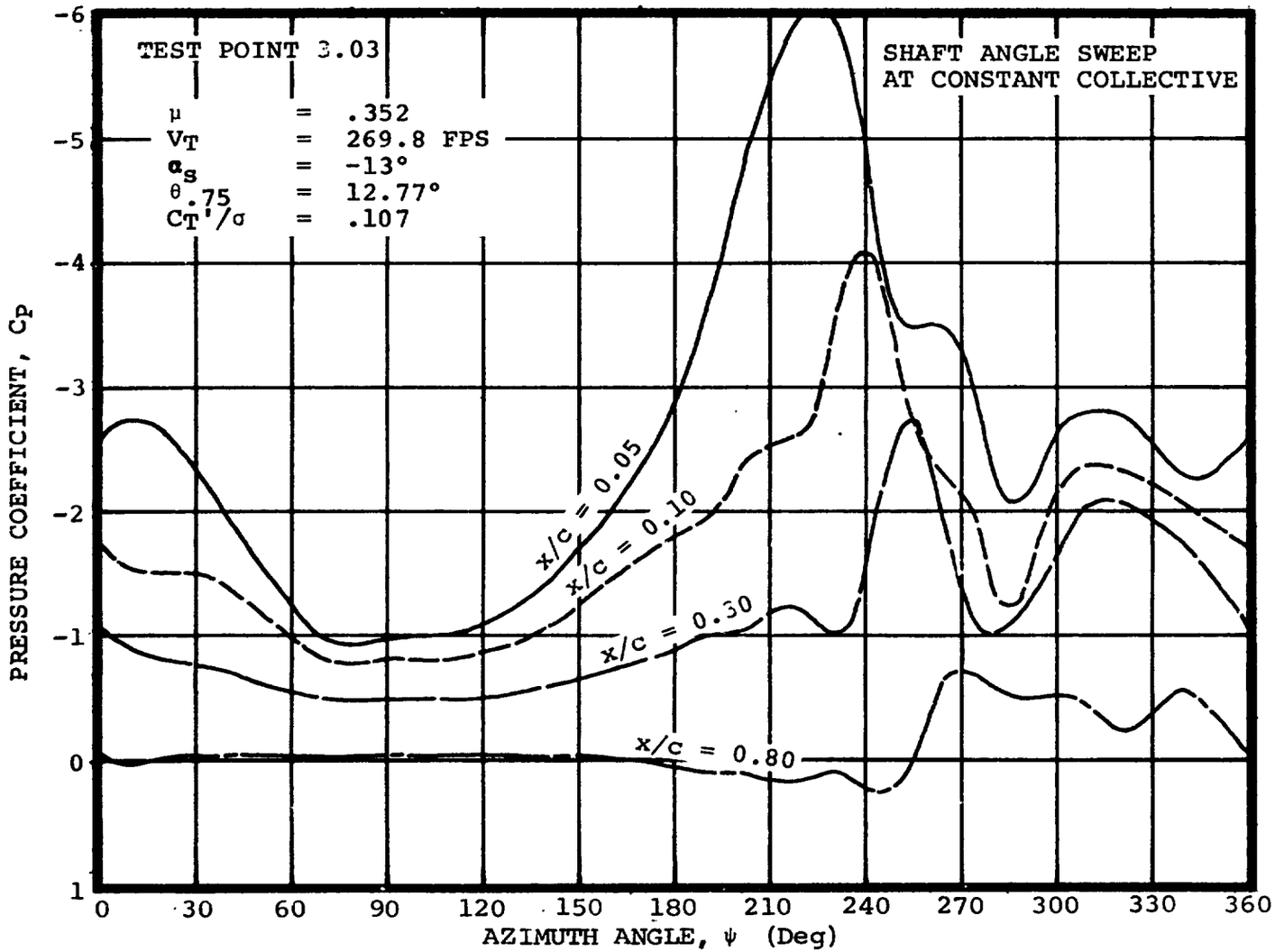

Figure 29 TIME HISTORIES OF UPPER SURFACE PRESSURES MEASURED AT r/R = 0.75

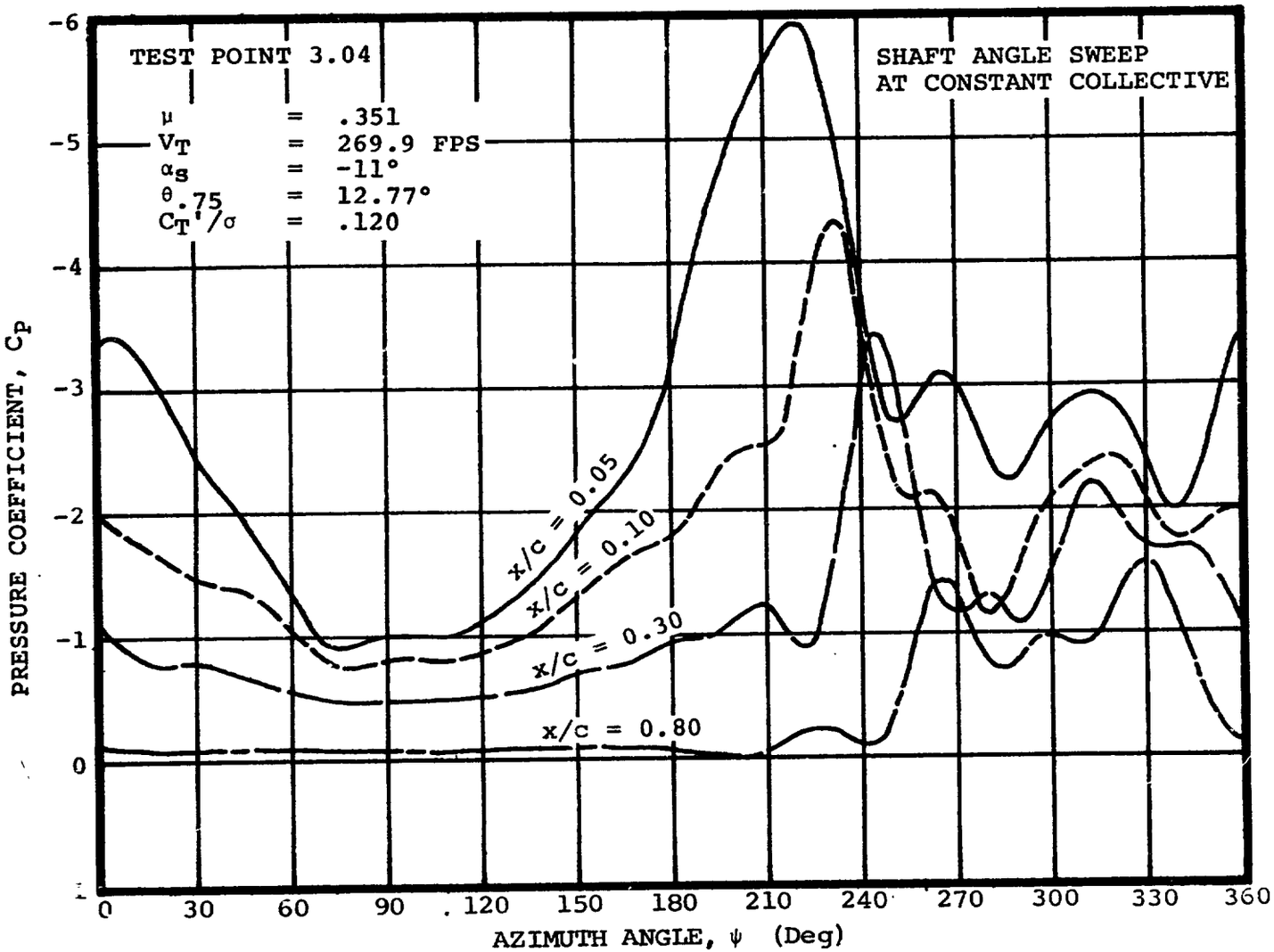

Figure 30 TIME HISTORIES OF UPPER SURFACE PRESSURES MEASURED AT r/R = 0.75

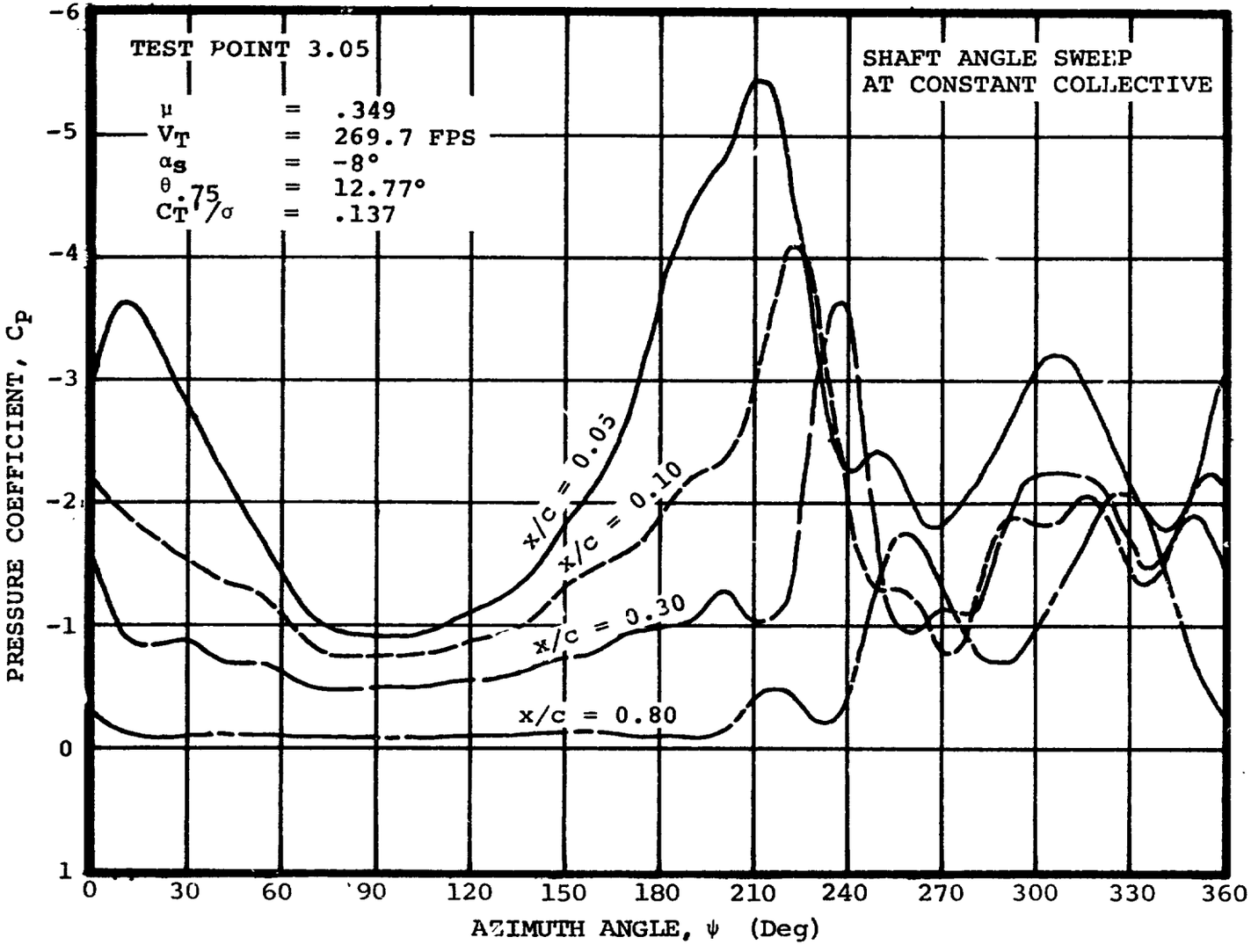

Figure 31 TIME HISTORIES OF UPPER SURFACE PRESSURES MEASURED AT r/R = 0.75

3.3.2 Shaft Angle Sweep at Reduced Collective, $\theta_{.75} = 8.83°$ (Test Points 3.06 and 3.07)

Figure 32 shows time histories of integrated normal force and pitching moment coefficients. Figures 33 and 34 show pressure time histories.

Both runs show some degree of stall, where the extent of stall is reduced by increasing the shaft angle and thus tilting the tip path plane into the wind.

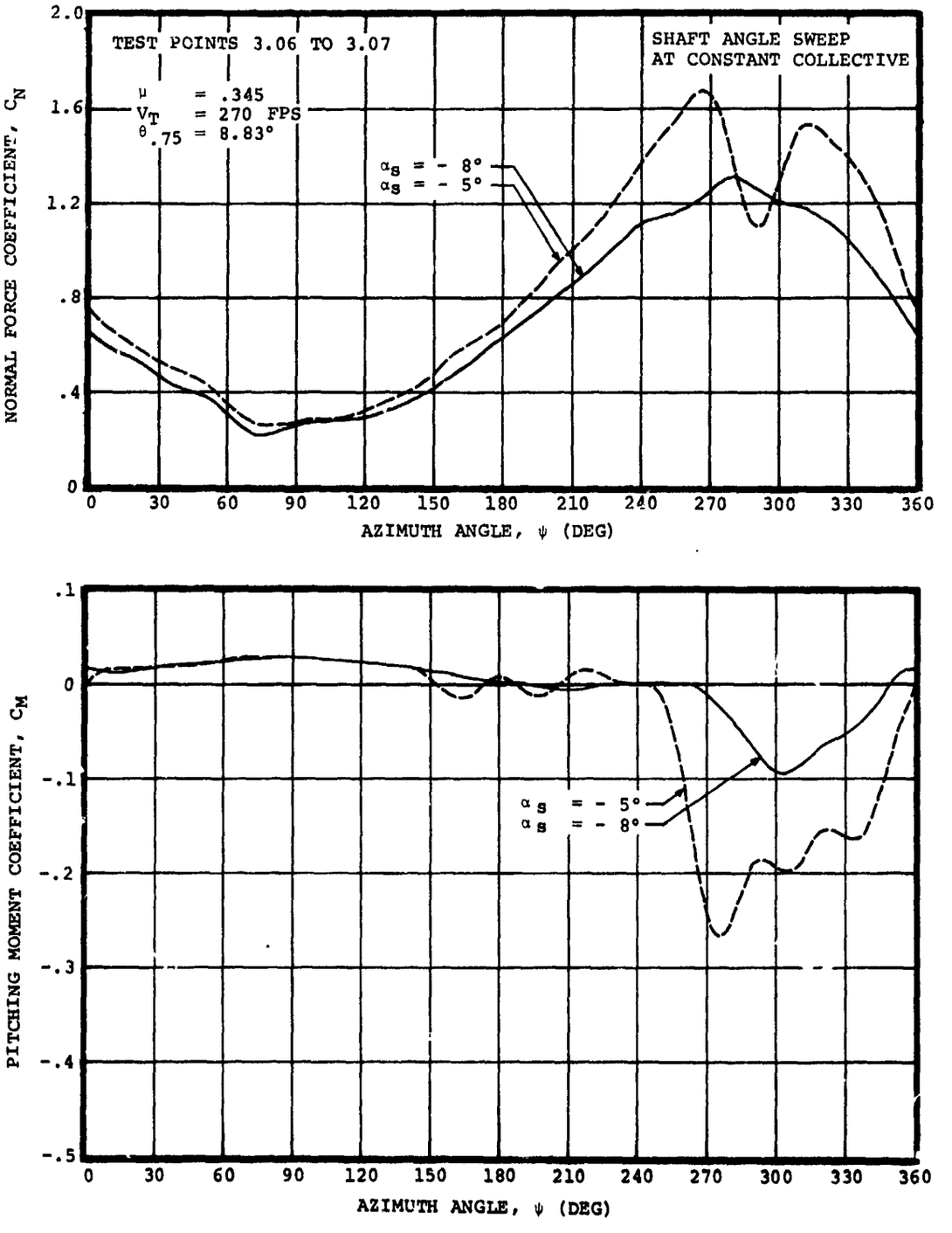

Figure 32 NORMAL FORCE AND PITCHING MOMENT COEFFICIENTS OBTAINED FROM INTEGRATED PRESSURES AT r/R = 0.75

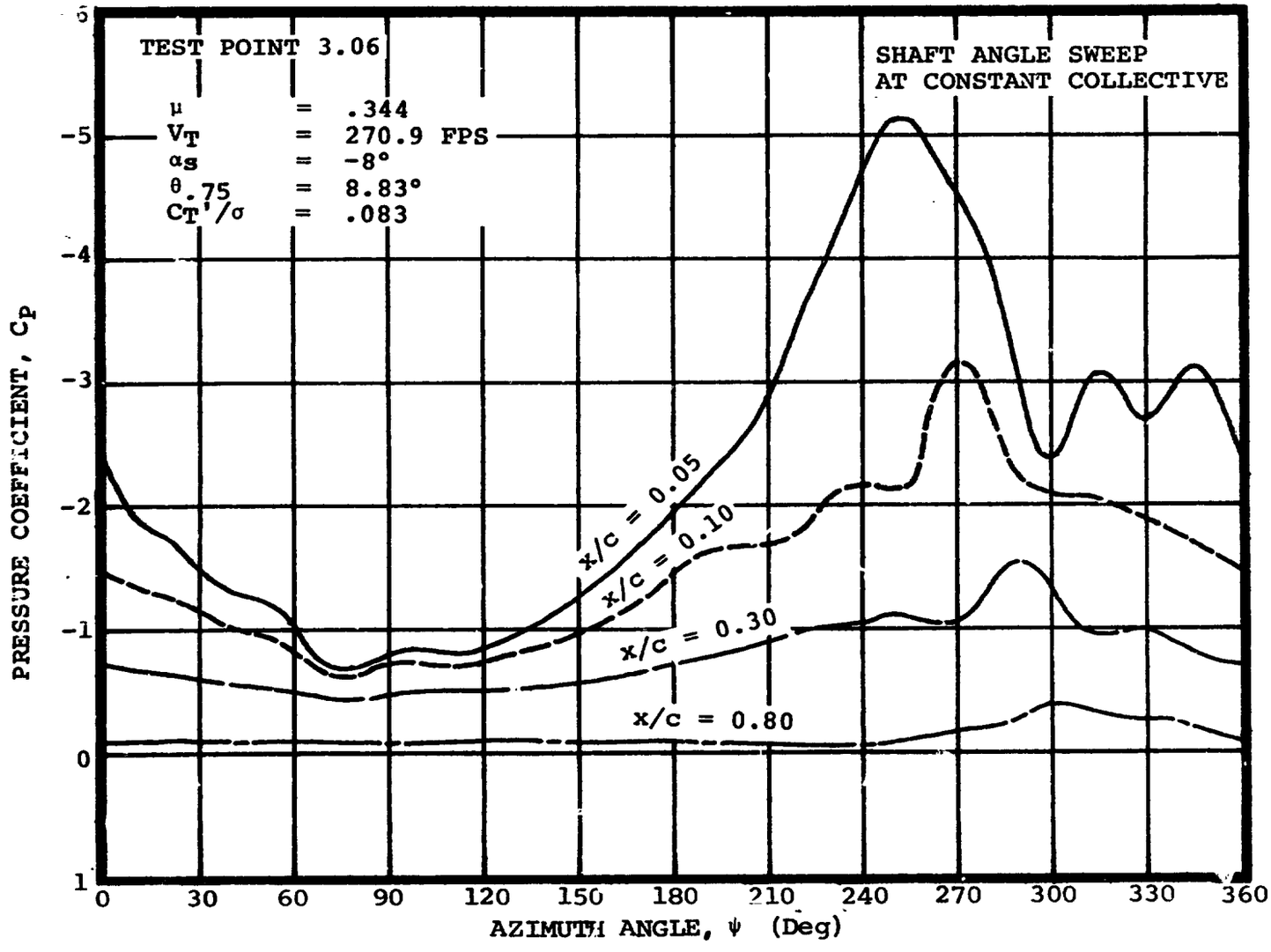

Figure 33 TIME HISTORIES OF UPPER SURFACE PRESSURES MEASURED AT r/R = 0.75

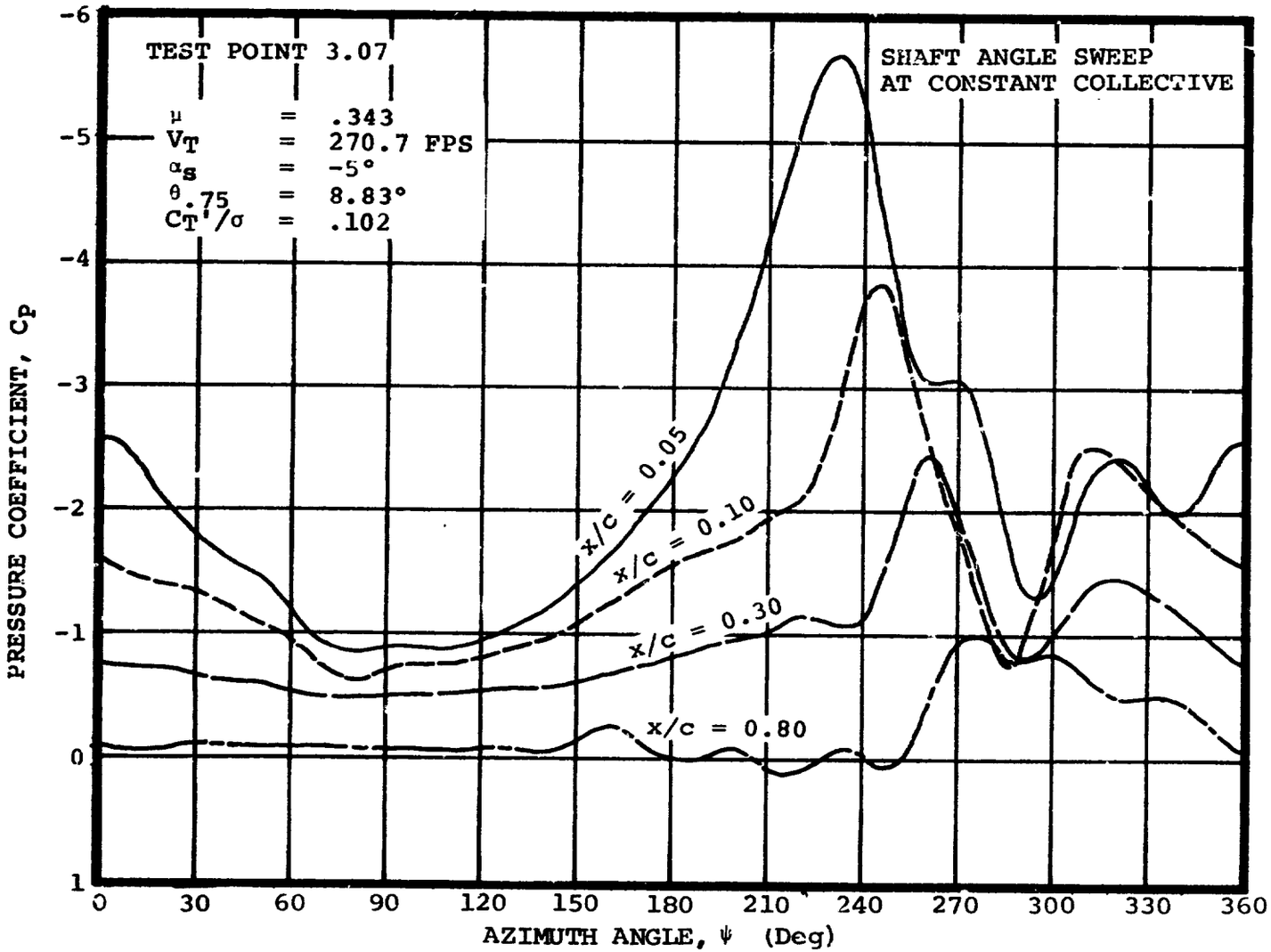

Figure 34 TIME HISTORIES OF UPPER SURFACE PRESSURES MEASURED AT r/R = 0.75

3.4 Additional Test Conditions (Test Points 3.09 and 3.10)

Test Points 3.09 and 3.10 repeat the conditions of Test Points 3.05 and 2.02 respectively. Pressure time history plots are shown in Figures 35 and 36. Pressure distributions for Test Point 3.10 are shown in Figure 37. No integrated loads are presented.

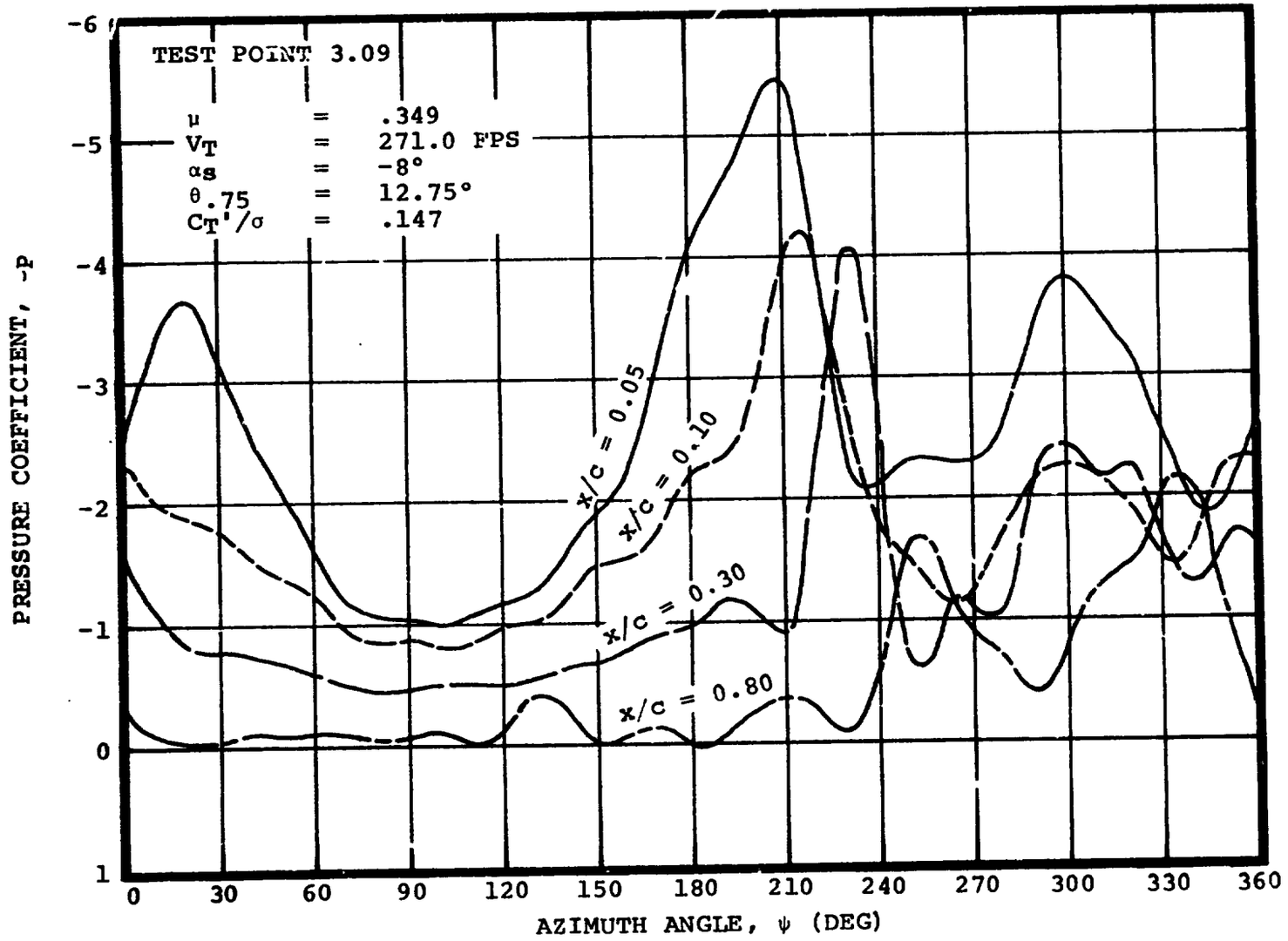

Figure 35 TIME HISTORIES OF UPPER SURFACE PRESSURES MEASURED AT r/R = 0.75

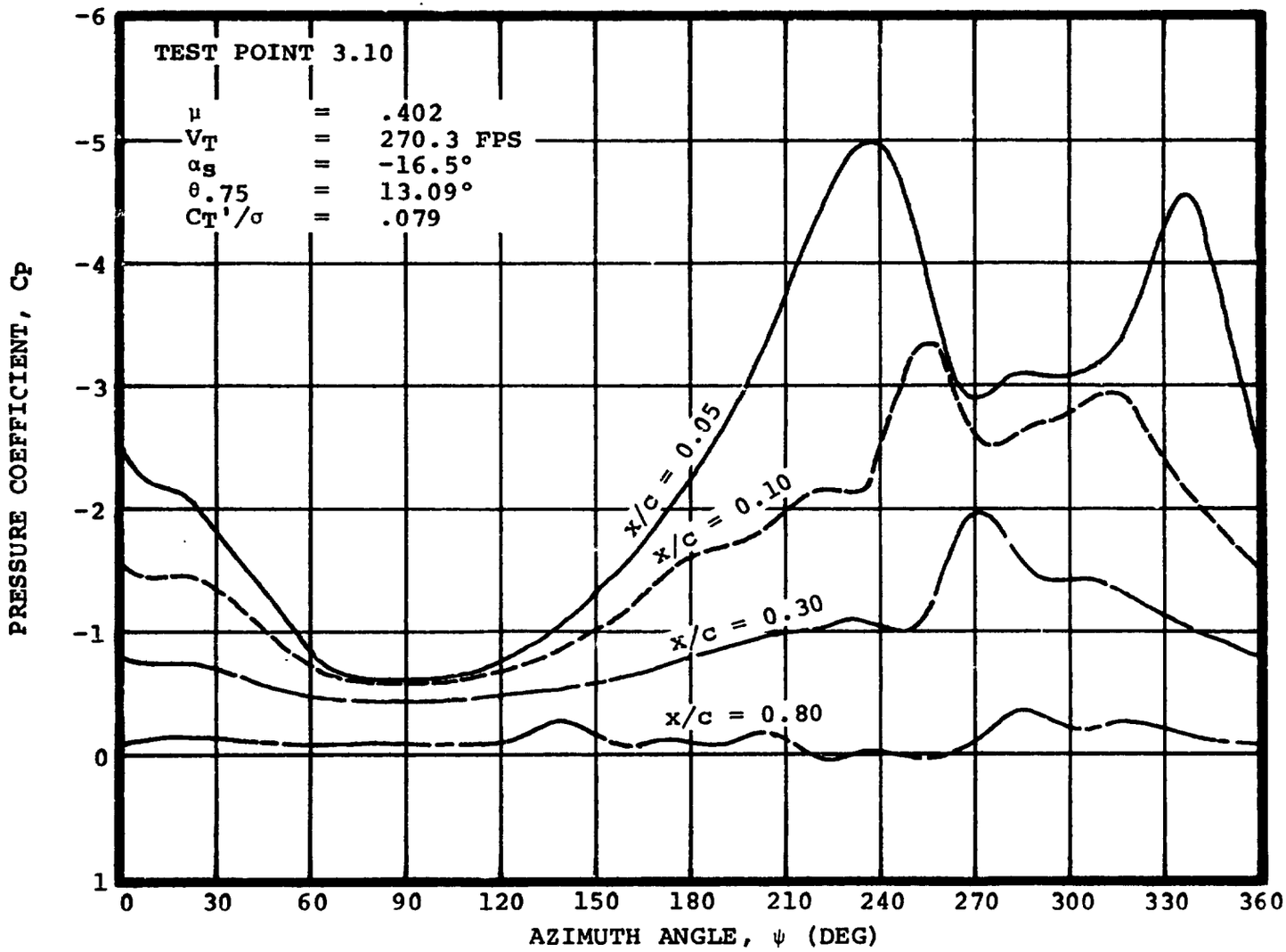

Figure 36 TIME HISTORIES OF UPPER SURFACE PRESSURES MEASURED AT r/R = 0.75

TEST POINT	μ	V_T (FPS)	α_{SHAFT} (DEG)	θ_{TPP} (DEG)	$\theta_{.75}$ (DEG)	C_T/σ	$X/qD^2\sigma$
3.10	.402	270.3	-16.5°	-5.6°	13.09°	.079	.08987

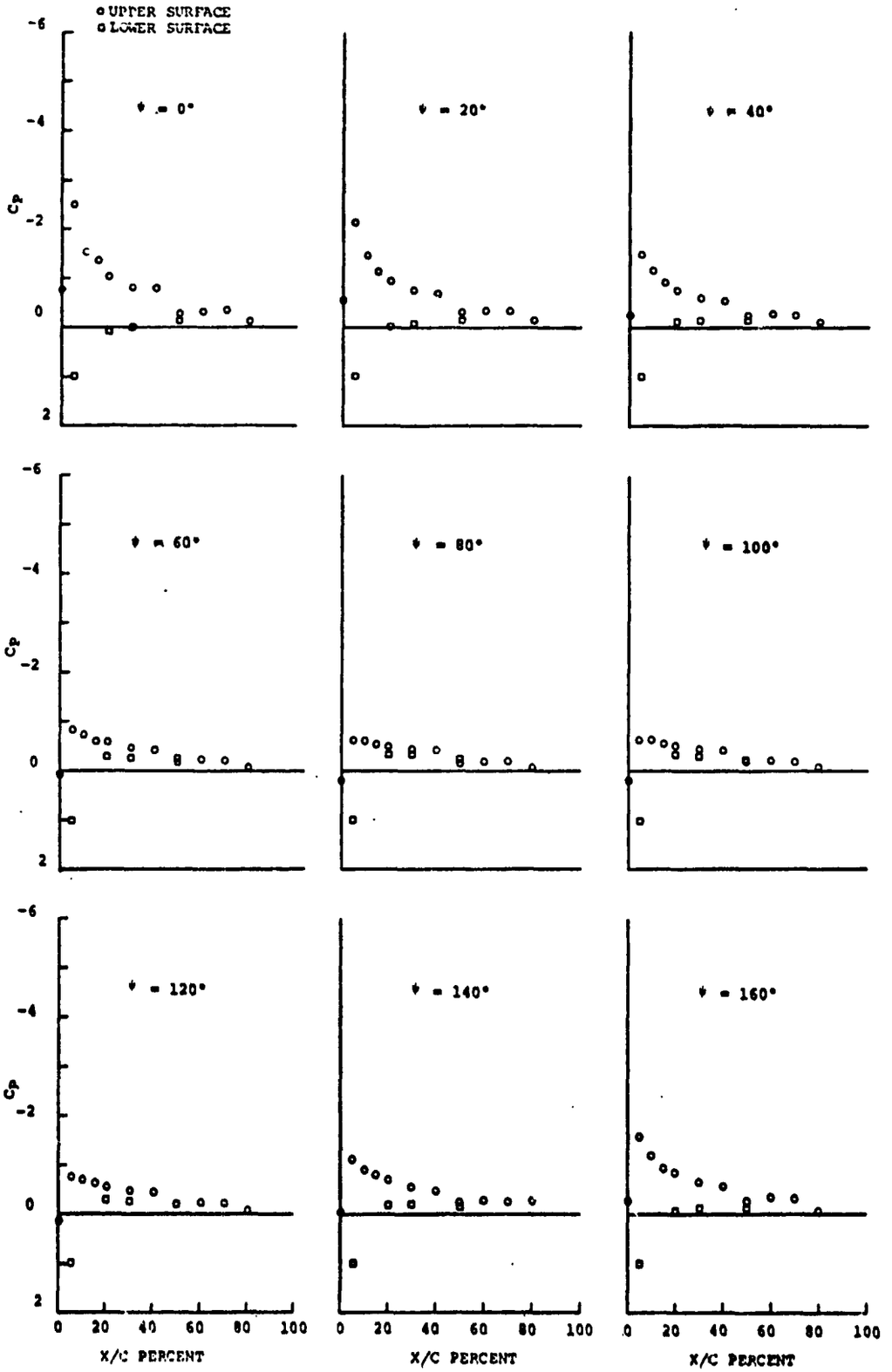

Figure 37 PRESSURE DISTRIBUTIONS MEASURED AT r/R = 0.75

TEST POINT	μ	V_T (FPS)	α_{SHAFT} (DEG)	α_{TPP} (DEG)	$\theta_{.75}$ (DEG)	C_T'/σ	$X/qD^2\sigma$
3.10	.402	270.3	-16.5°	-5.6°	13.09°	.079	.08987

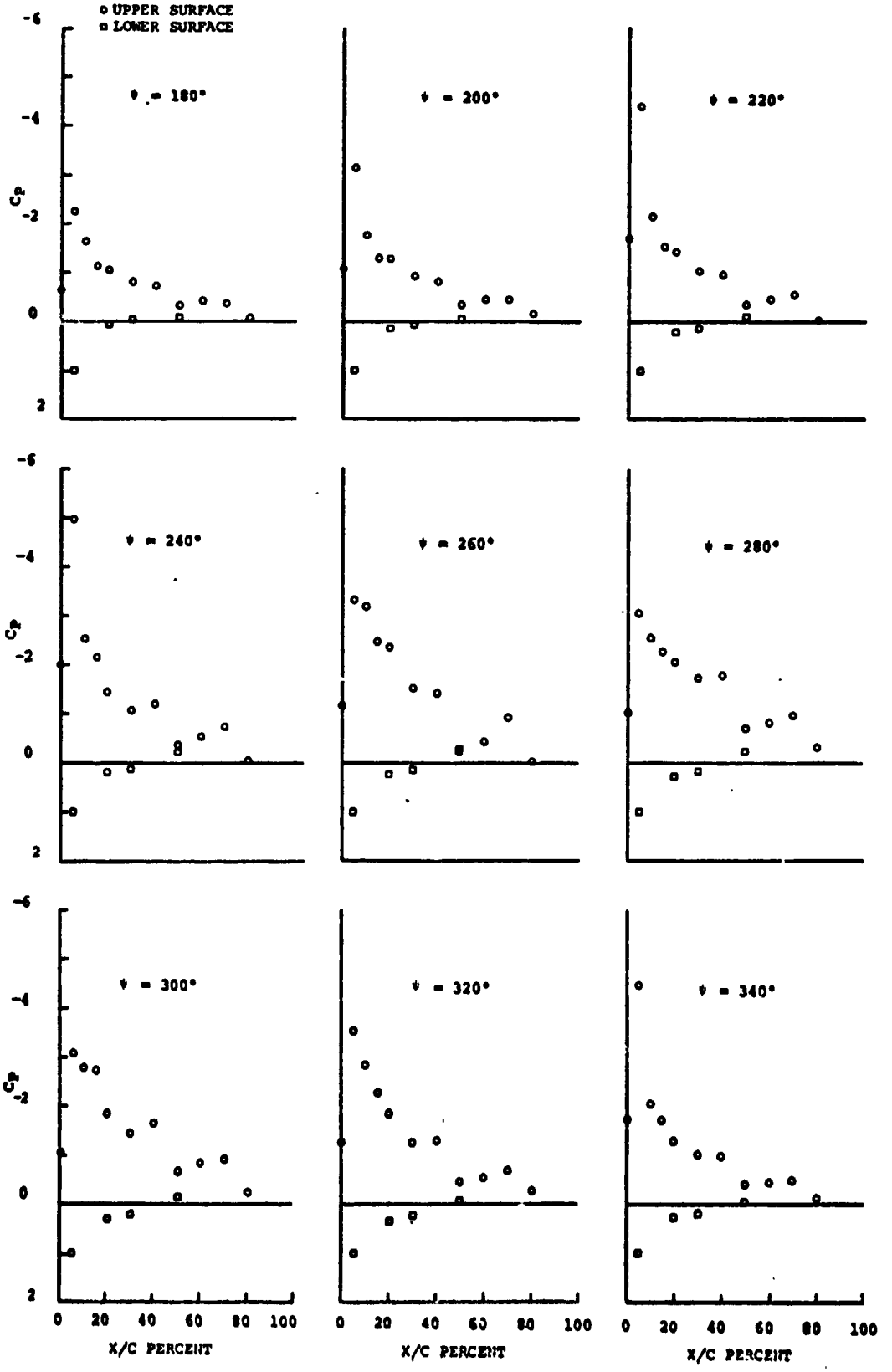

Figure 37 (Continued) PRESSURE DISTRIBUTIONS MEASURED AT r/R = 0.75

3.5 Acceleration Compensated Transducers (Test Points 4.01 to 4.12)

The last part of the present wind tunnel test was devoted to checking out a set of acceleration compensated transducers. The data are presented in a strip-out form in the Appendix. Transducer assignment and condition have been discussed in Section I, and the test conditions are summarized in Table VI.

A set of directly comparable data is presented in Figure 38 from Test Point 4.07. In Figure 38 one measurement was carried out with transducer TR A, which is compensated for accelerations, and the other with transducer TR2, of the conventional type. The transducers were mounted at the 0.75 R span station and 10% chordwise position on different blades. The pressure time histories show significant differences on the advancing side, but it is likely that such differences are due to airfoil contours because the "taped-over" data of Test Point 4.12 do not show a response of such magnitude on transducers TR 2, TR 4 and TR 5.

TRANSDUCER LOCATION: 0.10 c
0.75 R

TR A ACCELERATION COMPENSATED
TR 2 CONVENTIONAL TRANSDUCER

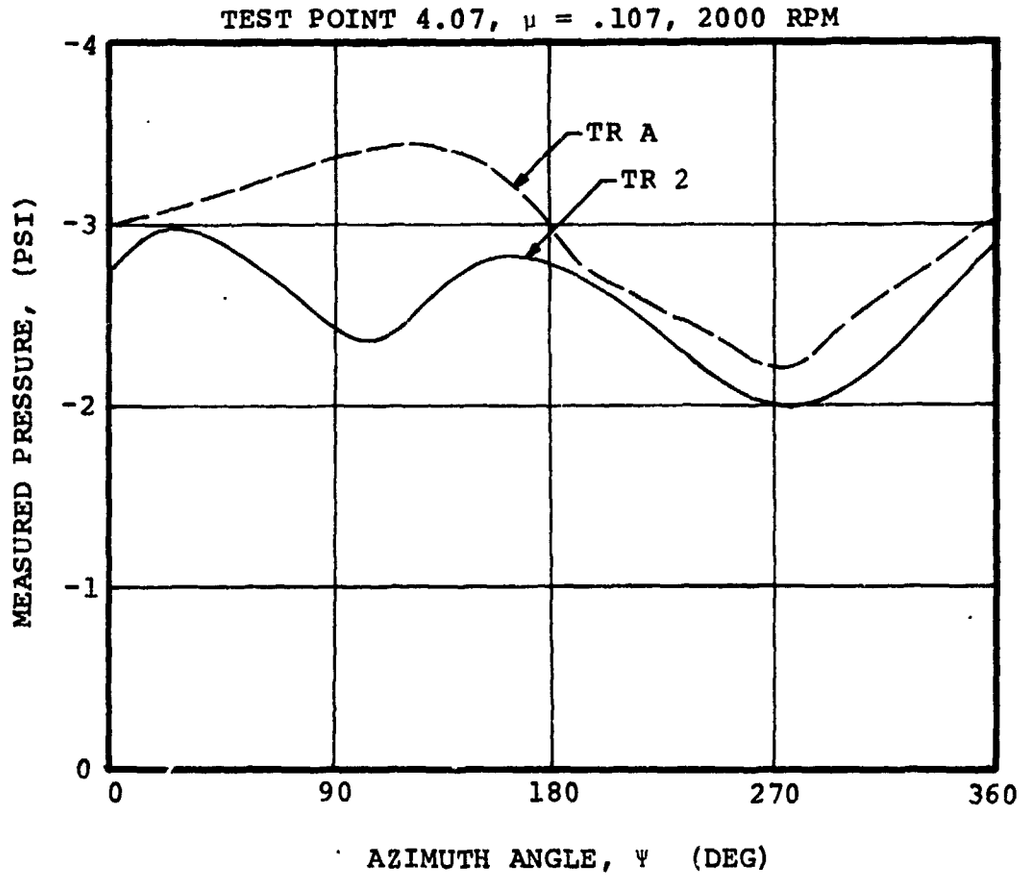

FIGURE 38 TIME HISTORY OF UPPER SURFACE PRESSURE AT r/R = 0.75. MEASURED WITH A CONVENTIONAL AND AN ACCELERATION COMPENSATED TRANSDUCER

4. CONCLUSIONS AND RECOMMENDATIONS

(a) The pressure data at the 0.75 R span station display fluctuations which can be attributed to the effect of tip vortex proximity.

(b) The lift computed by integrating the pressures measured at the 0.75 R station agrees with the lift determined by laser velocimeter measurements as reported in Reference (2).

(c) The data obtained to illustrate the growth of the stall region with increasing advance ratio revealed moderate leading edge separation followed by reattachment and the attainment of a second substantial pressure peak. The test results should be analyzed in more detail.

(d) The additional data to compare teetering and articulated rotors showed that the stall boundaries for the two rotors are much more similar than suspected after the first test (Reference 1). This casts some doubt on the integrated loads from the first test.

(e) The acceleration compensated transducers offer little or no advantage over the standard transducers employed in this test and in the previous test (Reference 1).

The following recommendations can be made as to the equipment necessary for future tests:

(a) The rotor hub should be equipped with cyclic pitch control.

(b) Having established the usefulness of absolute pressure data, future measurements should be limited to differential pressure data.

Additional work needs to be done in the following areas:

(a) A comparison between teetering and articulated rotors should be carried out with models having identical blades.

(b) More tip vortex data should be acquired and such data should be used to define or verify a tip vortex trajectory method applicable to helicopter performance prediction methodology.

(c) Future tests should be run in the Mach Number environment of actual helicopters, or at least with the advancing blade operating beyond the critical Mach Number.

5.0 APPENDIX

5.1 Summary of Data

A summary of reduced data is presented in Table V. A microfiche listing of the reduced data is available through G. Morehouse, Research Scientist, of the U. S. Army Air Mobility Research and Development Laboratory, at Moffett Field, California.

5.2 Test of Acceleration Compensated Transducers

Table VI summarizes the data taken for the acceleration compensated transducers.

Figures 39 through 50 show an oscillograph record of the data acquired.

The last three runs, 4.10, 4.11, and 4.12, display a significant wind-off-zero shift between the beginning and the end of each run. This is due to air leaking out of the transducer cavity around the tape covering the transducers. The pressure fluctuations seen during the runs are probably due to the air flow and do not reflect a transducer response to accelerations. The data are presented only for completeness.

5.3 Flow Visualization Study

A flow visualization study with tufts attached along a rotor blade was conducted by G. Morehouse and J. McCroskey, of the Ames Directorate, separately from the test discussed in this report. The results of such investigation have not been published yet.

Figure 51 summarizes the results of a study of the separation boundaries at conditions comparable to those of Test Points 3.05 and 3.09.

Figure 52 shows an example of the effectiveness of tufts in detecting flow separation. The flow conditions are the same as for Test Points 3.05 and 3.09, except for a tip speed reduction from V_T = 270 fps to V_T = 110 fps.

TABLE V SUMMARY OF REDUCED DATA

TEST POINT	μ	V_{TIP} (FPS)	α_{SHAFT}	$\theta_{.75}$	C_T'/σ	$P/\rho D^2 \sigma V$	$\bar{X}$	B_{1C}	B_{1S}
1.01	.278	109.9	-10.0°	8.62°	.131	.1108	.23632	-11.3°	-2.5°
02	.188	110.0	-10.0°	8.5°	.074	.17	.4	- 7.4°	-3.9°
03	.249	238.2	-10.0°	8.579°	.123	.0152	.25954	- 9.1°	-2.3°
04	.289	110.7	-5.0°	8.5°	.100	.2163	.02674	-11.6°	-3.0°
05	.289	110.7	-5.0°	8.5°	.100	.2163	.02674	- 7.8°	-2.1°
06	.189	238.2	-10.0°	8.5°	.084	.07865	.42503	- 4.2°	-1.3°
07	.191	238.7	-5.0°	8.5°	.099	.0759	.09892	- 4.8°	-1.6°
2.01	.304	270.1	-10.0°	8.5°	.074	.0151	.08906	- 6.3°	-0.7°
02	.405	270.6	-16.5°	12.726°	.074	.0063	.07693	- 9.9°	-0.5°
03	.455	269.8	-20.5°	13.103°	.079	.0052	.08773	-12.1°	-0.5°
04	.353	269.7	-13.5°	10.88°	.079	.0112	.09435	- 8.3°	-0.5°
05	.348	270.3	-12.0°	12.33°	.109	.0115	.10259	-10.7°	-1.1°
06	.302	270.5	-9.5°	9.722°	.104	.0177	.10347	- 8.8°	-1.4°
07	.408	270.6	-16.0°	14.73°	.108	.0071	.10026	-14.0°	-1.1°
3.01	.350	270.2	-19.0°	12.77°	.070	.0128	.17317	- 8.5°	-0.5°
02	.350	270.2	-16.0°	12.77°	.088	.0129	.15479	- 9.6°	-0.8°
03	.352	269.8	-13.0°	12.77°	.107	.013	.11925	-11.1°	-0.8°
04	.351	269.9	11.0°	12.77°	.120	.013	.08322	-12.0°	-1.2°
05	.349	269.7	-8.0°	12.77°	.137	.0132	.01482	-13.1°	-1.6°
06	.344	270.9	-8.0°	8.83°	.083	.0203	.02807	- 7.4°	-0.8°
07	.343	270.7	-5.0°	8.83°	.102	.0206	-.02616	- 8.6°	-1.1°
08	.348	270.5	-10.0°	8.83°	.070	.02	.04277	- 6.8°	-0.6°
09	.349	271.0	-8.0°	12.75°	.147	.02	.00127	-13.9°	-1.9°
10	.402	270.3	-16.5°	13.09°	.079	.0131	.08987	-10.9°	0.1°

TABLE VI. SUMMARY OF DATA FOR ACCELERATION COMPENSATED TRANSDUCERS

TEST POINT	μ	Ω (RPM)	α_S	$\theta_{.75}$	C_T'/σ	$\bar{X}$
4.01	.207	1363	-19°	-2.54°	-.059	-.904
02	.209	1365	-19°	.204°	-.043	-.651
03	.208	1364	-19°	9.52°	.069	.697
04	.208	1363	-19°	11.93°	.1015	.927
05	.014	2010	-19°	-1.55°	.0059	
06	.107	2005	-19°	4.11°	.037	1.60
07	.107	1926	-19°	6.55°	.063	2.73
08	.353	737	- 8°	12.42°	.145	-.0054
09	.354	736	- 8°	12.41°	.143	-.0073
10	.107	1798	-19°	4.38°	.048	1.94
11	.053	1804	-19°	4.4°	.053	
12	.109	1800	-19°	≈6.0°	.048	1.92

Figure 39

TEST POINT 4.01

μ = .207 $\quad$ α_S = -19° $\quad$ C_T'/σ = -.059

Ω = 1363 RPM $\quad$ $\theta_{.75}$ = -2.54° $\quad$ $\bar{X}$ = -.904

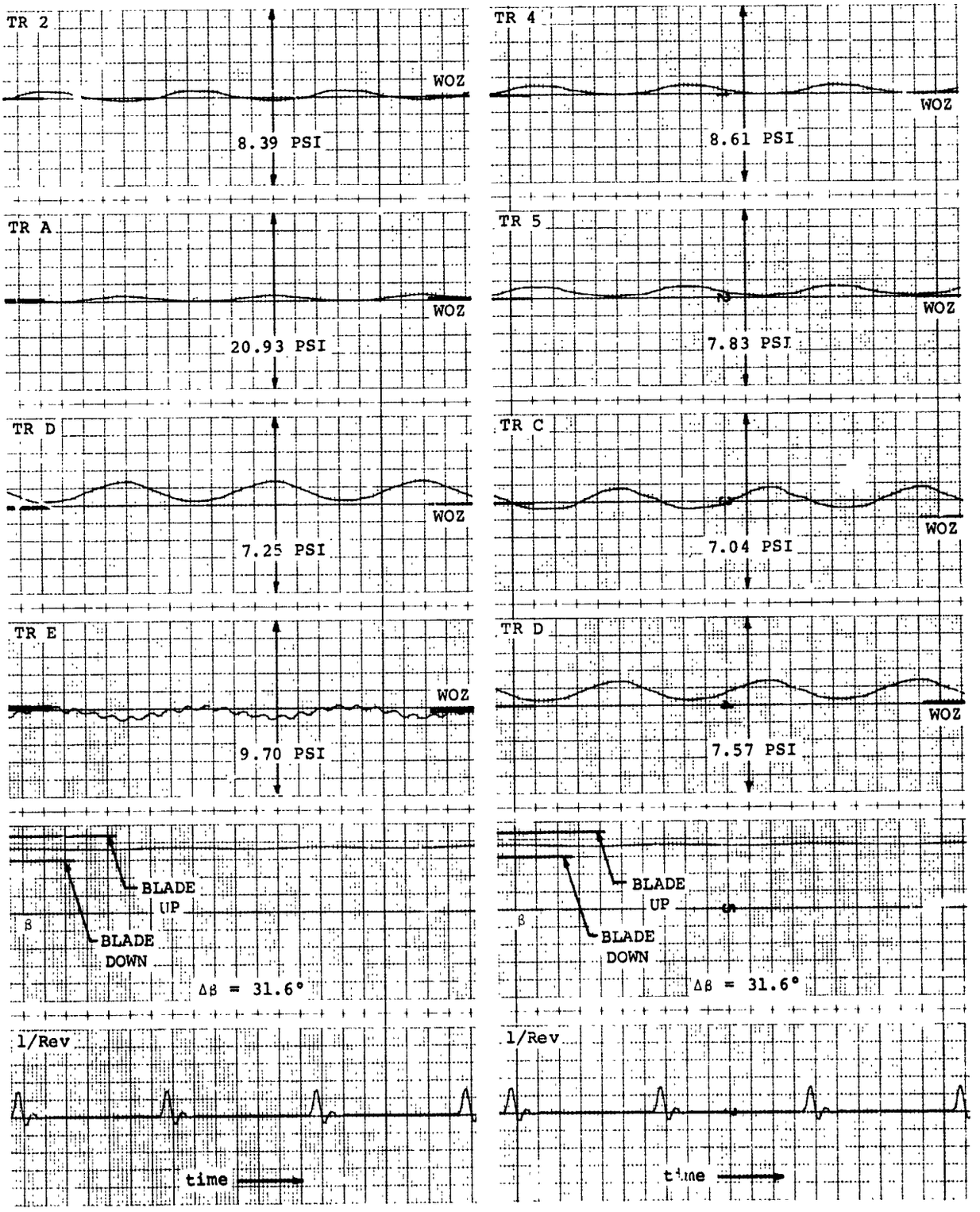

Figure 40

TEST POINT 4.02

μ = .209 $\quad$ α_S = -19° $\quad$ C_T'/σ = -.043

Ω = 1365 RPM $\quad$ $\theta_{.75}$ = .204° $\quad$ $\overline{X}$ = -.651

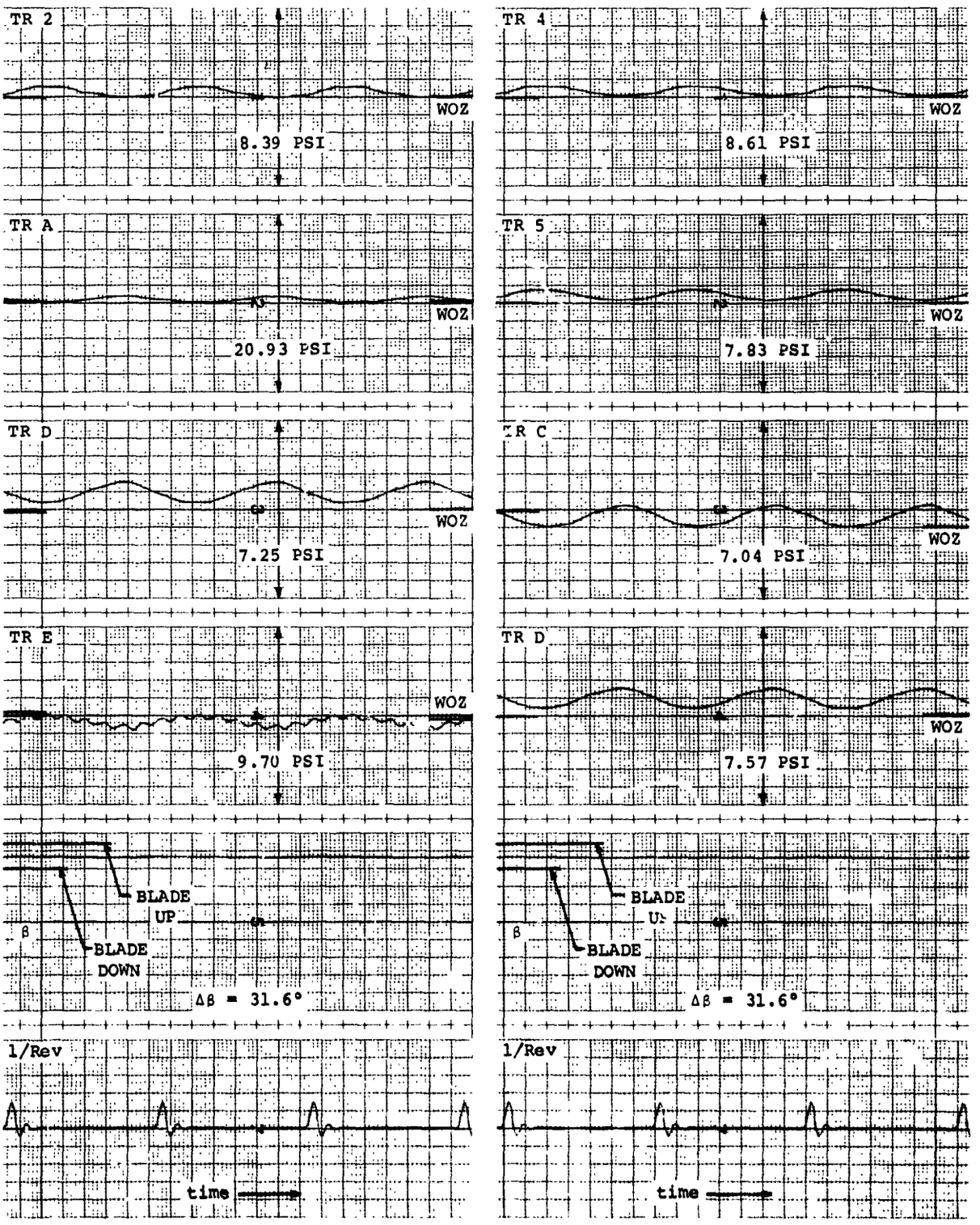

Figure 41

TEST POINT 4.03

μ = .208 $\quad \alpha_S$ = -19° $\quad \frac{C_T}{\sigma}$ = .069

Ω = 1364 RPM $\quad \theta_{.75}$ = 9.53° $\quad \bar{X}$ = .697

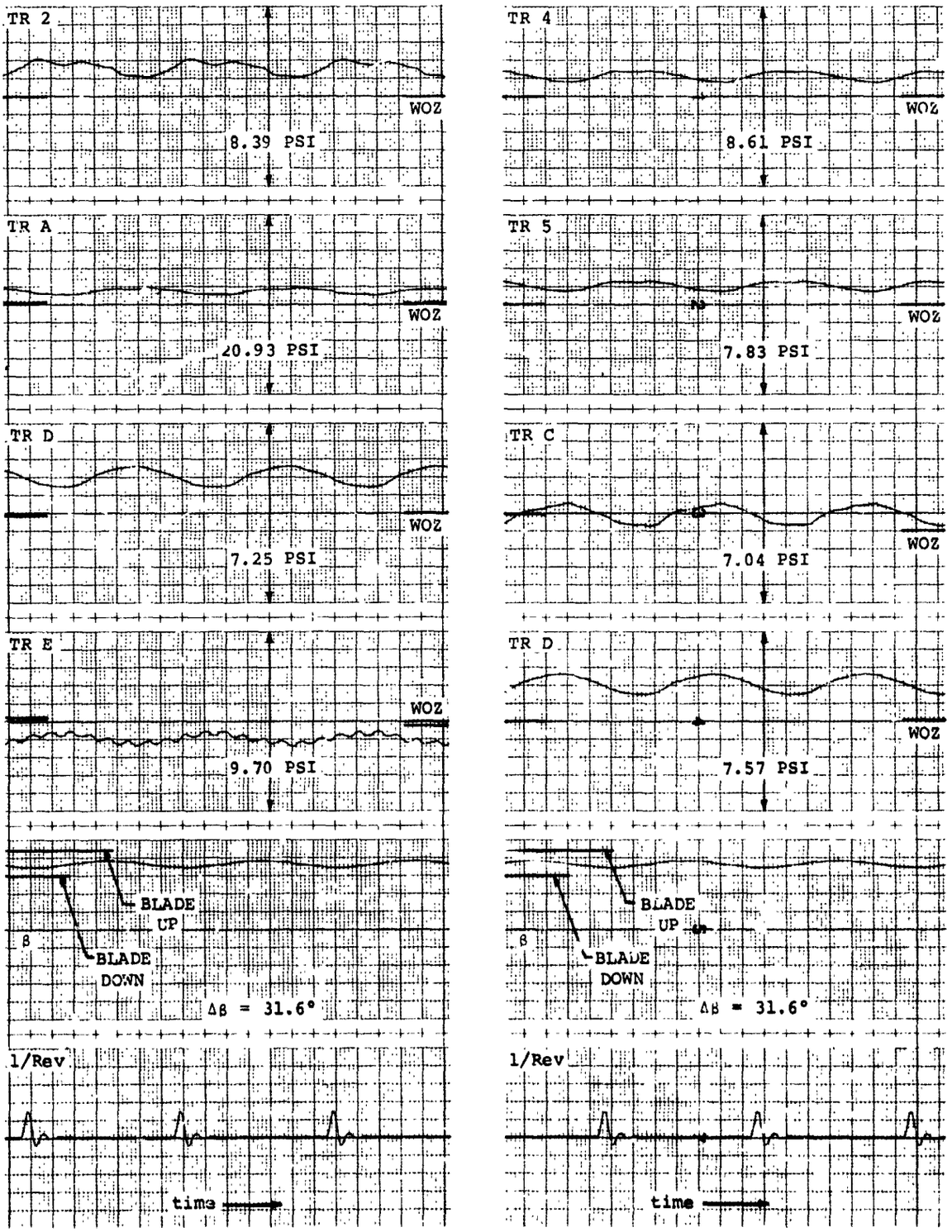

Figure 42
TEST POINT 4.04

μ = .208 $\quad \alpha_S$ = -19° $\quad C_T'/\sigma$ = .1015
Ω = 1363 RPM $\quad \theta_{.75}$ = 11.93° $\quad \bar{X}$ = .927

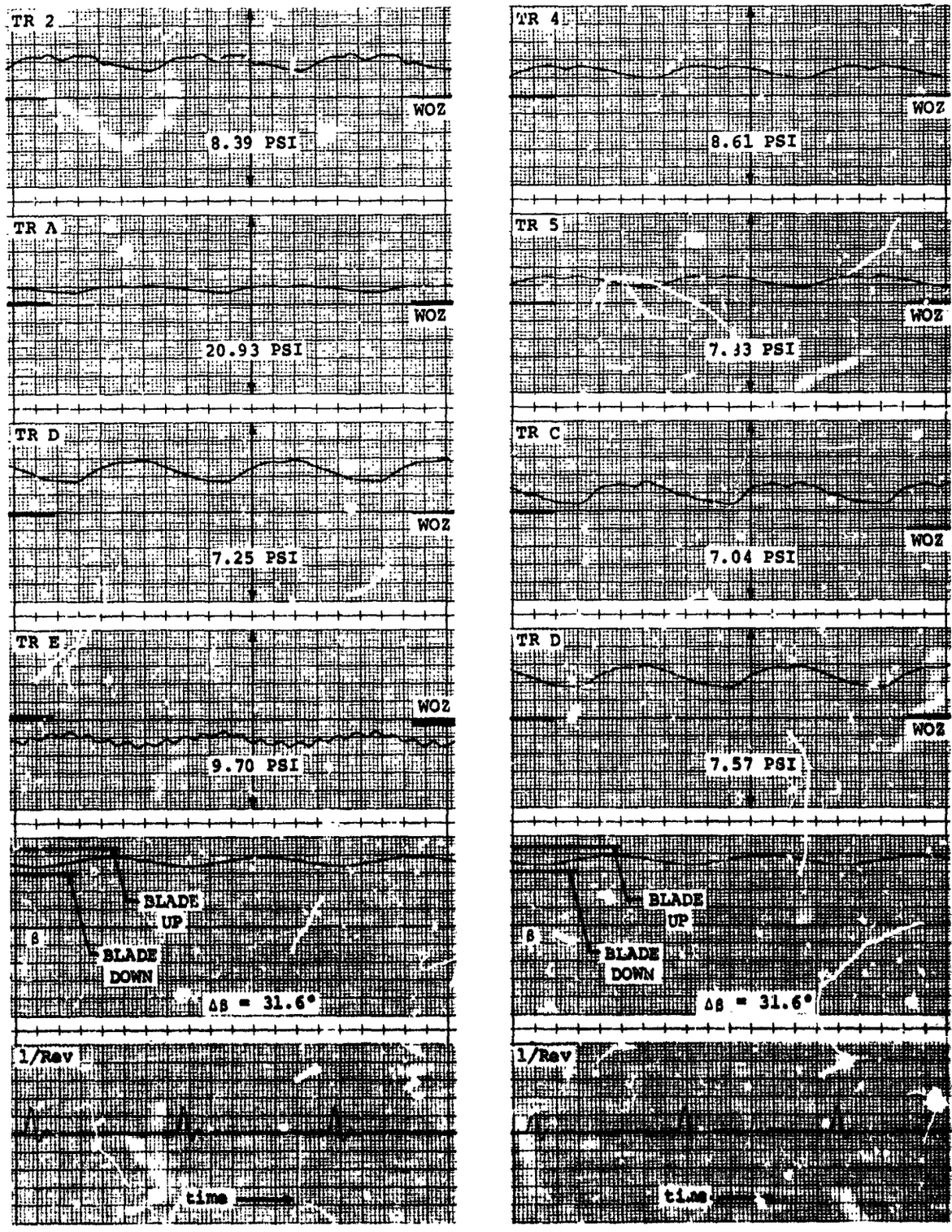

Figure 43
TEST POINT 4.05

μ = .014 $\quad$ α_S = -19° $\quad$ C_T'/σ = .0059
Ω = 2010 RPM $\quad$ $\theta_{.75}$ = 1.55° $\quad$ $\bar{X}$ = 17.71

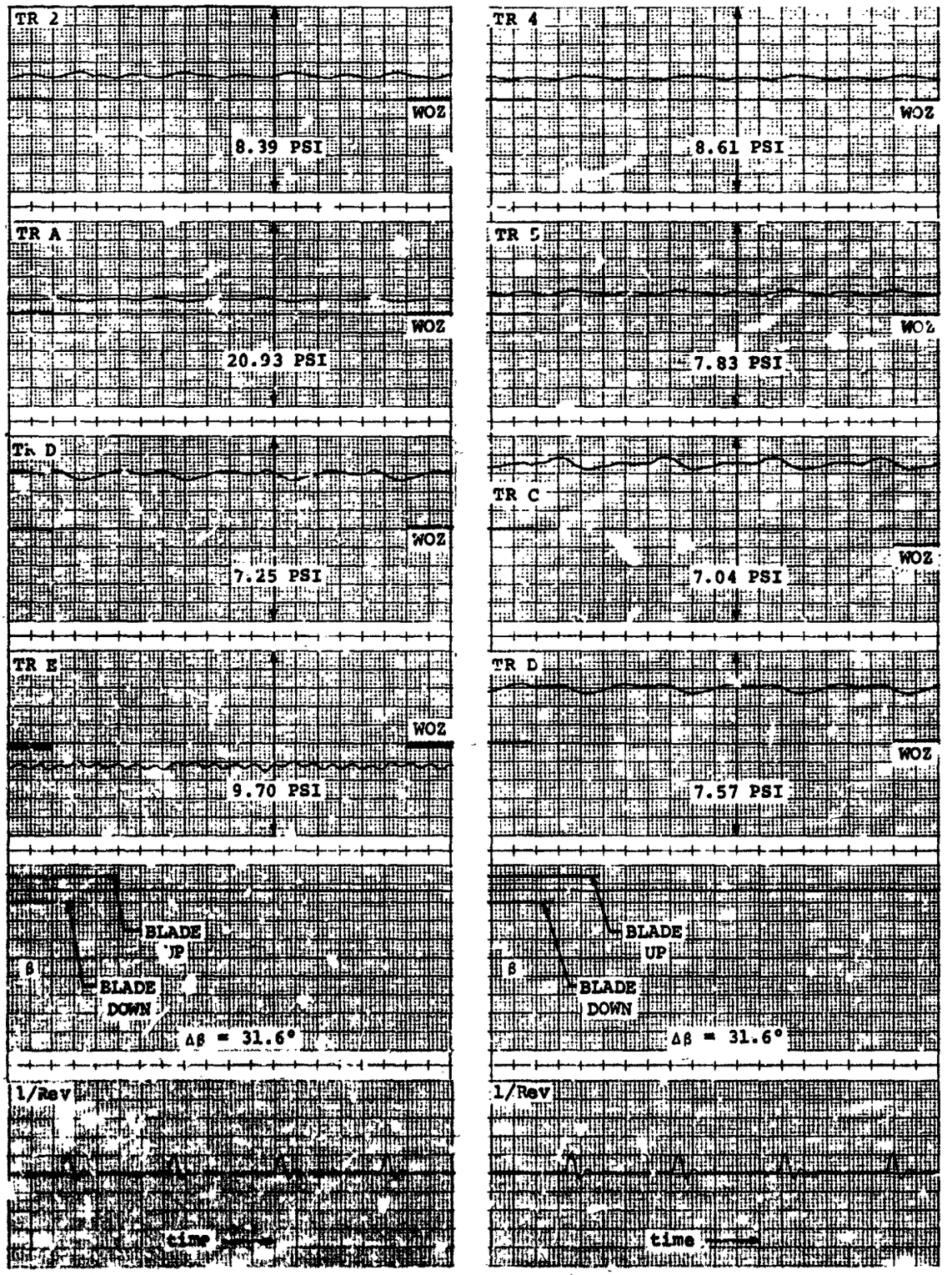

Figure 44
TEST POINT 4.06

μ = .107
Ω = 2005 RPM
α_S = -19°
$\theta_{.75}$ = 4.11°
C_T'/σ = .037
$\bar{X}$ = 1.60

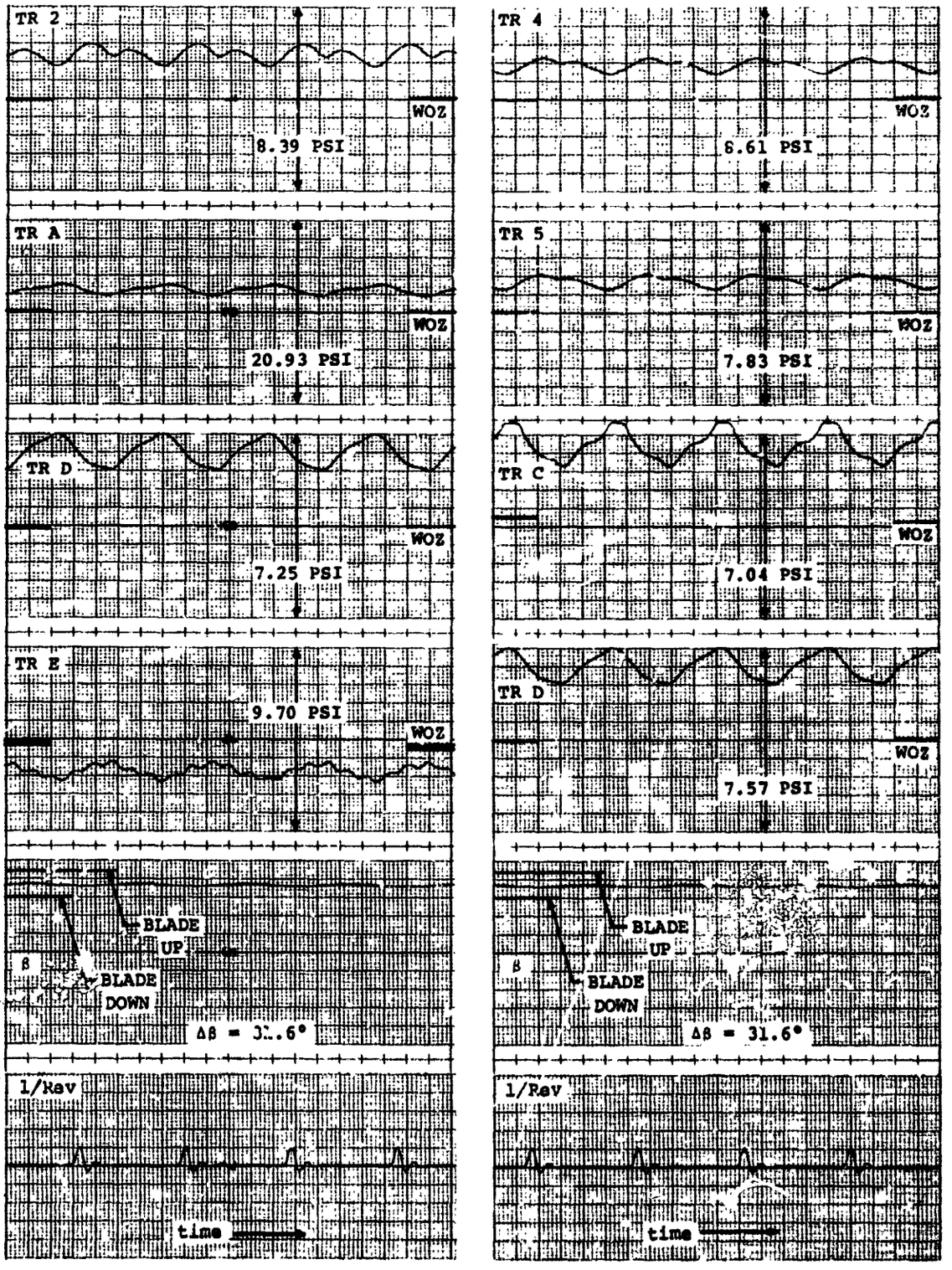

Figure 45

TEST POINT 4.07

μ = .107 $\quad \alpha_S$ = -19° $\quad \frac{C_T'}{\sigma}$ = .063

Ω = 1926 RPM $\quad \theta_{.75}$ = 6.55° $\quad \frac{C_T}{X}$ = 2.73

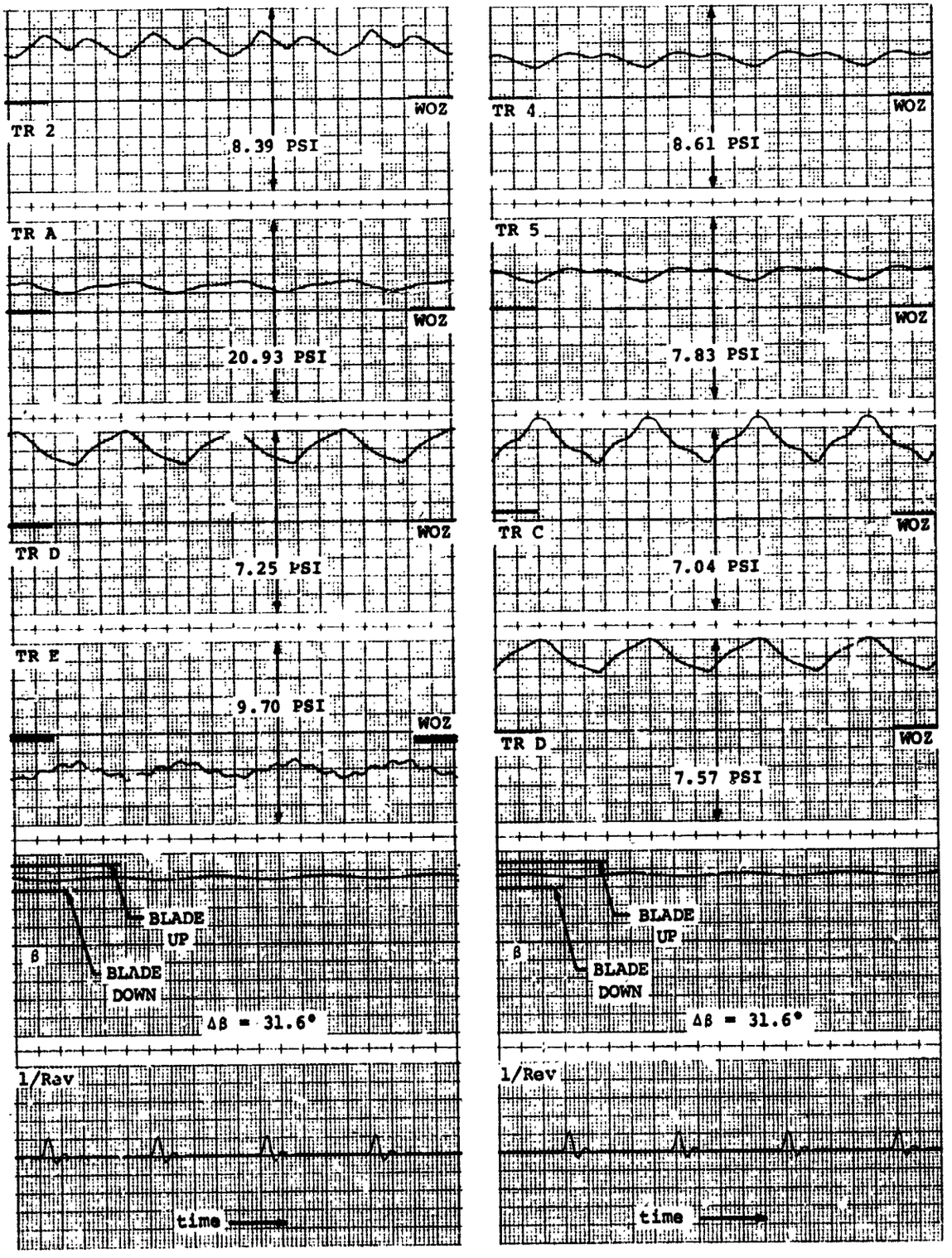

Figure 46
TEST POINT 4.08

μ = .353 $\quad \alpha_S$ = -8° $\quad \frac{C_T'}{\sigma}$ = .145
Ω = 737 RPM $\quad \theta_{.75}$ = 12.42° $\quad \bar{x}$ = -.0054

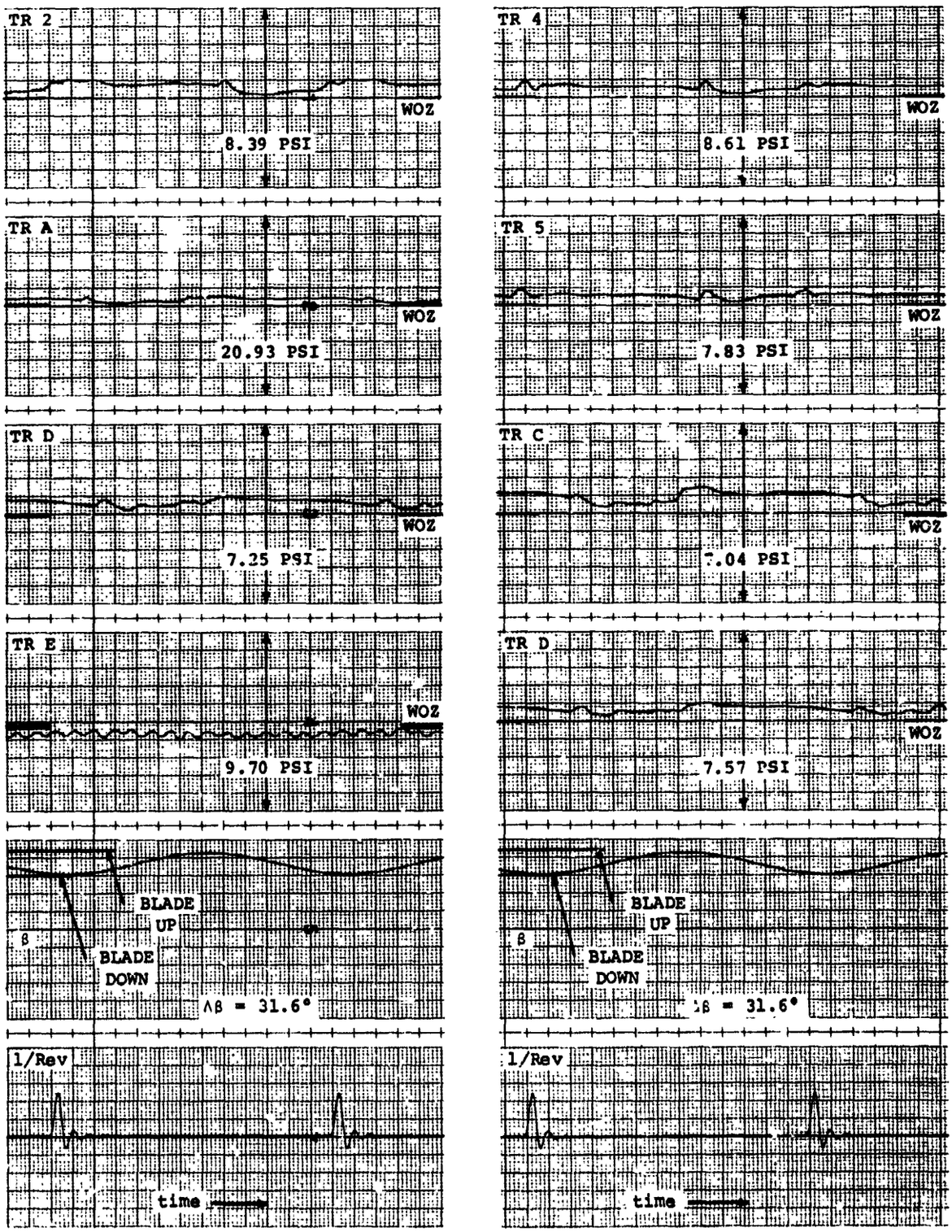

Figure 47
TEST POINT 4.09

μ = .354 $\quad \alpha_S$ = -8° $\quad C_T'/\sigma$ = .143
Ω = 736 RPM $\quad \theta_{.75}$ = 12.41° $\quad \bar{X}$ = -.0073

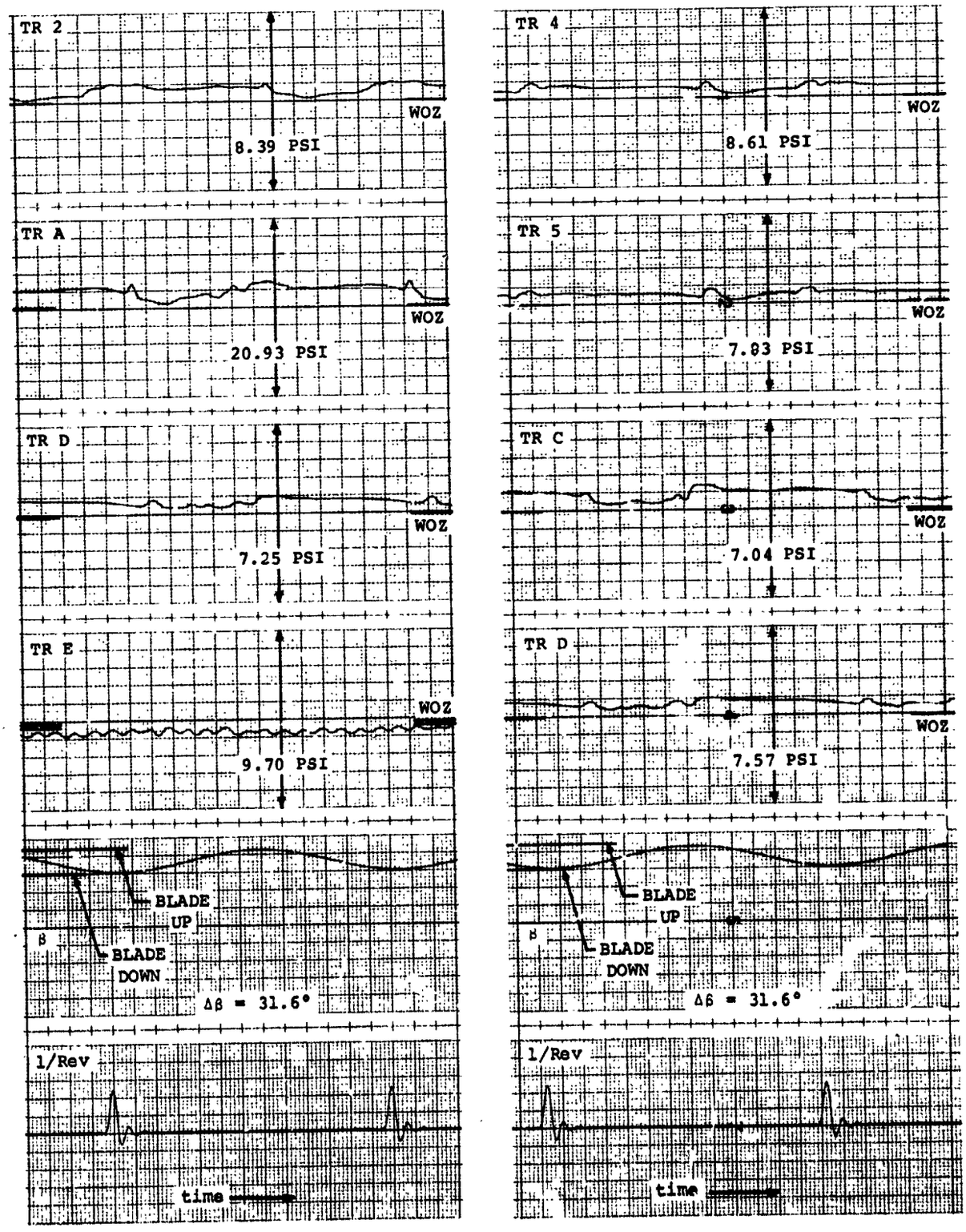

Figure 48
TEST POINT 4.10

A, B, C, D, E TAPED OVER

μ = .107 α_S = -19° C_T'/σ = .048
Ω = 1798 RPM $\theta_{.75}$ = 4.38° $\bar{X}$ = 1.94

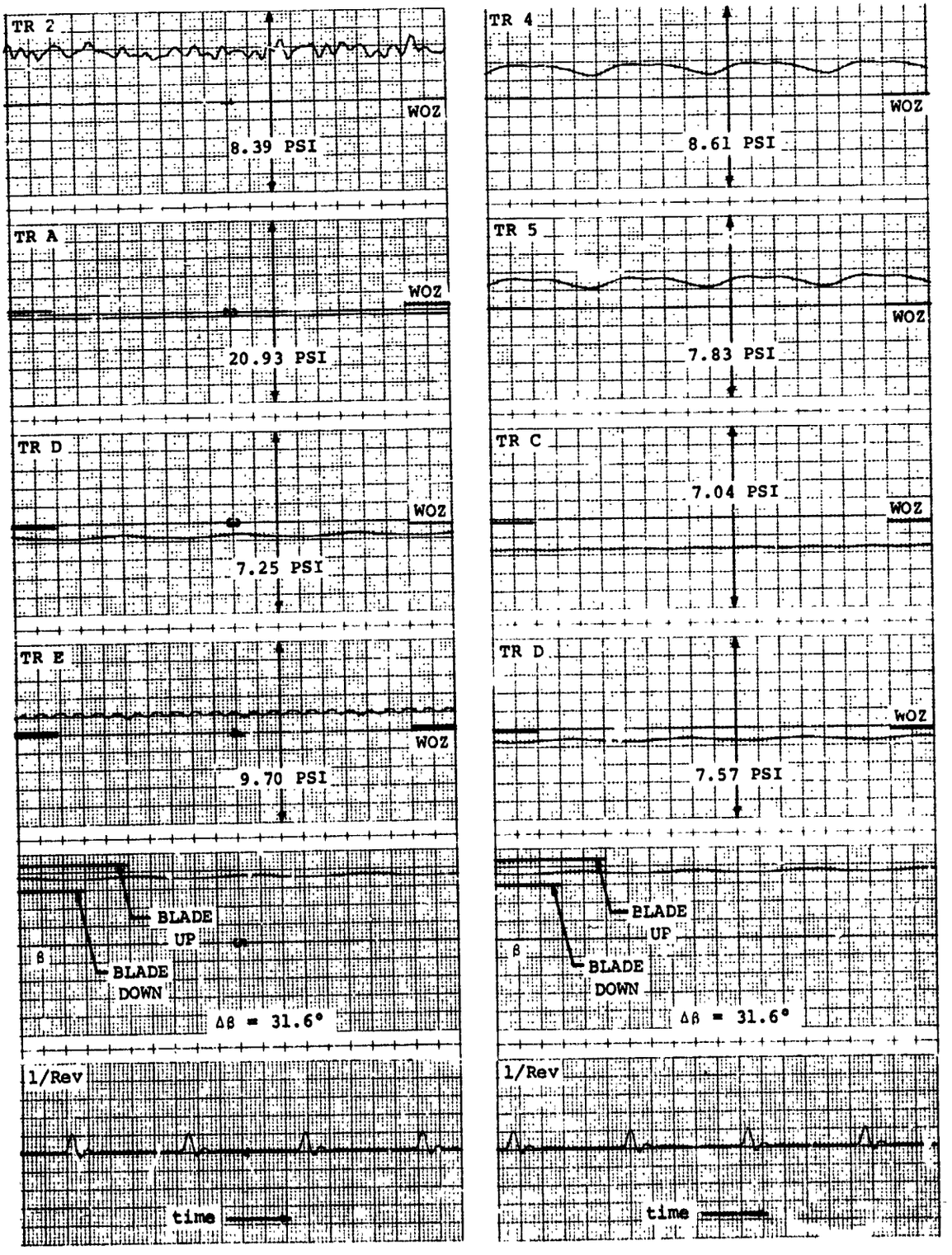

Figure 49
TEST POINT 4.11

ALL TRANSDUCERS TAPED OVER

μ = .053
Ω = 1804 RPM
α_S = -19°
$\theta_{.75}$ = 4.4°
C_T'/σ = .053
$\bar{X}$ = 10.34

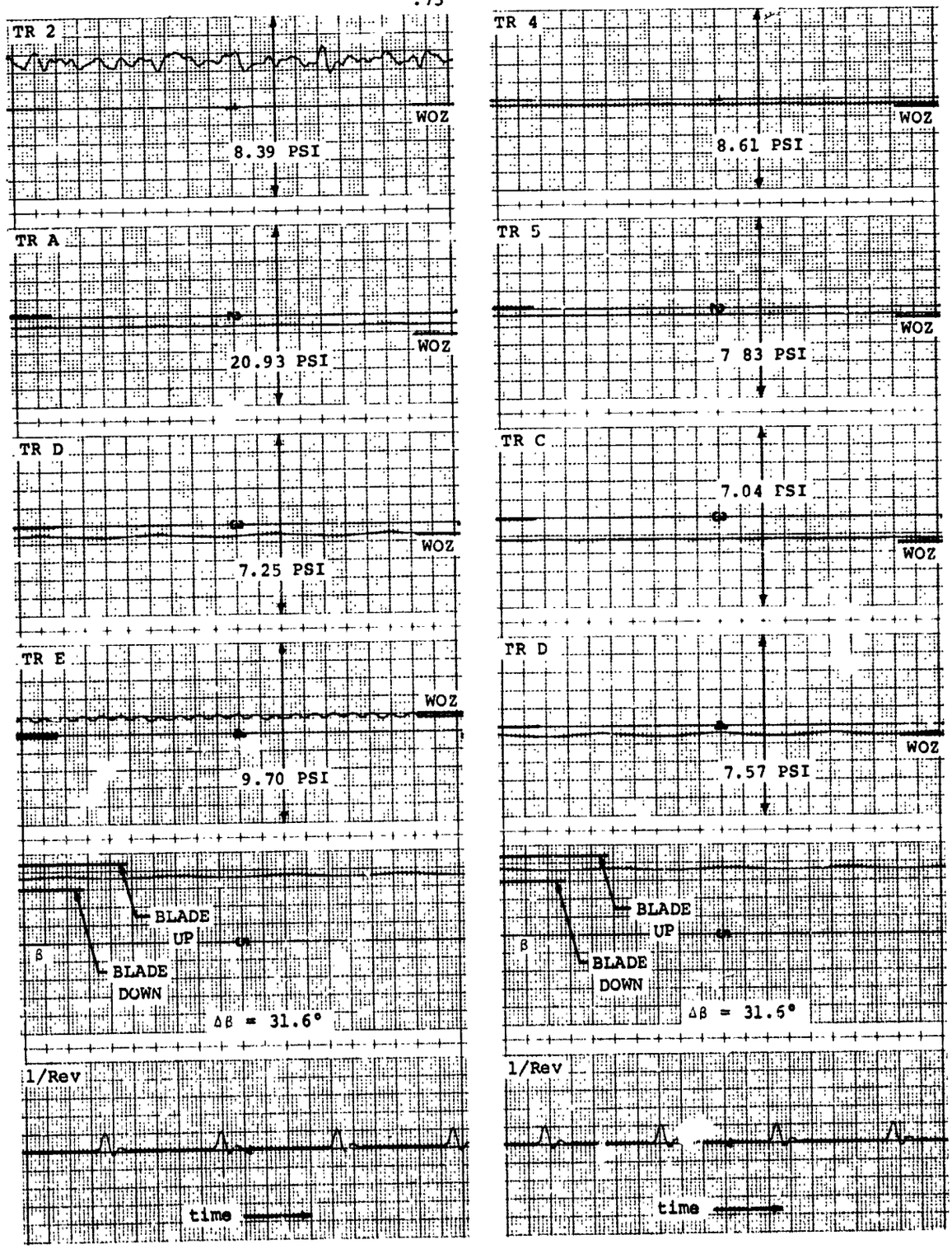

Figure 50
TEST POINT 4.12

ALL TRANSDUCERS TAPED OVER

μ = .109 α_S = -19° C_T'/σ = .048
Ω = 1800 RPM $\theta_{.75}$ = -6° $\bar{X}$ = 1.92

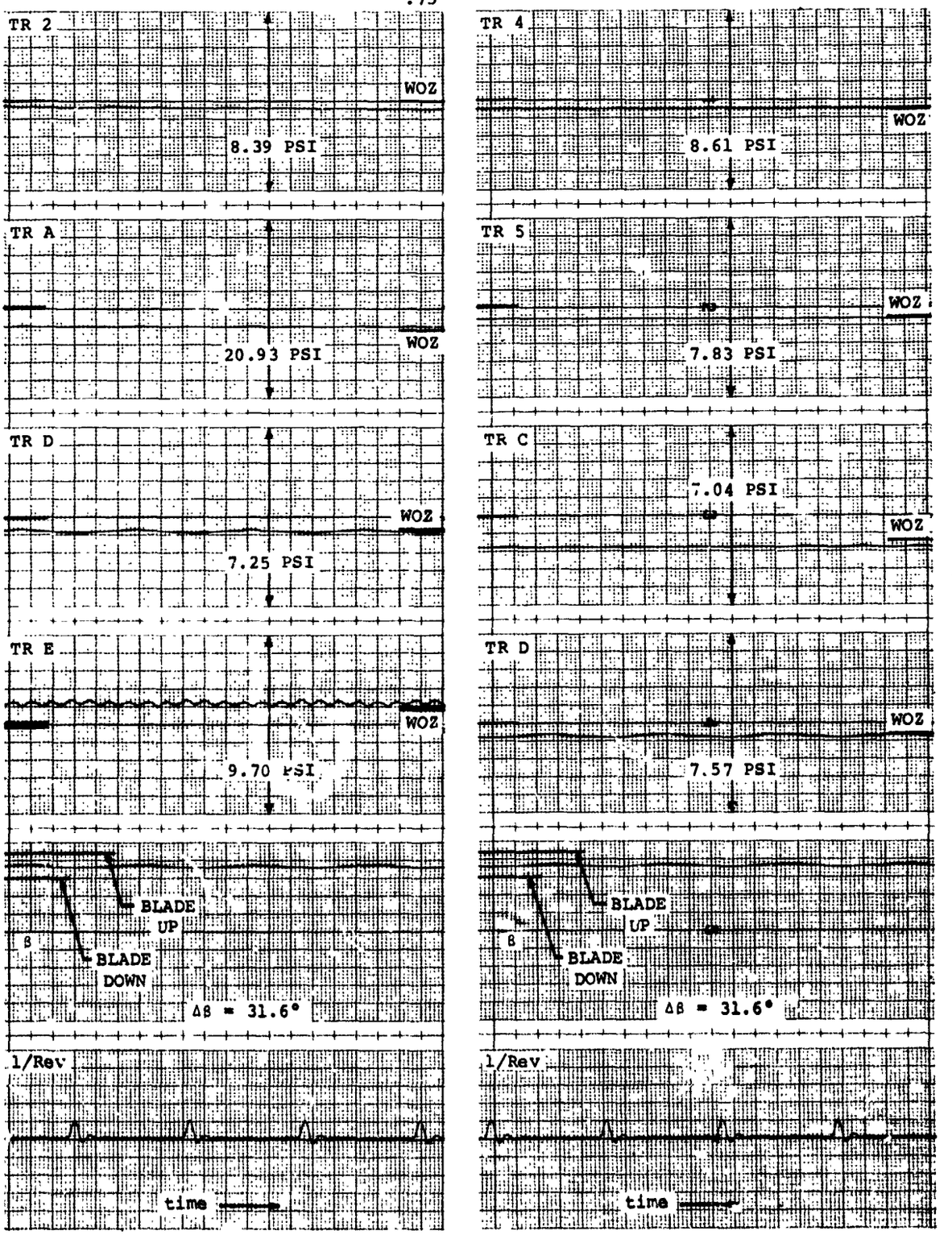

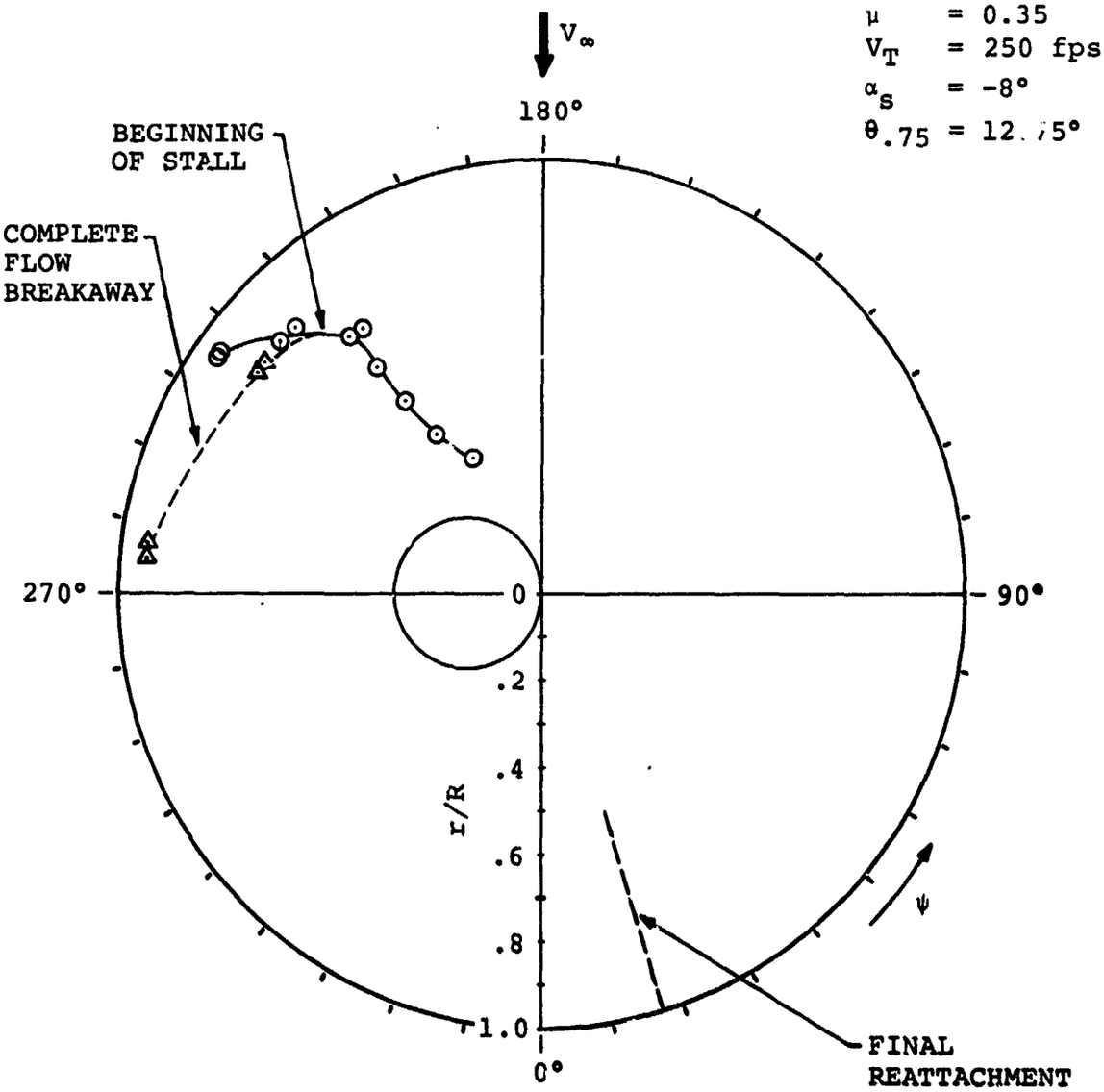

SYMBOL

o ONSET OF STALL

Δ COMPLETE FLOW SEPARATION

FIGURE 51 SUMMARY OF SEPARATION AND REATTACHMENT BOUNDARIES FROM TUFT FLOW VISUALIZATION STUDY

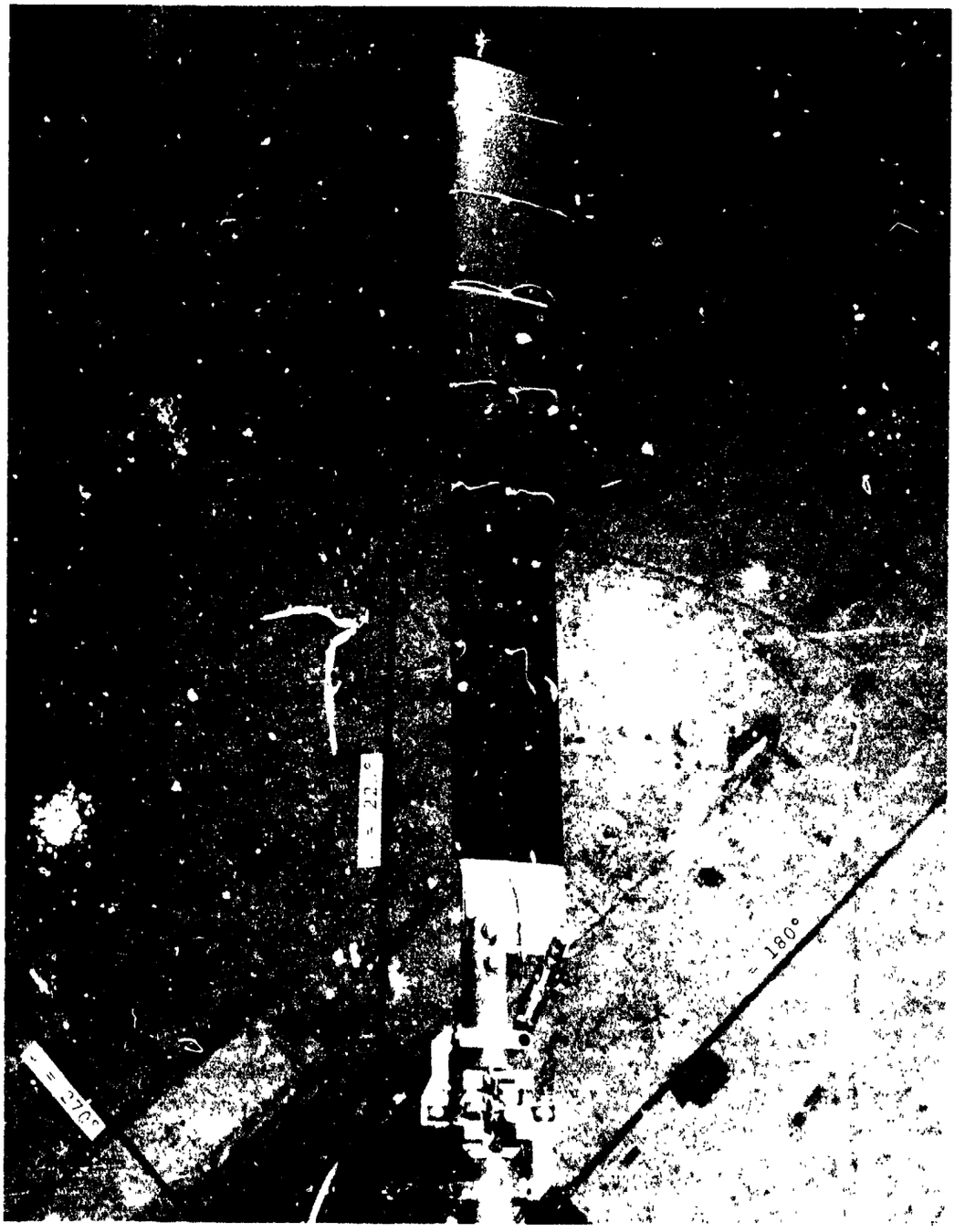

FIGURE 52 FLOW VISUALIZATION AT μ = 0.35, $\theta_{.75}$ = 12.75°, α_s = -8°, V_T = 110 fps

6. REFERENCES

1. Dadone, L. U., Fukushima, T., Investigation of Rotor Blade Element Airloads for a Teetering Rotor in the Blade Stall Regime, NASA CR-137534, September 1974.

2. Biggers, J. C., Sing Chu, Orloff, K. L., Laser Velocimeter Measurements of Rotor Blade Loads and Tip Vortex Rollup, presented at the 31st Annual National Forum of the American Helicopter Society, Washington, D. C., May 1975.

3. Bowden, T. H., Schockey, G. A., A Wind Tunnel Investigation of the Aerodynamic Environment of a Full-Scale Helicopter Rotor in Forward Flight, USAAVLABS TR-70-35, July 1970.

4. Fisher, R. K., Thompkins, J. E., Bobo, C. J., Child, R. F., An Experimental Investigation of the Helicopter Rotor Blade Element Airloads on a Model Rotor in the Blade Stall Regime, NASA CR-114424, September, 1971.